THYROID CANCER: A NOVEL INSIGHT INTO DIAGNOSTIC AND THERAPEUTIC APPROACH

FAISAL NOUMAN BAIG

Ph.D

The Hong Kong Polytechnic University

2018

The Hong Kong Polytechnic University

Department of Health Technology and Informatics

Thyroid Cancer: A Novel Insight into Diagnostic and Therapeutic Approach

FAISAL NOUMAN BAIG

A thesis submitted in partial fulfillment of the requirements for the degree of Doctor of Philosophy

August 2017

Certification of Originality

I hereby declare that this thesis is my own work and that, to the best of my knowledge and belief, it reproduces no material previously published or written, nor material which has been accepted for the award of any other degree or diploma, except where due acknowledgement has been made in the text.

_____(Signed)

Faisal Nouman Baig (Name of Student)

Dedication

To Almighty Allah, my loving parents, my dearest family, and friends with lots of love and respect

Abstract

There has been a substantial increase, worldwide, in the incidence of thyroid cancer over the past few decades. The diagnosis of thyroid cancer poses a clinical challenge to medical practitioners. Fine needle aspiration cytology (FNAC) is a current standard method to diagnose thyroid cancer. FNAC has a false-positive rate of 1% - 5% and a false-negative rate of 0% - 7.7%, whilst 20% - 30% of cases remain non-diagnostic. Grey-scale ultrasound is a useful imaging technique for the assessment of the thyroid gland, because it can characterize various features of thyroid nodules such as the number, site, size, shape, echogenicity, and internal architecture. However, grey-scale ultrasound has limited value in differentiating benign and malignant thyroid nodules because of its varied sensitivity (52% - 97%) and specificity (26% - 83%). The varied sensitivity and specificity of grey-scale ultrasound might be due to the qualitative analysis and subjective interpretation of the characteristics of thyroid nodules and renders it thus vulnerable to inter- and intra-observer variations. Nevertheless, certain features of thyroid nodules can be quantified, for example tissue stiffness and the vascularity index.

Shear wave elastography is a novel ultrasound technique that can quantify tissue stiffness by tracking the propagation of shear waves through thyroid nodules. In general, malignant thyroid nodules tend to be stiffer than benign nodules. Depending upon the differences in stiffness

values, thyroid nodules can be differentiated as benign or malignant. The first study of this thesis evaluated the feasibility of using shear wave elastography in predicting thyroid malignancy, and determined if any (and if so, which ones) of the shear wave elastography indices ($E_{maximum}$, E_{mean}, and $E_{minimum}$) are potential predictors of thyroid malignancy. The study further evaluated the diagnostic accuracy in differentiating benign and malignant thyroid nodules when grey-scale ultrasound was combined with shear wave elastography.

Vascularity is a dynamic feature usually detected on Doppler ultrasound. Central vascularity and hypervascularity are usually associated with malignant thyroid nodules. However, not all previous studies appreciate the usefulness of vascularity in predicting thyroid malignancy. Controversial results might be due to the fact that previous studies evaluated vascularity by visual assessment methods that involve subjective interpretation and thus result in high inter- and intra-observer variations. Moreover, in previous studies, the methods used to delineate a border between peripheral and central regions of a thyroid nodule were not standardized. In the second study in this thesis, we have thus developed a computer algorithm that can perform regional segmentation of thyroid nodules by using an 'offsetting' method, and quantify the overall vascularity as well as the vascularity in peripheral and central regions of thyroid nodules. Based on the differences in the vascularity indices, thyroid nodules can be differentiated into benign and malignant types. The study further evaluated the potential advantage of combining the

vascularity index with grey-scale ultrasound to enhance the diagnostic accuracy of thyroid malignancy.

In the first and second study, a total of 111 patients with solitary thyroid nodules were included. Each thyroid nodule was assessed with grey-scale ultrasound, shear wave elastography, and colour Doppler ultrasound. The diagnosis of the thyroid nodules was confirmed by FNAC and/or histological examination. Grey-scale ultrasound features including microcalcification (malignant: 77.8% versus benign: 7.1%), hypoechoic (92.6% versus 33.3%), irregular margins (55.6% versus 16.7%), and a height-to-width ratio > 1 (59.3% versus 13.1%) were found to be more frequently associated with malignant thyroid nodules than with benign thyroid nodules. The differences were statistically significant (all $P < 0.05$).

Regarding shear wave elastography, the results suggested that $E_{maximum} \geq 67.3$ kPa and $E_{mean} \geq 23.1$ kPa are independent predictors of thyroid malignancy. $E_{maximum}$ was found to be the best adjunct to grey-scale ultrasound. The combination of $E_{maximum}$ or E_{mean} with grey-scale ultrasound enhanced the diagnostic accuracy of grey-scale ultrasound from 58.5% to 80.2% and 78.4%, respectively ($P < 0.05$). The results of the vascularity index (VI) quantification showed that a 22% offset was optimal for regional subdivision of thyroid nodules. At the optimum offset, the mean VI of peripheral, central, and overall regions of malignant nodules were significantly higher than those of benign nodules (26.5 ±

16.2%, 21.7 ± 19.6%, 23.8 ± 4.6% versus 18.2 ± 16.7%, 11.9 ± 15.1%, and 16.6 ± 1.8%, respectively, $P < 0.05$). The optimum cut-off points of peripheral, central, and overall VI were 19.7%, 9.1%, and 20.2%, respectively. When compared to grey-scale ultrasound alone, a combination of VI assessment and grey-scale ultrasound evaluation of thyroid nodules increased the overall diagnostic accuracy from 58.6% to 79.3% ($P < 0.05$).

Studies 1 and 2 have clinical significance in establishing methods for accurate diagnosis of thyroid cancer. The results of Study 1 suggest that shear wave elastography has clinical importance in differentiating benign and malignant thyroid nodules. The combination of grey-scale ultrasound with $E_{maximum}$ or E_{mean} significantly improved the diagnostic accuracy in predicting thyroid cancer. Study 2 has devised a new method to perform regional segmentation of thyroid nodules and to quantify vascularity in each segment. This approach is objective and standardized to quantify thyroid vascularity and helps in differentiating benign and malignant thyroid nodules.

Colour Doppler ultrasound (CDU) and power Doppler ultrasound (PDU) are widely used for detecting the vasculature of tissues or organs. In the thyroid gland, CDU and PDU have been used for the differential diagnosis of, amongst others, Hashimoto's disease, Graves' disease, and Reidel's thyroiditis. Doppler ultrasound has also been used in monitoring treatment responses during therapy of thyroid disorders.

However, the detection of blood flow in minute blood vessels or vessels with low blood flow is challenging due to technical limitations of previously developed Doppler ultrasound modalities. Most recently, a new ultrasound technology, namely AngioPLUS (Planewave UltraSensitive™ imaging), provides superb sensitivity in the detection of tissue vascularity. The beauty of this technique is that all colour pixels of the tissue can be reconstructed in a single image. AngioPLUS provides high resolution and 3D wall filtering that allow efficient discrimination between blood flow and other soft tissues by analysing space, time, and amplitude information.

Study 3 aimed to evaluate the feasibility of using AngioPLUS imaging in assessing thyroid vascularity when combined with CDU or PDU. The study further evaluated whether the addition of AngioPLUS to CDU or PDU enhances the sensitivity in detecting vasculature of thyroid parenchyma. It also investigated whether there is any asymmetry of vascularity between the right and left thyroid lobes.

A total of 45 healthy volunteers underwent grey-scale ultrasound, CDU, CDU+AngioPLUS, PDU, and PDU+AngioPLUS evaluations of both lobes of the thyroid gland. Thyroid vascularity was evaluated using our in-house computer algorithm. The results showed that the combination of CDU+AngioPLUS (14.7 ± 9.4%) and the combination of PDU+AngioPLUS (13.4 ± 9%) had significantly higher thyroid VI than CDU (8.8 ± 7.3%) and PDU (4.7 ± 5.4%) alone (all $P < 0.05$). No

asymmetry was found between the VI of the right and left thyroid lobes ($P > 0.05$).

Study 3 highlights the differences in sensitivity of detecting thyroid vasculature assessed by different Doppler ultrasound modalities. The results suggest that AngioPLUS enhances the detection of vascularity when added to PDU or CDU. The clinical significance of the study lies in the detection of small blood vessels and vessels with low blood flow that may help disease diagnosis and treatment monitoring.

Study 4 highlights the scope of chemotherapeutic agents in treating papillary thyroid cancer. Current strategies to treat papillary thyroid cancer are largely based on surgery, where recurrence rate is high (up to 33%). Drug development is a costly and time-consuming process. Moreover, the identification of novel therapeutic targets is challenging. Study 4 introduces the concept of ‘repurposing of drugs’ that evaluates the therapeutic potential of already approved drugs beyond the scope of their primary clinical usage.

Cannabinoids are derivatives of the marijuana plant. They have been used for recreation and to relieve pain. Two cannabinoid receptors (CB1 and CB2) are known to be distributed over different body organs and systems in humans. Cannabinoids receptor expression has been noted in many cancers including breast cancer, prostate cancer, hepatic cancer, lung cancer, and colorectal cancer. Anti-cancer actions, including

antiproliferation, antimigration, antiangiogenesis, and apoptosis, have been validated in *in vitro* experiments in various cancer cell lines. In a recent study, immunohistochemistry analysis of surgical specimens of 87 thyroid nodules demonstrated that CB1 and CB2 receptor expression was more significantly associated with papillary thyroid cancer than with benign thyroid nodules. It was further found that CB2 expression was significantly higher than CB1 receptor expression.

In Study 4, the therapeutic potential of CB2 receptor agonist (JWH-133) in treating papillary thyroid cancer was evaluated. A normal thyroid follicular cell line (N-thy-ori-3) was used as the control, and BCPAP was the papillary thyroid cancer cell line used in this study. Both cell lines were treated with JWH-133 at 0, 5, 10, 15, 20, 25, and 30-µM concentrations for 24, 48, and 72 hours. Cellular metabolic activity and cell viability were evaluated using an MTT assay.

The results demonstrated that 25 µM was the lethal dose concentration for BCPAP cells at which cell viability was reduced to 50% after the optimal 48 hours of incubation. The results also suggested that BCPAP cells were more sensitive to the JWH-133 as compared with N-thy-ori-3. The cytotoxic effect mediated by JWH-133 was not significantly inhibited by CB2 receptor antagonist SR144528 in both cell lines. The results of the study demonstrated that JWH-133 has a potent cytotoxic effect, more pronounced in a papillary thyroid cancer cell line (BCPAP) than in a normal follicular thyroid cell line (N-thy-ori-3). Study 4 suggests

that JWH-133 induces cell death in papillary thyroid cancer cells, whilst the survival of normal thyroid follicular cells can be maintained at an acceptable level.

Presentations and Publications

Conference Presentations

1. **Faisal N Baig**, Shirley YW Liu, Helen KW Law, Shea-Ping Yip, and Michael Ying. Can ultrasound shear wave elastography be used as a diagnostic tool to differentiate between malignant and benign thyroid nodules? 21st Asia-Australasia Conference of Radiological Technologists (AACRT) in conjunction with 5th Asian Radiotherapy Symposium (ARS) and 3rd Hong Kong Radiographers and Radiation Therapists Conference (HKRRTC) at Hong Kong Science Park, from 23-25 June 2017, Hong Kong.
2. **Faisal N Baig**, Jurgen TJ van Lunenburg, Shirley YW Liu, Shea-Ping Yip, Helen KW Law, Michael Ying. A novel method to quantify regional vascularity of thyroid nodules for prediction of malignancy: 21st Asia-Australasia Conference of Radiological Technologists (AACRT) in conjunction with 5th Asian Radiotherapy Symposium (ARS) and 3rd Hong Kong Radiographers and Radiation Therapists Conference (HKRRTC) at Hong Kong Science Park, from 23-25 June 2017, Hong Kong.
3. **Faisal N Baig**, Shirley YW Liu, Helen KW Law, Shea-Ping Yip and Michael Ying. Shear wave elastography index (SWEI): a tool to differentiate between malignant and benign thyroid nodules: 15th

International Thyroid Congress and 85th Annual meeting of the American Thyroid Association (ATA), Lake Buena Vista, Florida, 2015, USA

Publications

1. **Baig, F.N.;** Liu, S.Y.W.; Lam, H.-C.; Yip, S.-P.; Law, H.K.W.; Ying, M. Shear Wave Elastography Combining with Conventional Grey Scale Ultrasound Improves the Diagnostic Accuracy in Differentiating Benign and Malignant Thyroid Nodules. Appl. Sci. 2017, 7, 1103.
2. **F.N. Baig,** J.T.J.v. Lunenburg, S.Y.W. Liu, S.-P. Yip, H.K.W. Law, M. Ying, Computer-aided assessment of regional vascularity of thyroid nodules for prediction of malignancy, Scientific Reports, 7 (2017) 14350
3. **Faisal N Baig**, Shea-Ping Yip, Helen KW Law, Michael Ying. AngioPLUS enhances the sensitivity of color flow imaging and directional color power imaging in assessing vascularity of thyroid gland (submitted to PLOS ONE)
4. **Faisal N Baig**, Helen KW Law, Shea-Ping Yip, Michael Ying. JWH-133 (Cannabinoid receptor 2 agonist) induces death in papillary cancer cell line (under preparation)
5. **Faisal N Baig**, Helen KW Law, Shea-Ping Yip, Michael Ying. Review: Update on ultrasound diagnosis of thyroid cancer (under preparation)

Acknowledgements

All praises to Almighty Allah Who bestowed me with knowledge and opportunities to complete this thesis.

My special thanks to Dr. Michael YING, my chief supervisor, for his continuous support, professional guidance, enthusiasm, motivation, and immense knowledge throughout my Ph.D. studies without whom this thesis was not possible.

My sincere gratitude to Dr. Helen K.W.LAW and Professor Shea-Ping YIP, my co-supervisors, for their kind help and invaluable suggestions to my study. Dr. Helen LAW trained me in cell culture technique and always kept me motivated. She was a big source of inspiration in completing my tasks throughout my Ph.D. studies.

My special thanks to Dr. Vincent W.C. Wu for his professional guidance in subject “Special Topic in Radiography” and for the provision of in-depth knowledge about radiotherapy of nasopharyngeal carcinoma patients. I would like to extend my gratitude to Dr. Shirley Y.W. Liu who helped us in recruiting patients and collection of data.

Thanks, are also extended to my colleague Jurgen TJ van Lunenburg who helped me in learning the MATLAB software and guided me during computational analysis of my data.

My sincere gratitude to my dearest friend Ali Majid, Waleed, and Rahim Rajwani for their advice, support, and encouragement.

I have to thank admission selection committee of The Hongkong Polytechnic University for accepting me as a Ph.D. candidate and provided me a chance to study at this prestigious institute.

In the last but not the least, I must say thanks to my loving parents, my siblings and my all other family members for their unfailing love, continuous support, and encouragement throughout my academic career.

Faisal Nouman Baig

Table of Contents

List of Figures

List of Tables

List of Abbreviations

AACE	American Association of Clinical Endocrinologists
AME	Associazione Medici Endocrinologi
AMPK	Adenosine Monophosphate-Activated Protein Kinase.
AngioPLUS	Angio Planewave UltraSensitive™ imaging
ARFI	Acoustic radiation force impulses
ATA	American Thyroid Association
ATC	Anaplastic thyroid carcinoma
ATF-6	Activating Transcription Factor 6
AUS	Area under study
CB1	Cannabinoid receptor 1
CB2	Cannabinoid receptor 2
CDU	Color Doppler Ultrasound
CEA	Carcinoembryonic antigen
CHOP	CAAT/enhancer binding protein C/EBP homologous protein
CNS	Central Nervous system
CT-scan	Computed Tomography scan
DNA	Deoxyribonucleic acid
E	Elasticity
ER	Endoplasmic Reticulum
ERK	Extracellular Receptor Kinase
ETA	European Thyroid Association
FDG	Flouro-deoxyglucose

FNAC	Fine needle aspiration cytology
FTC	Follicular thyroid carcinoma
GABA	Gamma Amino Butyric Acid
GSU	Grey-scale Ultrasound
HIF1	Hypoxia Inducible Factor 1
HIV	Human Immunodeficiency Virus
HSESC	Human Subject Ethics Sub-committee
I^-	Iodide
^{123}I	Iodine -123
IFP	Interstitial Fluid Pressure
K^+	Potassium Ion
keV	Kilo electron volt
kPa	Kilopascal
Li	Lithium
MAPK	Mitogen-Activated Protein Kinase
MHz	Mega Hertz
MTC	Medullary Thyroid carcinoma
MNG	Multinodular goiter
MRI	Magnetic resonance imaging
mTOR	Mammalian Target of Rapamycin
Na^+	Sodium Ion
NFV	Nelfinavir
NPV	Negative Predictive Value
PDU	Power Doppler Ultrasound
PET	Positron Emission Tomography
PPV	Positive Predictive Value
PTC	Papillary thyroid carcinoma
PNS	Peripheral Nervous System
PRF	Pulse Repetition Frequency
ROI	Region of interest

SE	Strain elastography
SEN	Sensitivity
SPE	Specificity
SPSS	Statistical Package for the Social Sciences (software)
SR	Strain ratio
SWE	Shear wave elastography
SWEI	Shear wave elastography index
$t_{1/2}$	half-life
$^{99m}TcO^-_4$	Technetium Pertechnetate
T_3	Triiodothyronine
T_4	Thyroxine
Tg	Thyroglobulin
TRIB3	Tribbles homolog 3
TRH	Thyroid-releasing hormone
TSH	Thyroid stimulating hormone
USE	Ultrasound elastography
USPSTF	US Preventive Services Task Force
VA	Valproic Acid
VEGF	Vascular endothelial growth factor
VI	Vascularity Index

Chapter One

Introduction

Thyroid cancer is the most common endocrine malignancy and accounts for 3.8% of all malignant cases (Nguyen et al., 2015). Diagnosis of thyroid cancer is critical and poses a challenge to medical professionals. Benign thyroid nodules are common, whereas 5% - 15% of thyroid neoplasms harbour malignancy (Veyrieres et al., 2012a, Brito et al., 2013, Guth et al., 2009). Among thyroid malignancies, papillary thyroid cancer (PTC) constitutes 80% - 85% of all differentiated thyroid malignancies (Abboud and Tannoury, 2010). Currently, the diagnosis of thyroid cancer relies on invasive techniques such as fine needle aspiration cytology (FNAC) and/or histopathological examinations of surgical sections of thyroid tissues (Haugen, 2016, Cooper et al., 2009). However, 25% - 30% of thyroid aspirates remain non-diagnostic and repeated cytology examinations are required (Yoon et al., 2011b). The potential reasons for inconclusive FNAC results might include inadequate sampling or ‘skipping’ of the diagnosis, due to the highly complex and variable pathological features of thyroid neoplasms.

The US Preventive Services Task Force (USPSTF), the American Association of Clinical Endocrinologists (AACE), the Associazione Medici Endocrinologi, and the European Thyroid Association (Cooper et al.,

2009, Gharib et al., 2010) emphasize that ultrasonography of the thyroid gland should be performed in all patients with clinically diagnosed or suspected thyroid nodules. Grey-scale ultrasound (GSU) can correctly identify malignant features of thyroid nodules such as microcalcification, absent halo sign, heterogeneity, irregular border, and a height-to-with ratio > 1 (Asteria et al., 2008, Ünlütürk et al., 2012). However, the sensitivity and specificity of GSU vary considerably, from 52% - 97% and from 26% - 83%, respectively (Sun et al., 2014b).

In our current study, we have established novel methods that, in conjunction with GSU, quantitatively assess elastic modulus and hemodynamic properties of thyroid nodules to differentiate them as benign or malignant. We have also determined the value of a new ultrasound technology, AngioPLUS (PLanewave UltraSensitive™ imaging), in conjunction with colour Doppler ultrasound and power Doppler ultrasound, in the detection of thyroid vascularity. These ultrasound imaging methods are objective, their results are highly reproducible, and they can therefore facilitate the diagnosis of thyroid disorders. In the study, we have further investigated the therapeutic potential of currently available non-cancer drugs as anti-cancer agents to broaden our understanding of the chemotherapeutic management of thyroid cancer.

In our first research study (Chapter 3), we have evaluated the feasibility of using the shear wave elastography index (SWEI: $E_{maximum}$,

E_{mean}, $E_{minimum}$) to quantify the elastic properties of thyroid nodules for distinguishing benign and malignant nodules. This study was based on the rationale that malignant thyroid nodules tend to be stiffer than benign thyroid nodules, and that this variation of tissue stiffness of the nodules can be evaluated and measured by shear wave elastography (SWE) (Dudea and Botar-Jid, 2015). Shear waves travel faster in harder medium than in softer counterparts, and their velocity is directly proportional to the square root of Young's modulus assuming homogeneous density of the medium (Kim et al., 2002, Papini et al., 2002). The tissue stiffness can thus be determined by tracking the speed of shear waves through the region of interest (ROI). Most malignant thyroid nodules, due to the presence of excessive collagen, excessive myofibroblasts, and desmoplastic transformation, tend to have firm stroma and thus tend to be harder (Dighe, 2014, Koperek et al., 2007, Sun et al., 2014b). In Chapter 3, we presented a comprehensive comparison of elastic properties of benign and malignant thyroid nodules, and a detailed investigation of the value of SWE in conjunction with GSU in the differential diagnosis of benign and malignant thyroid nodules.

Angiogenesis is considered an important manifestation in the proliferation and survival of tumours and is usually associated with malignancy (Gacche, 2015). Colour Doppler and power Doppler ultrasound are common imaging tools for the detection of vasculature in thyroid nodules. Previous studies have highlighted the importance of the usage of vascular patterns (central and peripheral vascularity) in thyroid

nodules as a determinant of malignancy; central and hypervascularity, for example, are frequently found in malignant thyroid nodules (Rosario et al., 2015, Anil et al., 2011). However, not all studies agree that vascular patterns of nodules are associated with thyroid malignancy, and some authors have suggested that vascularity and vascular distribution patterns are not useful for the prediction of thyroid malignancy (Moon et al., 2010, Khadra et al., 2016). Since vascularity is a dynamic feature, it should be quantitatively evaluated rather than using a non-standardized qualitative method (visual assessment). The advantages of using an objective method are that the results are more reproducible and that the risk of inter- and intra-observer variations is minimized. In the assessment of regional vascularity of thyroid nodules, there is a lack of standardized and objective methods to divide a nodule into peripheral and central regions. In previous studies, regional subdivision was performed manually and there were no standardized guidelines to delineate the border between peripheral and central regions of the nodule (Sultan et al., 2015). Chapter 4 presented a novel image processing method that can quantify regional vascular density of a thyroid nodule in Doppler ultrasound images to predict malignancy. Our method was based on a customized computer algorithm that uses an ‘offsetting’ principle to perform regional subdivision (into peripheral and central regions) and quantify the regional vascularity of thyroid nodules in Doppler ultrasound images. The method allowed objective and standardized quantification of thyroid nodule vascularity, and eliminated human errors associated with manual outlines of ROIs on Doppler

ultrasound images. The association between regional vascularity of thyroid nodules and thyroid malignancy, as well as the value of assessing thyroid nodule vascularity in conjunction with GSU in differentiating benign and malignant nodules, were presented in this chapter. To the best of our knowledge, this is the first study to use a customized algorithm to perform automatic segmentation of peripheral and central regions of thyroid nodules and to quantify their regional vascular density in Doppler ultrasound images.

Vascularity is an important feature required by any organ or biological tissue to maintain proliferation and homeostasis. Certain pathological conditions alter the blood flow to affected organ/tissue. Likewise, certain thyroid diseases, for example Grave's disease and acute thyroiditis, are associated with a hypervascular status of the thyroid gland (Arslan et al., 2000). In contrast, hypothyroidism and Riedel's thyroiditis cause reduced blood supply to the thyroid gland (Shrestha and Hennessey, 2015). Whether thyroid vascularity is a predictor of malignancy is a matter of debate and has led to controversial reports in the literature; however, hypervascular thyroid nodules with central vascularization raise the suspicion of malignancy (Hoang et al., 2007). In addition, tracking the vascularity status of an organ with the help of colour Doppler ultrasound or power doppler ultrasound during therapy might be a useful strategy to estimate the patient's response to the therapy. Angiogenesis (an essential manifestation of malignancy) involves the formation of several tiny new blood vessels. Detection of blood vessels

with very small diameter (< 100 μm) or blood flow at a very low poses a challenge (due to low frame rate and slow wall filtering) to previously developed CDU and PDU (Bercoff, 2011). Therefore; there is a need for new imaging modalities that can depict microvasculature with higher sensitivity. In our third study (Chapter 5), we have comprehensively investigated the value of AngioPLUS in conjunction with colour Doppler and power Doppler ultrasound in the detection of thyroid vascularity in a group of healthy volunteers. The study demonstrated the potential of AngioPLUS in enhancing the sensitivity of colour Doppler and power Doppler ultrasound in the detection of the vasculature of thyroid glands. The study also compared the vascularity of the left and right thyroid lobes. This is the first study that investigated the added value of AngioPLUS in colour Doppler and power Doppler ultrasound examinations. The result of the study provided novel insights into the detection of micro-vasculature of soft tissues.

Drug discovery is a long process and is associated with a financial burden due to various complexities regarding drug regulation and approval. Currently, surgery is the ultimate option for the management of thyroid cancer. The role of chemotherapeutic drugs in treating thyroid cancer is very limited. Our fourth study (Chapter 6) introduced the concept of ‘drug repositioning’ and evaluated the therapeutic potential of using non-cancer drugs as anti-cancer agents in treating papillary thyroid cancer. Cannabinoids (e.g. Nabilone) have been approved for medical use in patients with cancer in Canada by the Canadian Cancer Society

(Kramer, 2015) to alleviate chemotherapy-related symptoms (e.g. nausea and pain). Chapter 6 presented an *in vitro* study in which a normal thyroid follicular cell line (N-thy-ori-3) was used as the control and a PTC cell line (BCPAP) was used to investigate the anti-cancer effect of a member of the group of cannabinoid agonist type 2 receptors (CBR2) called JWH-133. We hypothesized that CBR2 can induce cancer cell death by inducing endoplasmic stress while the survival of normal thyroid follicular cells can be maintained at an acceptable level. The findings of this study shed light on the potential of non-cancerous drugs in treating cancer.

Chapter Two

Literature Review

2.1 The thyroid gland

The word ‘thyroid’ is derived from the Greek word ‘thyreos’ meaning ‘shield’. It was first described by Thomas Wharton in 1656 (Balasubramanian, 2015). The thyroid gland is the largest endocrine gland in the body and it works in coordination with other organs to maintain homeostasis (Greenspan and Gardner, 1997).

2.1.1 Embryology and histology of the thyroid gland

The thyroid is the first endocrine gland to develop in the embryo. The development of the thyroid gland initiates around 24 days post fertilization by the fusion of the median endoderm (at the junction of the base of the tongue) and the primitive pharynx called ‘thyroid primordium’ (Figure 2.1a). With the development of the tongue, the growing thyroid descends into the neck and passes ventrally to the developing hyoid bone and the laryngeal cartilages (Figure 2.1b). When approaching the seventh week of gestation, the thyroid gland reaches its destination in the neck and adopts its definitive shape. Finally, at the tenth week of gestation, the thyroid primordium is surrounded by vascular

mesenchyme and splits into numerous follicles lined by an epithelial monolayer (Sofferman and Ahuja, 2011).

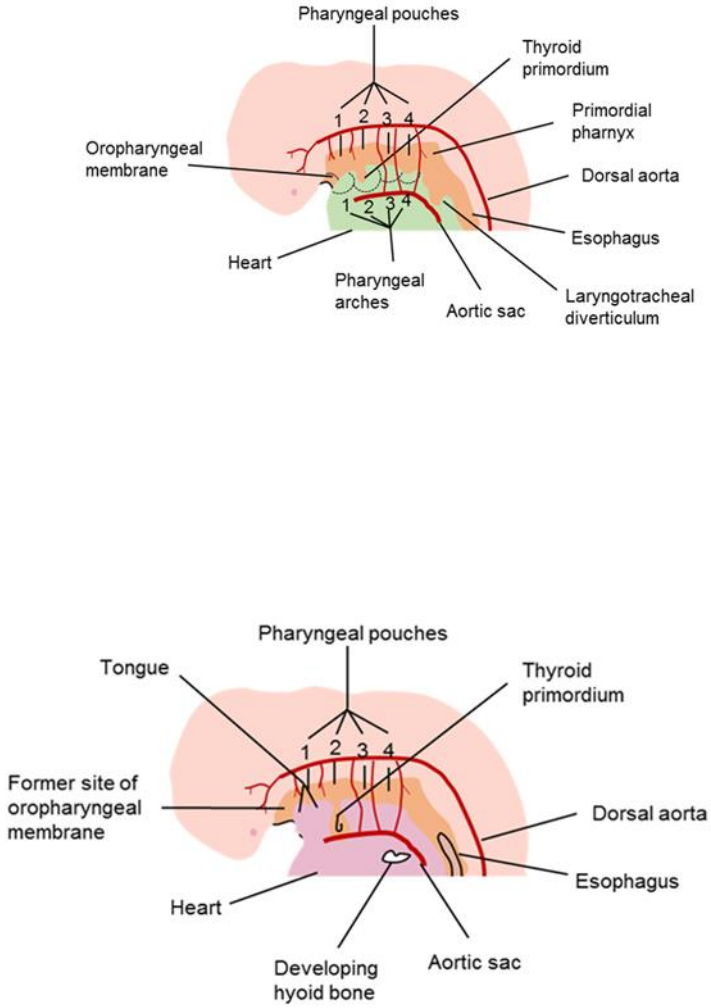

Figure 2.1 Sagittal sections (A and B) of the head and neck of embryos at 4th and 5th week of gestation. (A) illustrates the developing thyroid gland as “Thyroid primordium” arising from 1st and 2nd pharyngeal pouches (B) Illustrates passage of descent of thyroid. Figures are amended and redrawn, the concept originated from Moore et al. (2000).

The thyroid gland is composed of follicles. Follicles are spherical cells filled with thyroglobulin (iodinated glycoprotein), and each follicle is about 200 - 300 micron in diameter (Moore et al., 2000). Follicles absorb iodine from blood in the form of Iodide (I^-), and the absorbed iodine is used for the synthesis and storage of thyroid hormones (Carrasco, 1993). Follicles are grouped in the form of 'lobules' and are nourished by an 'end artery' (McDougall, 2013). Parafollicular cells are scattered around the follicular cells and secrete a linear polypeptide hormone called 'calcitonin' that is involved in the metabolism of calcium and phosphorus in the human body (Fujimori et al., 2013).

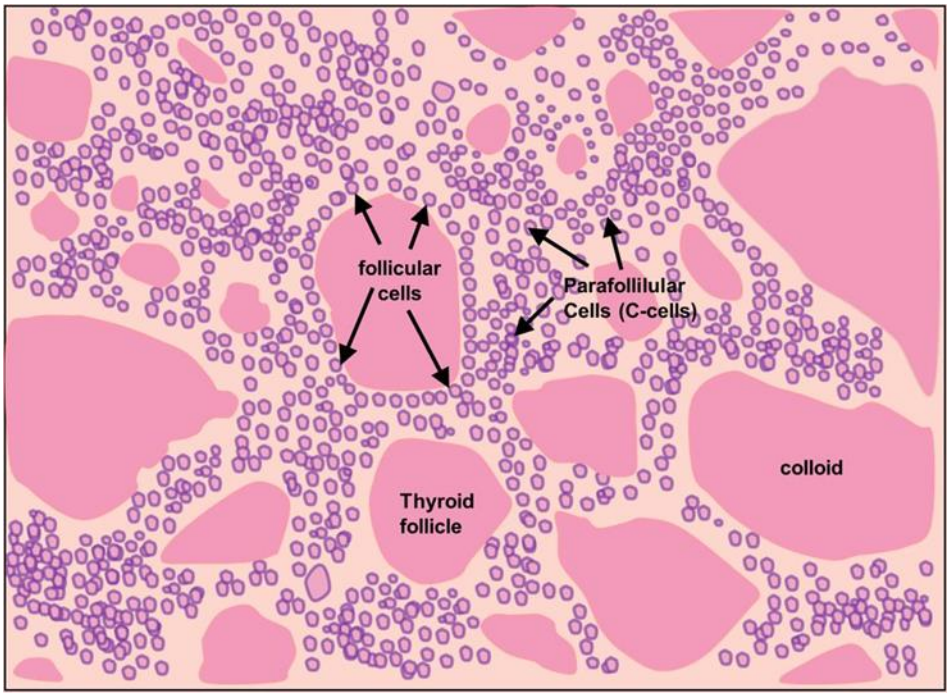

Figure 2.2 Schematic illustration of histological features of the normal thyroid gland.

2.1.2 Anatomy of thyroid gland

The thyroid is a soft, red-coloured, butterfly-shaped endocrine gland located in the anterior neck. The gland is in the anterior neck behind the platysma, the sternohyoid, and the sternothyroid muscles and extends from the sixth cervical vertebra to the first thoracic vertebra. It weighs around 15 - 25 g in adults (Imam, 2016).

The thyroid gland has two lobes on each side of the neck that are interconnected by a thin slice of thyroid tissue, called isthmus, at the level of the second, third, and fourth tracheal rings. Medially, the trachea and the oesophagus are bound to each thyroid lobe. Sternocleidomastoid and strap muscles (superior belly of the omohyoid, sternothyroid, and sternohyoid) lie anterolaterally, while the carotid sheath, containing the common carotid artery, the internal jugular vein, and the vagus nerve, is located posterolaterally to the thyroid gland (Stewart and Rizzolo, 2012).

The pyramidal lobe is a small projection that arises from the isthmus and extends upward towards the left of the midline. The pyramidal lobe is present in 15% - 75% of patients with thyroid diseases (Sinos and Sakorafas, 2015). In addition to its own capsule, the thyroid gland is also unsheathed by the pretracheal fascia that attaches posteriorly to the ‘cricoid cartilage’ and the ‘suspensory ligament of Berry’ to facilitate upward and downward movements of the gland during deglutition.

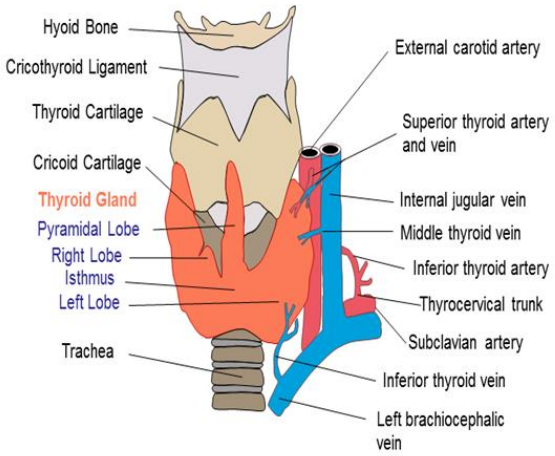

Figure 2.3.1 Anatomical relations and blood supply of thyroid gland

The red appearance of the thyroid gland owes to its rich blood supply. The superior thyroid artery (a branch of the external thyroid artery) descends bilaterally to reach the superior pole of each thyroid lobe. It runs parallel to the external laryngeal nerve, pierces the thyroid fascia, and gives off anterior and posterior branches. The anterior branch of the superior thyroid artery bathes the anterior aspect of the thyroid gland and the posterior branch supplies to the medial and lateral regions of the gland. The inferior thyroid artery branches from the thyrocervical trunk which is originated from the subclavian artery. The inferior thyroid artery crosses the carotid sheath and reaches the middle and inferior poles of the thyroid gland, where the artery gives off superior and inferior branches and supplies to the posterior and inferior regions of the thyroid gland. A small fraction (3% - 10%) of the general population, show an uncommon variant of blood vessels called ‘thyroid ima artery’. The thyroid ima artery is an unpaired, persistent embryonic vessel and has various origins including the subclavian artery, the inferior thyroid artery, the aortic arch, the brachiocephalic trunk, and the common carotid artery. The artery ascends along the anterior surface of the trachea to reach the isthmus of the thyroid gland. The presence of ima artery must be noted while performing thyroidectomy or tracheostomy, as it is a potential source of heavy bleeding during surgery (Youn et al., 2014).

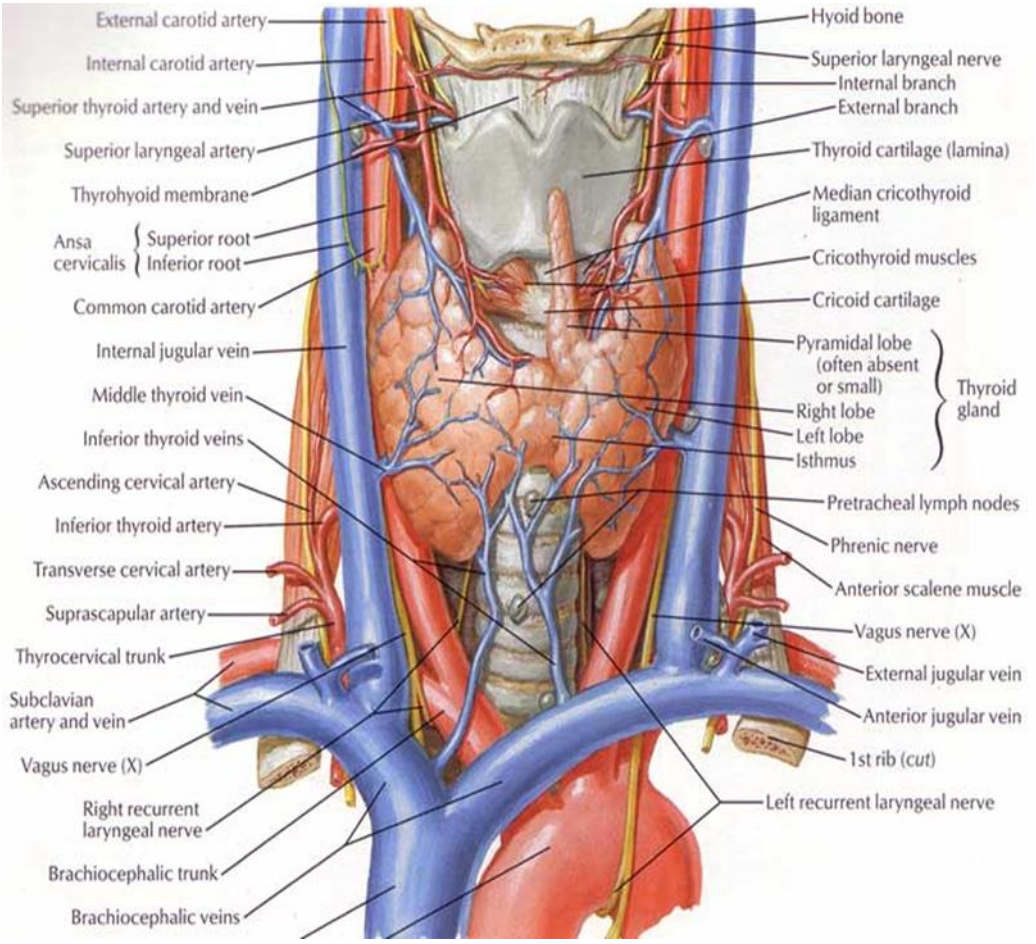

Figure 2.3.2 Gross Anatomy of the thyroid gland and its anatomical relations (Netter, 2014)

The thyroid venous plexus is a composite of the superior, middle, and inferior thyroid veins, and is located on the anterior surface of the thyroid gland. The superior thyroid vein runs along with the superior thyroid artery. It emerges from the upper pole of the thyroid gland and drains into the internal jugular vein. The middle thyroid vein drains the lateral aspect and inferior surface of the thyroid gland. Like the superior thyroid vein, the middle thyroid vein drains into the internal jugular vein. There are about three to four inferior thyroid veins, and they originate from the venous plexus of the thyroid gland. Inferior thyroid veins drain directly into the brachiocephalic veins (Kanani et al., 2014).

Lymphatic drainage of the thyroid gland is extensive and multidirectional, as it bathes the interlobular connective tissues first and then proceeds to the prelaryngeal, pretracheal, paratracheal, and mediastinal lymph nodes. Some lymphatic vessels drain into the brachiocephalic lymph nodes and the deep cervical nodes, whereas others drain directly (without involving lymph nodes) into the thoracic duct (Youn et al., 2014).

The nerve innervation of the thyroid gland is derived from both the sympathetic and the parasympathetic nervous system. Sympathetic distribution involves superior, middle, and inferior cervical sympathetic ganglia. They cause vasoconstriction of blood vessels. Parasympathetic

fibres arise from the vagus nerve. The right vagus nerve gives rise to the right recurrent laryngeal nerve, which circles around the subclavian artery and ascends to the right lobe of the thyroid gland. The left vagus nerve branches into the left recurrent laryngeal nerve, which circles around the aortic arch and traverses posteriorly to reach the left lobe of the thyroid gland (Mizrachi et al., 2015).

2.1.3 Synthesis of thyroid hormones

The thyroid gland synthesizes and secretes two important hormones; thyroxine (T_4) and triiodothyronine (T_3). The synthesis of thyroid hormones (TH) involve various steps (Mullur et al., 2014, Braverman and Cooper, 2012).

1st step: Iodide uptake by thyroid follicular cells by means of 'active transport', utilizing a Na^+ / I^- symporter.

2nd step: Oxidation of Iodide to Iodine by NADPH-dependent thyroperoxidase (TPO) enzyme in the lumen of thyroid follicles.

3rd step: Binding of oxidized iodine with thyroglobulin tyrosine to form iodotyrosine.

4th step: Monoiodotyrosine and diiodotyrosine are coupled to form T_3 and T_4.

After synthesis, thyroid hormones are stored in the colloid of thyroid follicles. Hormonal release from the thyroid gland is auto-regulated by the hypothalamus-hypophysis-thyroid axis. Low levels of thyroid hormone in circulation stimulate the hypothalamus to release thyroid releasing

hormone (TRH), that is synthesized and taken to the frontal lobe of the hypophysis via portal circulation to stimulate the release of thyroid stimulating hormone (TSH). TSH is then secreted into the blood stream and is taken to the thyroid gland for synthesis and secretion of T_3 and T_4. The effect of TSH and TRH is controlled by a negative feedback system in which higher levels of T_3 and T_4 decrease the secretion of TSH and optimum levels of thyroid hormone are restored (McKerns, 2013).

2.1.4 Functions of thyroid hormones

Thyroid hormones are essential in the human body, and they play important functional roles in the body metabolism (Mullur et al., 2014, Christiansen et al., 2007).

1. Thyroid hormones accelerate the basal metabolic rate of the body which increases oxygen utilization and general thermogenesis.

2. Thyroid hormones speed up cardiac output and heart rate by increasing the β-adrenergic count without affecting catecholamine secretion.

3. Thyroid hormones stimulate several metabolic activities. In case of lipid metabolism, plasma fatty acid concentrations are directly related to the levels of thyroid hormone concentrations in peripheral blood circulation. Thyroid hormones facilitate the oxidation of fatty acids in body tissues (Pucci et al., 2000). Serum concentrations of triglycerides and cholesterol are inversely proportional to thyroid hormone levels in plasma. In carbohydrate metabolism, thyroid hormones promote

gluconeogenesis and glycolysis to liberate free glucose and enhance insulin-dependent glucose entry into the cells (Sinha et al., 2014). At desired physiological concentrations, thyroid hormones stimulate the synthesis and degradation of proteins into amino acids (Müller and Seitz, 1984).

4. Thyroid hormones potentiate the effects of insulin and epinephrine, and therefore increase the secretion of growth hormones.

5. Thyroid hormones are essential for the pre- and post-natal development of the brain. Thyroid hormones play an important role in myelinization of the nerves. Deficiency of thyroid hormones during the foetal period causes, for example, mental retardation, retardation in deep reflexes, and cerebral hypoxia.

2.2 Thyroid nodules and thyroid cancer

Thyroid nodules constitute abnormal growth in the thyroid parenchyma, and may represent thyroid heterogeneity due to genetic and epigenetic involvement (Sofferman and Ahuja, 2011). Thyroid nodules are detected in 3% - 7% of the general population by 'palpation' (Tunbridge et al., 1977), whereas 20% - 76% of thyroid nodules are found by grey-scale ultrasound and in autopsy records (Feng et al., 2012, Ross, 2008). Thyroid nodules at an estimate of 20% - 48% are incidentalomas which are found incidentally with or without clinical symptoms (Tan and Gharib, 1997). Incidental thyroid lesions are commonly found on ultrasound, computed tomography (CT), magnetic resonance imaging (MRI) (Shetty et al., 2006), and ^{18}F-flourodeoxy-glucose positron emission tomography (PET) (Choi et al., 2006), performed for unrelated medical reasons.

Most thyroid nodules are benign, whilst 5% - 15% of nodules are malignant (Ali et al., 2013, Krátký et al., 2014, Ciledag et al., 2016, Hussein et al., 2013). Thyroid nodules are frequently found in elderly people and in individuals with iodine deficiency. They are more common in females than males (4:1). Other risk factors involved in the development of thyroid nodules include an iodine-deficient diet, an irradiation treatment history in childhood for cancers such as lymphoma, Wilms tumour, or neuroblastoma, a family history of thyroid cancer, a history of Hashimoto's disease, environmental chemicals (e.g.

thiocyanate, lithium), drugs (e.g. aniline derivatives, thionamides), flavonoids, and various chemical carcinogens (e.g. thiamine compounds, aminotriazole, nitrosamine, oxydianiline, methylene benzylamine, etc.) (Salabe, 2001).

Thyroid cancer is the most common endocrine malignancy and accounts for 2% - 3% of all cancers. The prevalence of thyroid cancer is 3 - 4 times higher in females than in males. A recent study claimed that over 77% of all patients with thyroid cancer worldwide are female (Kitahara and Sosa, 2016). More than 95% of thyroid cancer cases are differentiated carcinomas (originated from thyroid follicles and with the ability to concentrate iodine). Papillary thyroid carcinoma (PTC) and follicular thyroid carcinoma (FTC) are classified as differentiated thyroid carcinoma. PTC alone constitutes 80% to 85% of all thyroid malignancies and is the most common form of thyroid malignancy, with a relatively better prognosis than other types of thyroid cancer. FTC represents 10% to 15% of all thyroid malignancies. Under the microscope, follicular thyroid carcinoma resembles the microscopic features of the normal thyroid gland. Although FTC is a well-differentiated carcinoma, it is overtly or minimally infiltrating and has the potential to spread to distant organs via the blood stream. FTC is a slow-growing carcinoma and has a favourable prognosis, with a mean mortality rate of 1.5% in females and 1.4% in males. Lymphatic involvement is rare in FTC and the mean survival rate is < 60% after 10 years of first occurrence (Sobrinho-Simoes et al., 2011).

Anaplastic carcinoma (1% - 2% of all thyroid malignancies) is classified as undifferentiated or poorly differentiated thyroid carcinoma, and has a much worse prognosis than any other form of thyroid cancer. Anaplastic carcinomas arise from the follicular cells and present with rapidly growing mass in older people. Patients usually present with advanced stages of the cancer where surgery is inappropriate and external radiation beam therapy or intensive modulated radiation therapy with or without concurrent chemotherapy are the preferred therapeutic options (Gharib et al., 2016).

Medullary thyroid carcinoma (MTC) originates from parafollicular cells (C-cells) that are involved in the synthesis of calcitonin. MTC constitutes 2% - 3% of thyroid malignancies and has a poor prognosis. Cervical lymph node metastasis is common. An elevated level of serum calcitonin or carcinoembryonic antigen (CEA) may help to establish the diagnosis. Total thyroidectomy is the standard treatment for MTC. The 10-year survival rate of patients with MTC is 75%. The prognosis is poorer than that for PTC and FTC but better than that for ATC (Bomford et al., 1993).

Table 2.1 List of high-risk factors for thyroid malignancy (Gharib et al., 2016)

High-risk factors for thyroid malignancy
1. Male sex 2. Age less than 14 years or greater than 70 years 3. Irradiation history 4. Consistency: firm or hard; fixed not movable 5. A persistent cough not related to cold, dyspnoea /dysphonia/dysphagia

Table 2.2 List of common causes for the development of thyroid nodule (Pacini)

Common causes for thyroid nodule development
1. Anaplastic carcinoma 2. Benign nodule/goiter 3. Chronic lymphocytic thyroiditis 4. Follicular adenomas/carcinomas 5. Haemorrhagic cyst 6. Hürthle cell carcinoma 7. Medullary thyroid carcinoma 8. Papillary thyroid carcinoma 9. Primary lymphoma 10. Sarcoma/Teratoma

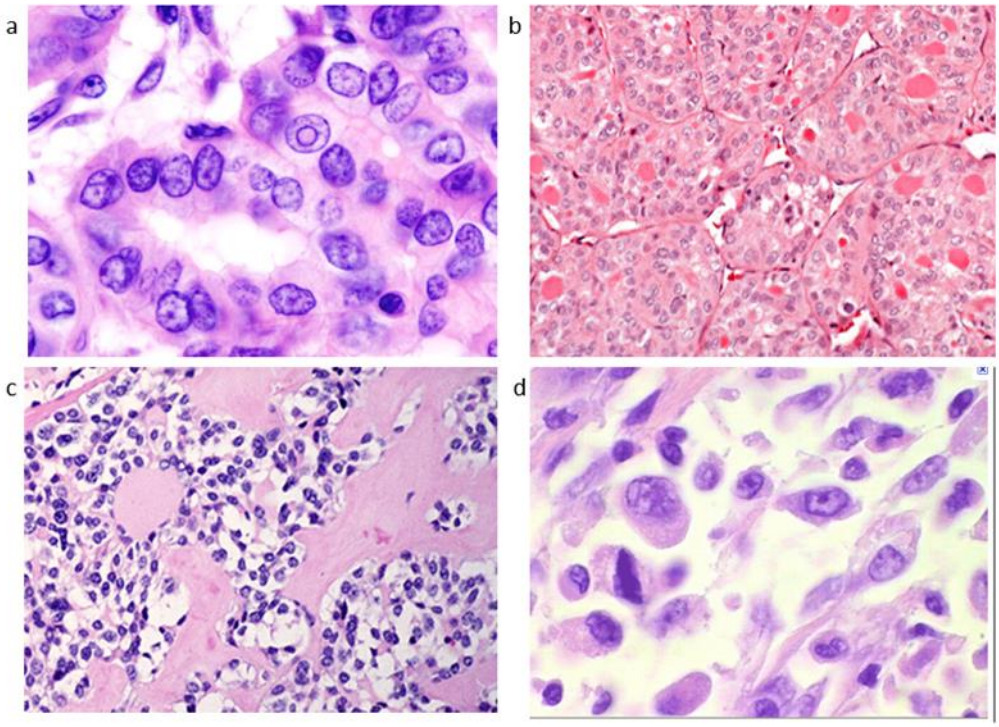

Figure 2.4 Histological features of (a) Papillary thyroid cancer; illustrating orphan annie eye and Psammoma bodies (b) Follicular thyroid carcinoma; showing capsular/vascular invasion (c)Medullary thyroid carcinoma; featured amyloid deposition (d) Anaplastic thyroid cancer; pleiomorphic giant tumor cell nuclei. Source: http://www.thyroidmanager.org/chapter/thyroid-cancer/

Thyroid cancer, Furio Pacini, Professor of Endocrinology, Director, Section of Endocrinology and Metabolism University of Siena, Siena, Italy.

2.2.1 Diagnostic approaches for thyroid cancer

2.1.1 Signs and symptoms

The presence of an unusual lump or swelling near the Adam's apple is the most common sign of thyroid cancer. In most cases, the lump is painless. However, pain over the anterior aspect of the neck and radiating to the ears is suspicious for thyroid cancer. Rapidly growing thyroid nodules also raise suspicion of thyroid malignancy and demands immediate investigation. Changes in the voice or hoarseness that are not relieved with medication may also be suggestive of thyroid cancer. Patients with thyroid cancer may present with difficulties in breathing or complaints of a persistence cough that is not related to the cold. In few cases, thyroid nodules may cause difficulties in swallowing (Bomford et al., 1993, Nix et al., 2005).

2.2.1.2 Palpation

Palpation is one of the physical examination methods that is commonly performed for patients with suspected thyroid nodules. Palpation can be used to assess the texture (e.g. solid, cystic) and consistency (firm/mobile) of thyroid nodules. Based on the mechanical properties of soft tissues, palpation methods can differentiate between soft and hard nodules. Moreover, the mobility or fixity of the nodule can be determined. Malignant thyroid nodules tend to appear hard on palpation (Gharib et al., 2010). Palpation is sensitive for assessing large and superficial thyroid lesions but not for small and deeply situated thyroid nodules. In addition, small malignant thyroid lesions are often

devoid of suspicious features of palpation, such as hardness and fixed nodules, compared to larger malignant nodules (Tan et al., 1995). Therefore, palpation may not be useful for assessing smaller thyroid nodules. In addition, the accuracy of palpation also depends on the experience of the examiner. The sensitivity, specificity, and diagnostic accuracy of palpation in assessing thyroid nodules are 63%, 67%, and 65%, respectively (Kharchenko et al., 2010).

Because of the limited accuracy of palpation in assessing thyroid nodules, the American Association of Clinical Endocrinologists (AACE), the Associazione Medici Endocrinologi (AME), and the European Thyroid Association (ETA) suggest that all palpable thyroid nodules or clinically suspicious thyroid nodules should be evaluated with GSU (Gharib et al., 2016).

2.2.1.3 Blood test

During routine clinical practice, a serum blood test to detect changes in thyroid hormone levels to rule out thyroid malignancy is not performed (Andersen et al., 2002). However, increased serum levels of calcitonin and carcinoembryonic antigen (CEA) are common predictors of MTC (Barbet et al., 2005). Serum levels of thyroid hormones, such as free thyroxine (T4), triiodothyronine (T3), and thyroid stimulating hormone (TSH) are usually performed to determine physiological functioning of the thyroid gland (DAVIES, 2017). Depending upon the stage of the thyroid cancer, most thyroid cancers are found to be

euthyroid (Hwang et al., 2016). However, abnormal thyroid hormone levels do not exclude the risk of malignancy and should be correlated with other clinical investigations.

2.2.1.3.1 Thyroid function test

Measurements of serum TSH should be the first step in evaluating physiological functions of the thyroid gland. The reference values for normal serum TSH levels, free T4, and free T3 range between 0.5 and 6 uU/ml, 0.7 and 1.9 ng/dl, and 230 and 619 pg/d, respectively. However, the reference values used to detect normal thyroid hormone function vary among different laboratories. A chronic increase in TSH levels raises the risk of thyroid cancer (Haymart et al., 2008), whereas TSH levels below the normal physiological range are associated with lower risks of papillary thyroid cancer (Fiore et al., 2009).

2.2.1.3.2 Serum thyroglobulin levels

Serum levels of thyroglobulin (Tg) are measured before, during, and after thyroidectomy to detect recurrence of cancer or identification of residual tumour cells after surgery. Ideally, thyroglobulin levels should be very low or undetectable after thyroidectomy followed by radioiodine treatment. Persistent detection of thyroglobulin indicates recurrence of thyroid cancer (Spencer et al., 1999).

2.2.1.4 Fine needle aspiration cytology (FNAC)

FNAC is a minimally invasive, cost-effective, and current standard method to characterize thyroid nodules. Fine needle aspirates may be reported as benign (e.g. colloid nodule, hyperplastic nodules, cystic lesions, lymphocytic or granulomatous lesions), malignant (ATC, MTC, FTC, or PTC), non-diagnostic (poor cellularity and/or poor fixation of specimen), or as follicular lesions (e.g. Hürthle cell neoplasm and follicular variants of PTC) (Perros et al., 2014, Yoon et al., 2011b). FNAC is commonly performed by endocrinologists because they have the necessary skill to palpate the nodule and can perform adequate sampling (Veyrieres et al., 2012a). Nevertheless, FNAC yields a wide range of sensitivity (54% - 94%) and specificity (60% - 98%) in the diagnosis of thyroid cancer (Cantisani et al., 2015, El Hennawy et al., 2013, Luck et al., 2017). Due to the high complexity of cellular features, there is a greater likelihood of skipping diagnosis in histology-proven 'non-diagnostic' nodules (Cantisani et al., 2015).

Ultrasound-guided fine needle aspiration cytology (FNAC) has played a vital role in the assessment of thyroid nodules. In comparison with palpation-guided FNAC, ultrasound-guided FNAC has significantly decreased the numbers of inadequate sampling or false-negative aspirates due to the appropriate selection of suspicious areas of the nodule that resulted in a reduction of unnecessary surgeries. The reported sensitivity, specificity, positive predictive value, negative predictive value, and diagnostic accuracy of ultrasound-guided FNAC are

96.7%, 85.9%, 76.6%, 98.2%, and 89.4%, respectively (Yoon et al., 2011a).

Nodule selection for FNA biopsy

Most recent guidelines for the selection of a nodule to perform FNAC are provided by the AACE/AME/ETA thyroid nodule guidelines 2016 (Gharib et al., 2016) (Figure 2.7). A thyroid nodule should receive FNAC if it meets one of the following criteria:

1) Solid and hypoechoic on GSU, and diameter > 1.0 cm.
2) Extra thyroidal extension or cervical lymph node involvement; nodule of any size.
3) Previous history of neck irradiation; family history of PTC or MTC; nodule of any size.
4) GSU feature involvement (microcalcification, height-to-width ratio > 1, irregular border or hypoechogenicity); suspicious of malignancy highly increases if more than one GSU features are found; nodule size > 10 mm.
5) Incidentaloma discovered on CT-scan or MRI should be evaluated with GSU before FNA is suggested.
6) Incidentaloma discovered on ^{18}F-flourodeoxy glucose carry a high risk of malignancy and should be evaluated by GSU and ultrasound-guided FNA.

7) Specimen should only be collected from a solid component of the nodule facilitated by ultrasound-guided FNA when complex (solid-cystic) nodules are encountered.

8) In the case of multinodular goitre (MNG), if cervical lymph node involvement is evident, then a biopsy is indicated for both nodules.

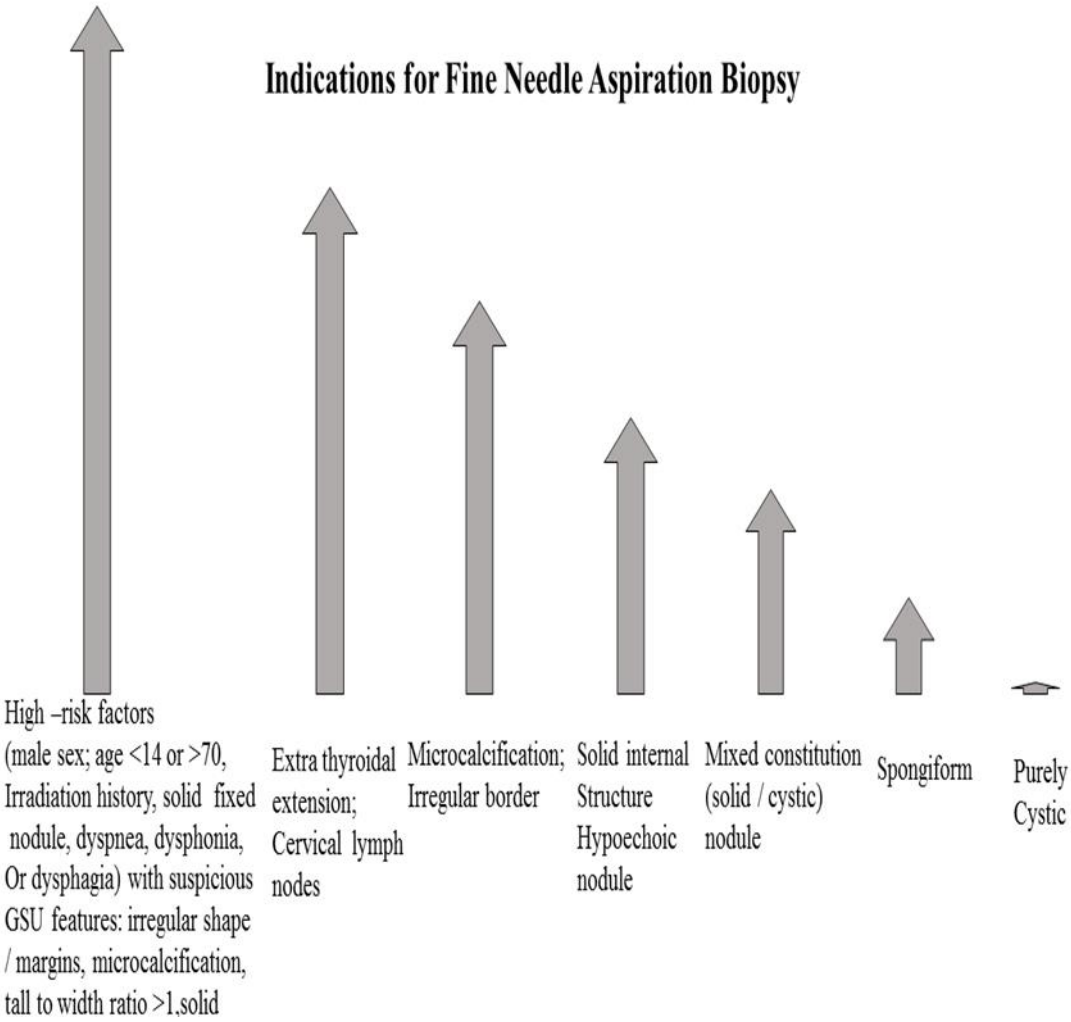

Figure 2.6 Illustration of guidelines to perform fine needle aspiration biopsy on thyroid nodules. Concept based on information provided in the guidelines of AACE/AME/ETA (Gharib et al., 2016)

2.2.1.5 Medical imaging techniques for thyroid assessment

2.2.1.5.1 Scintigraphy

The primary role of thyroid scintigraphy is to differentiate hot and cold thyroid nodules based on the uptake of radioactive tracers (Iodine-123 and Technetium-99m pertechnetate), compared to extranodular tissue uptake (Van Nostrand et al., 2016). A cold thyroid nodule has a reduced tracer uptake, and a hot nodule has an increased tracer uptake. In common clinical practice, more than 85% thyroid nodules appear 'hot' and are classified as benign, whilst up to 15% of cold nodules are malignant. However, it must be noted that not all 'cold' nodules are malignant and vice versa (Treglia et al., 2013). Iodine-123 (^{123}I) and Technetium-99m (^{99m}Tc) pertechnetate are the common radioactive tracers for thyroid scintigraphy. The American Thyroid Association (ATA) guidelines (2015) recommend the use of ^{123}I over ^{99m}Tc pertechnetate, because of the high resolution and image quality and a reduced radiation burden associated with the former tracer. (Haugen, 2016) However, the European Association for Nuclear Medicine suggests that both ^{123}I and ^{99m}Tc pertechnetate are useful for thyroid scintigraphy (Verburg et al., 2016).

In comparison to ^{99m}Tc pertechnetate, ^{123}I is expensive and not readily available. In contrast, ^{99m}Tc pertechnetate is available at a low price and has an uptake similar to that of ^{123}I. Moreover, it takes comparatively less time (10 - 20 minutes) after intravenous injection of ^{99m}Tc pertechnetate for the tracer to concentrate in the thyroid and thus

for the subject to be ready for imaging. The uptake time of ^{123}I is longer and imaging must therefore be delayed for almost 24 hours (Ramos et al., 2002). Altogether, these factors have made ^{99m}Tc pertechnetate the radioactive tracer of choice for assessing the functional characteristics of the thyroid gland. However, it should be noted that ion organification is absent with ^{99m}Tc pertechnetate, and that it can therefore not replace ^{123}I in cases where iodide organification is required, such as for example dyshormonogenic hypothyroidism and organification defects in autoimmune chronic thyroiditis (Harbert et al., 1996, Agrawal et al., 2015)

Table 2.3 Characteristics of Radiopharmaceuticals Used in Thyroid Imaging (Agrawal et al., 2015, Van Nostrand et al., 2016)

	^{99m}Tc-Pertechnetate	^{123}I-Iodide
Physical half-life ($t_{1/2}$)	6 h	13.2 h
Photon energy	140 keV	159 keV
Beta emission and energy	No	No
Mechanism of uptake	Trapped by the thyroid	Trapped and organified
Advantages	Easily available Less expensive Quicker examination Low radiation burden	Good for visualization of retrosternal tissue Better image quality Low radiation burden
Disadvantages	No organification Poor image quality when uptake is low Not good for retrosternal mass characterization	Less readily available Relatively expensive Delayed imaging at 24 hours is required Higher radiation burden compared with ^{99m}Tc-pertechnetate

Normal Thyroid Scan

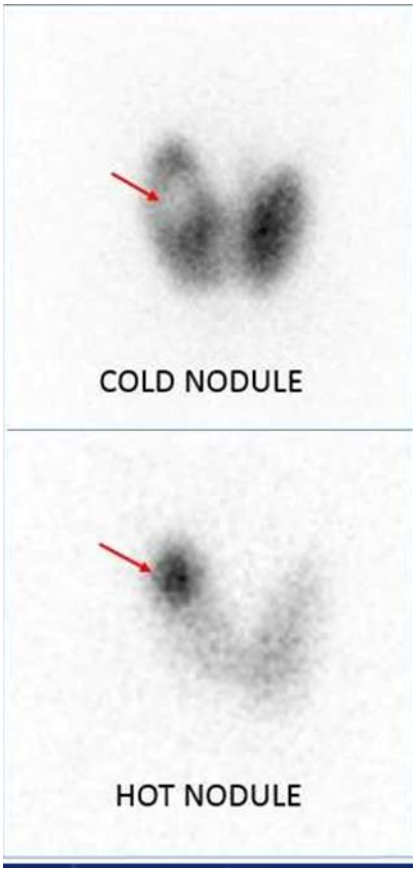

Figure 2.7.1 Thyroid scintigraphy with ^{123}I (Ain and Rosenthal, 2010)

2.2.1.5.2 Positron Emission Tomography (PET)

PET is promising imaging technique with benefits of higher spatial resolution and quantitative measurements of metabolic activities compared to gamma camera.^{18}F-fluorodeoxyglucose (FDG) is a PET radiotracer which targets glucose metabolism in tumors (Lin and Iagaru, 2010). Most of the thyroid cancer are differentiated thyroid cancer such as papillary thyroid carcinoma (PTC) and follicular thyroid carcinoma (FTC) altogether constitutes up to 95% of all thyroid malignancies. Differentiated thyroid cancer, recurrent tumors, and metastatic cancer have slow growth rate and consume more glucose than normal body tissue and this makes the best strategy of using ^{18}F-FDG in diagnosing recurrent and metastatic differentiated thyroid cancer (Haslerud et al., 2016). In complicated cases, where the tumor is undetected on scintigraphy after thyroidectomy and recurrence are suspected due to the persistent elevated level of thyroglobulin, ^{18}F-FDG-PET can help to identify cancer cells on the basis of high glucose metabolic rate (Wimmer and Pichler, 2016). A meta-analysis by Dong et al. (2009) evaluated 571 patients with metastatic or recurrent differentiated thyroid carcinoma and found that ^{18}F-FDG was effective in diagnosing metastatic thyroid lesions with elevated TSH levels. The pooled sensitivity and specificity of the study was 84% for both diagnostic parameters (Dong et al., 2009). Another study suggested a change in TNM staging due to the ^{18}F-FDG results in 21% of the patients. The authors suggested that ^{18}F-FDG should be established as an initial-stage modality in high-risk patients with differentiated thyroid carcinoma (Rosenbaum-Krumme et al., 2012)

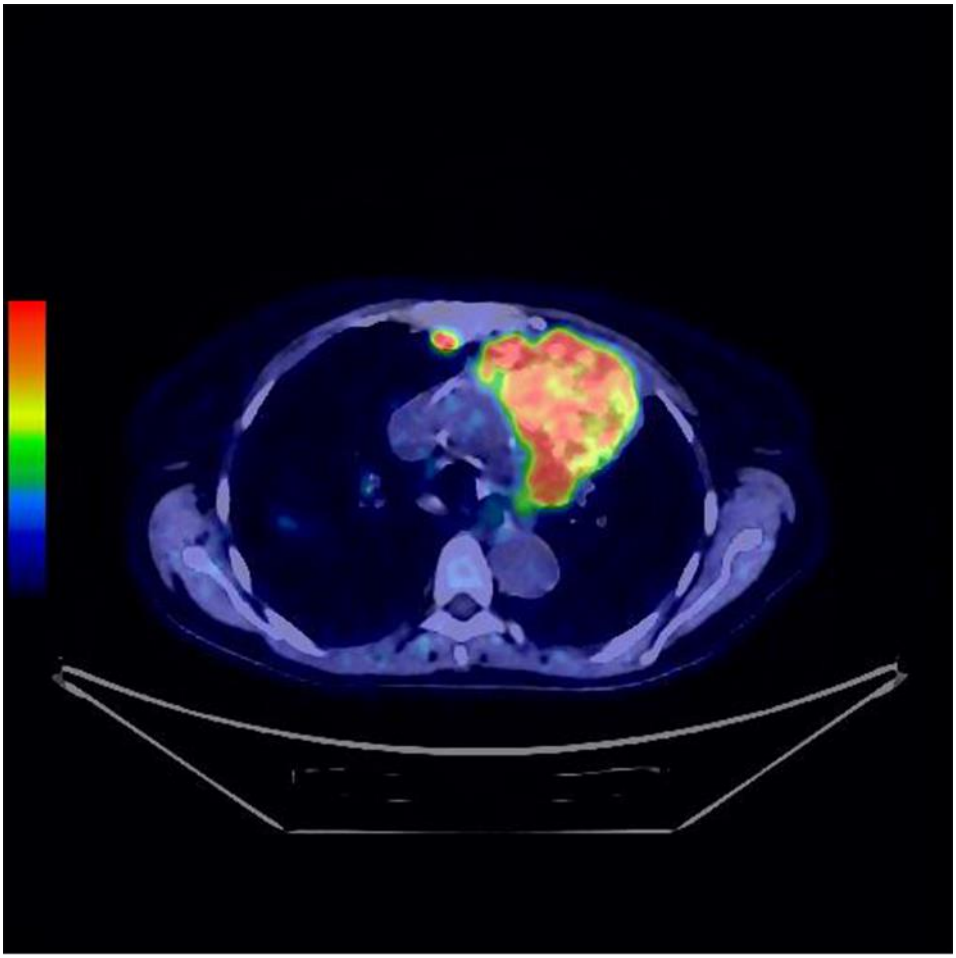

Figure 2.7.2 ^{18}F-FDG -PET scan of medullary thyroid carcinoma (Wimmer and Pichler, 2016)

2.2.1.5.3 Computed tomography (CT)

CT scans provide important information regarding the local extension of cancer or the presence of mass effect, and they are useful in evaluating recurrent disease. Furthermore, CT examination plays a crucial role in preoperative surgical planning for patients with symptomatic goitre (Saeedan et al., 2016).

CT features of benign and malignant thyroid nodules are not well established, compared to grey-scale ultrasound. Ill-defined margins and extrathyroidal extension such as lymph node involvement or invasion to surrounding thyroid parenchyma are suspicious features of malignancy on CT scans of thyroid nodules. However, the absence of these features does not eliminate the risk of malignancy (Weber et al., 2000).

One recent study suggested that the most common CT features for PTC were taller-than-wide shape and homogenous low attenuation. The author of the study further concluded that the degree of enhancement (sensitivity 84.5%, specificity 47.8%), the pattern of enhancement (sensitivity 81.9%, specificity 58.7%), and ill-defined margins (sensitivity 40.5%, specificity 80.4%) were important features in differentiating between benign and malignant thyroid nodules (Kim, 2014). Twol other studies reported that calcifications, nodular attenuation values > 130 HU on contrast-enhanced CT, and nodular attenuation ≥ 55 HU on non-enhanced CT were associated with malignant thyroid nodules; the results

of these studies were statistically significant (all $P < 0.05$) (Ahmed et al., 2012, Kim, 2014).

CT and MR imaging are indicated for larger tumours (greater than 3 cm in diameter) that extend outside the gland to adjoining structures, including the mediastinum and the retropharyngeal region. Metastatic lymph nodes in the neck and invasion of the aero digestive tract are also in the realm of the diagnostic possibilities of CT and MR imaging. In addition, CT is usually the imaging modality of choice for the detection of pulmonary metastasis of thyroid cancer (Kabala, 2006).

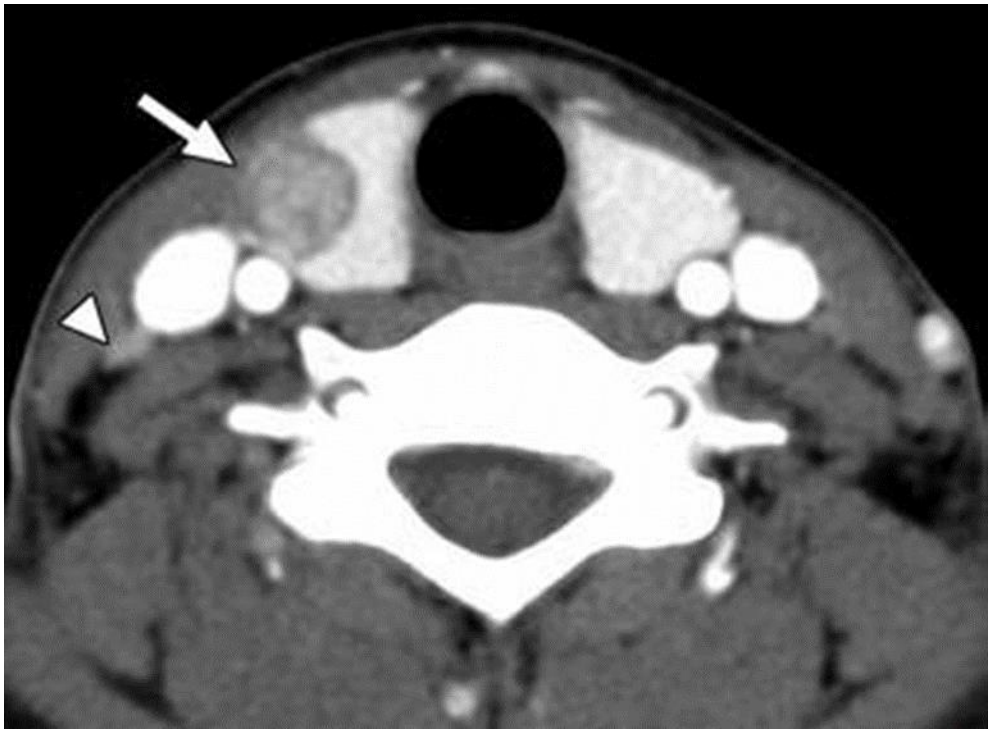

Figure 2.7.3 Illustrates CT-scan image of Papillary thyroid carcinoma in the right lobe of 28 years old female. The arrow shows malignant mass with extrathyroidal extension. The arrowhead represents a small lymph node with contrast enhancement at right level III. (Choi et al., 2009).

2.2.1.5.4 Magnetic Resonance Imaging (MRI)

MRI has the potential to depict very fine details of thyroid tissue. However, there is very little information available in the literature regarding the description of MRI characteristics of benign and malignant thyroid nodules. One recent study showed that MRI T2-weighted imaging can accurately differentiate between benign and malignant thyroid nodules with 86% sensitivity and 100% specificity (Noda et al., 2015).

The use of CT and MRI in thyroid cancer is indicated in the following situations (King, 2008):

(1) Preoperative assessment

(2) Follow-up of disease

(3) Suspicion of a locally advanced tumour

(4) Assessment of recurrent disease

(5) Tumour staging

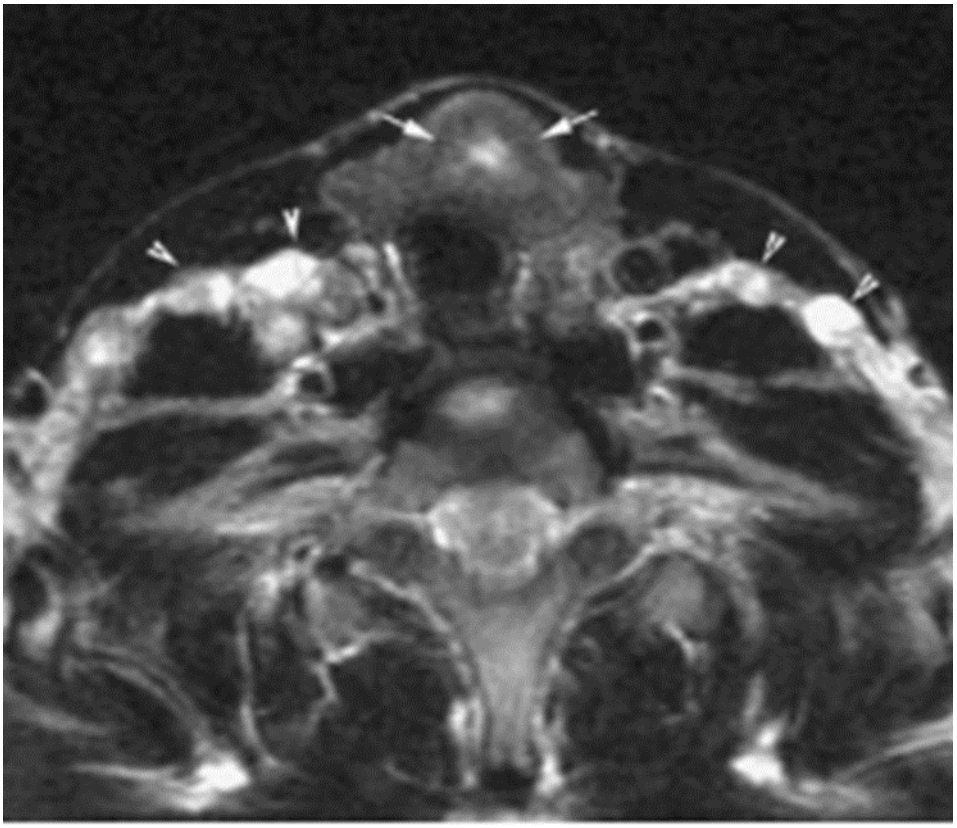

Figure 2.7.4 Illustrates transverse MRI scan (T2 weighted image) of PTC (arrows) with central cystic change. Several abnormal lymph nodes with cystic changes can be observed bilaterally (arrowheads) in the internal jugular and posterior cervical chains (Kabala, 2006).

2.2.1.5.5 Ultrasonography

High-frequency (1 - 30 MHz) sound waves are classified as ‘ultrasound waves’. Ultrasound waves are longitudinal waves that travel at a velocity of 1540 m/sec in human soft tissues. Ultrasound imaging of the thyroid gland provides detailed anatomical information and identifies pathological features associated with various thyroid diseases. As suggested by the American Thyroid Association (ATA), grey-scale USG is a useful imaging modality to assess the thyroid gland and its pathology (Cooper et al., 2009, Blum). USG is a safe, inexpensive, and widely available technique with relatively fair specificity and good sensitivity. It can clearly differentiate cystic from solid nodules (Hegedüs and Bennedbæk, 2005, Shapiro, 2003) (Figure 2.5). Up to 68% of thyroid nodules are detected by USG in randomly selected individuals (Sun et al., 2014b). Grey-scale ultrasonography is suitable for thyroid imaging because it depicts the internal structure of the gland without applying ionizing radiation (Butch et al., 1985) and produces an image with a high correlation to the thyroid anatomy. Ultrasound is also of great clinical significance in guiding fine needle aspiration cytology (Danese et al., 1998, Manning et al., 2017).

In general, the normal thyroid gland has a ground-glass appearance (homogenous echotexture). It is hyperechoic as compared to adjacent tissues (e.g. sternocleidomastoid). In adult humans, the thyroid volume ranges from 5 - 20 cm^3, and can easily be influenced by sex, age, body weight, and other physiological and environmental factors.

Each thyroid lobe has a globular appearance (height = 3 - 4 cm, width = 1 - 1.5 cm, depth = 1 cm) and is interconnected with the isthmus (identified as a uniform, smooth structure lying anterior to the trachea), approximately 0.5 cm in height and 2 - 3 cm in depth. The pyramidal lobe is usually not visible in adults but can be observed in young children. The trachea is filled with air and does therefore not transmit ultrasound waves. Placing the transducer obliquely near the trachea may allow the visualization of the region behind the trachea. The oesophagus is located slightly to the left; air and fluid fill the lumen appearing as a hypoechoic centre surrounded by a hypoechoic rim due to the presence of oesophageal musculature, altogether giving a characteristic ‘bull’s eye’ shape on grey-scale ultrasonogram. Bones and other calcified tissues or calcified lesions (e.g. micro/macro calcifications) block the ultrasound waves and appear as bright, echo-free shadows on grey-scale images. Organs and fleshy structures exhibit ground-glass appearance whereas cysts exhibit homogeneous hypoechoic appearance.

Image brightness can be controlled by adjusting the ‘gain control knob’. Blood vessels are usually echoless and can be best visualized by CDU; using this approach, the blood vessels can be differentiated from cystic lesions. The jugular vein usually appears in collapsed condition and can be distended by a Valsalva manoeuvre for best visualization. Other manoeuvres, such as swallowing of water for identification of the

oesophagus and various degrees of hyperextension of the neck can be adopted to enhance image quality.

For large goitres, panoramic ultrasound has been suggested in which images with a large ‘field of view’ are produced. However, the performance and interpretation of sonograms is subjective and therefore prone to inter- and intra-observer variation. One previous study has suggested that inter-observer variation can be minimized by selecting a curved transducer instead of a linear transducer (Peeters et al., 2003). It is recommended that a low-energy transducer should be used to delineate the fine anatomy of the thyroid. Usually, 15 - 4 MHz is optimal for all except large goitres. Some of the GSU features are correlated with malignancy. The underlying pathology can be related to the gross appearance of nodules characterized by GSU.

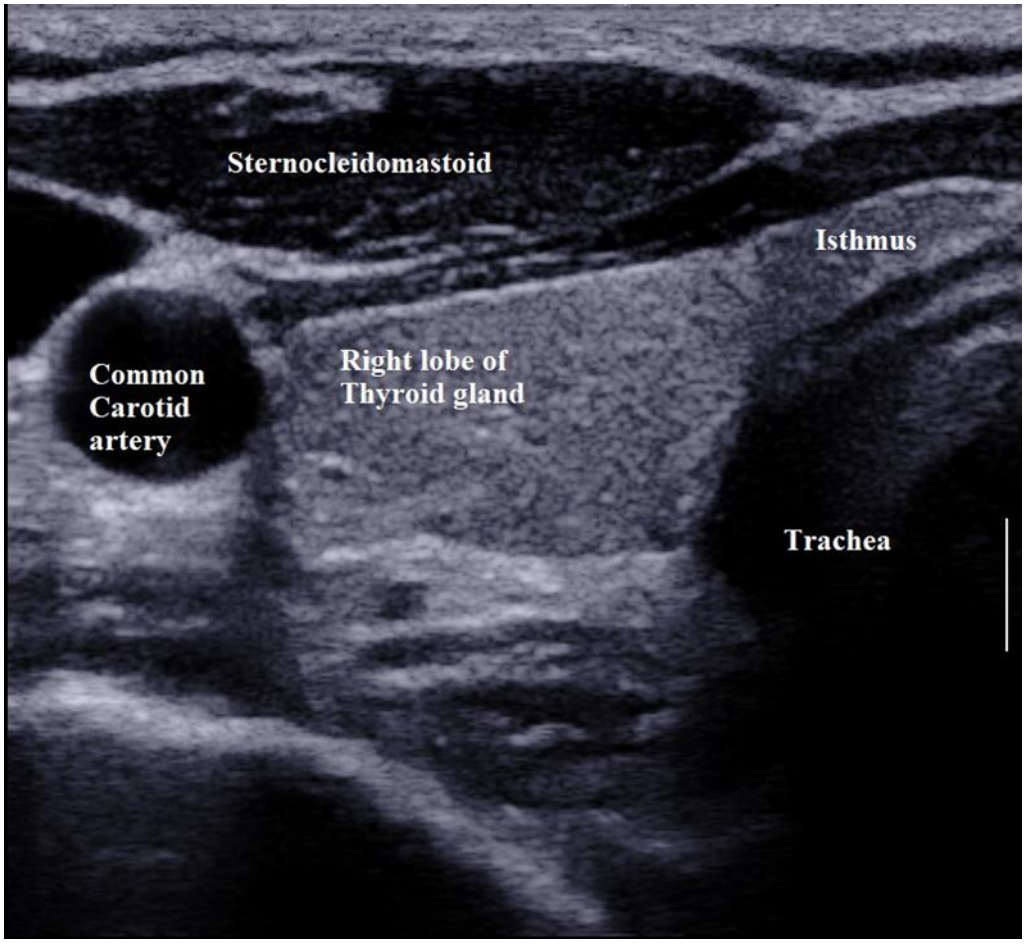

Figure 2.7.5 Grey-scale ultrasound features of normal thyroid gland and its anatomical relationship.

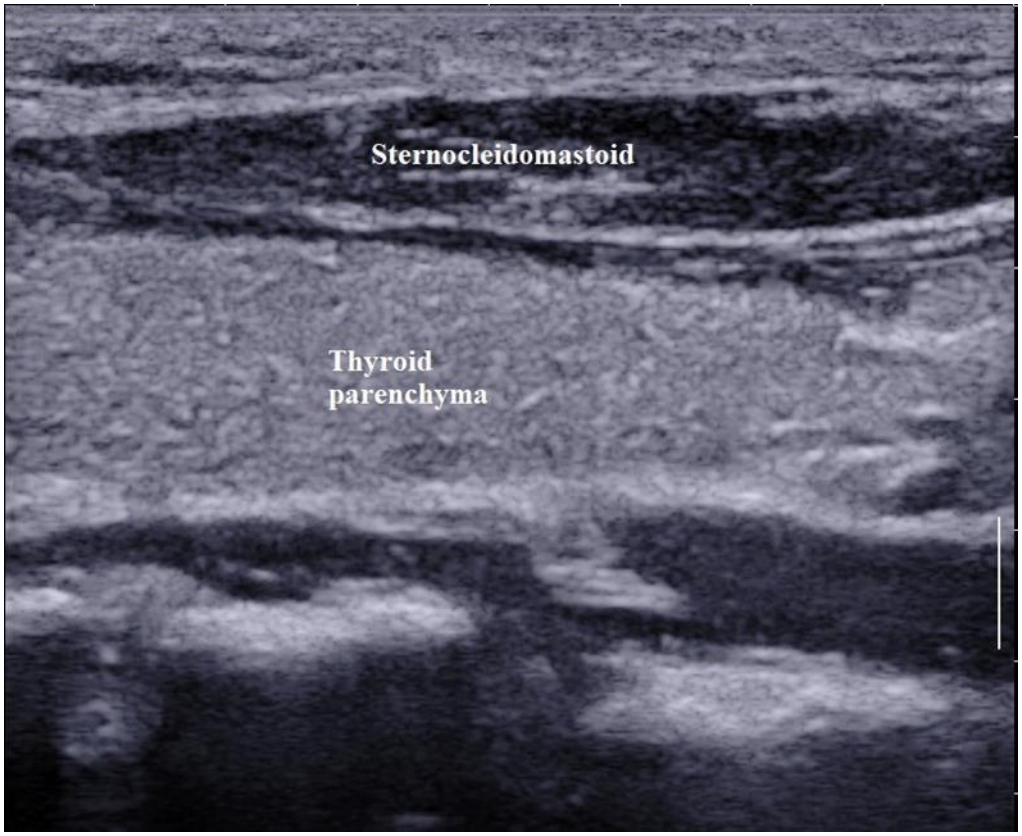

Figure 2.7.6 Grey-scale ultrasound Longitudinal section of left lobe of the normal thyroid gland

2.2.1.5.5.1 Grey-scale ultrasound features of malignant thyroid nodules

Echogenicity

Solid tumours (e.g. PTC) are packed with denser material (e.g. collagen) and have higher interstitial fluid pressure (IFP) compared to normal thyroid follicles. This may reduce the interface with acoustic impedance and decrease ultrasound reflection that results in the hypoechoic appearance of thyroid nodules (Figure 2.8.8).

Irregular shape

Thyroid tumour cells proliferate in an uneven manner that gives rise to the irregular shape on grey-scale USG scans (Figure 2.8.9).

Microcalcification

Microcalcifications appear as hyperechoic points without acoustic shadows on grey-scale ultrasonograms. Ultrastructural investigation shows thickening of the base lamina of neoplastic papillae followed by calcification, collagen production by necrotic tumour cells, and formation of ‘Psammoma bodies’ (Figure 2.8.9).

Solidity

The higher stiffness of malignant thyroid nodules is multifactorial. There is increased permeability of tumour vessels, leakage of plasma protein not effectively drained by lymphatic vessels, overproduction of vascular endothelial growth factor (VEGF) by tumour cells, infiltration of activated macrophages and immune cells, and inward diffusion of extracellular matrix and collagen fibres. Therefore, malignant cells become stiffer compared to normal thyroid follicular cells. Although GSU can accurately identify suspicious features for malignancy (e.g. micro-

calcification, irregular margins, hypoechogenicity, and irregular shape) the sensitivity and specificity of GSU vary considerably, between 52% and 97% and 26% and 83%, respectively (Sun et al., 2014b). Moreover, these findings are based upon subjective and qualitative assessments and vulnerable to inter- and intra-observer variability. The American Thyroid Association (ATA) suggests that no single feature or combination of GSU features are sensitive or specific enough to detect all malignant thyroid nodules(Ahuja and Evans, 2000, Cerbone et al., 2000). Some USG features are quantitative (e.g. vascularity, the stiffness of the nodule) and should be assessed by objective methods so that their clinical values can be evaluated (Figure 2.8.8).

Aspect ratio (taller-than-wide or anterior-posterior diameter/transverse diameter) > 1

This feature has repeatedly been reported to be associated with malignant thyroid nodules only (Popli et al., 2012, Anil et al., 2011, Johnson et al., 1988). The presence of this feature raises the suspicion of malignant potential of a thyroid nodule. Papillary thyroid carcinoma more commonly express taller-than-wide shape (Michels et al., 2007). Tall cell variants of papillary thyroid carcinoma might be responsible for such characterization of PTC (Harach and Zusman, 1991) (Figure 2.9).

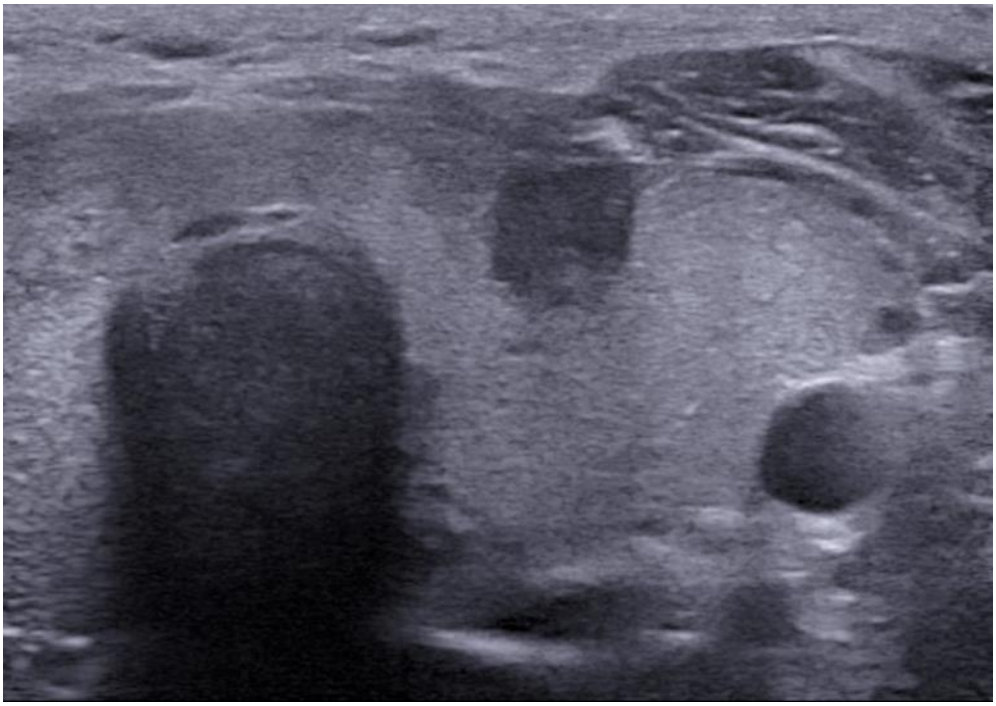

Figure 2.7.7 Transverse grey-scale sonogram illustrating papillary thyroid carcinoma (PTC) in the left lobe of the thyroid gland of the 43-year-old female patient. PTC is hypoechoic with respect to healthy thyroid parenchyma and adjacent muscles.

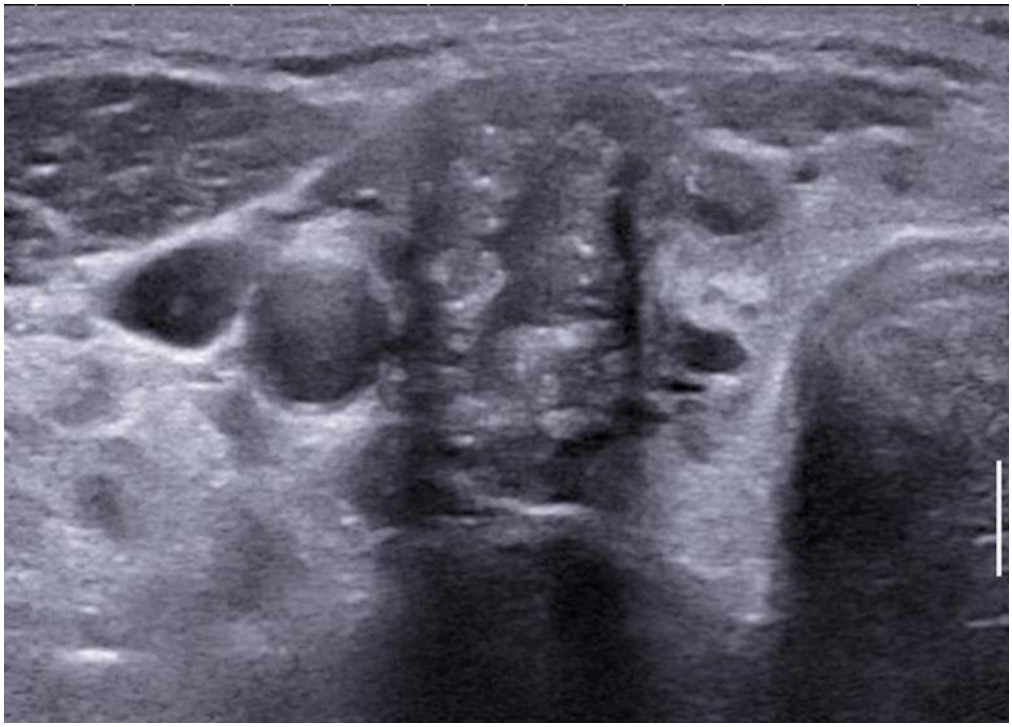

Figure 2.7.8 Transverse sonogram of right lobe of thyroid gland illustrating papillary thyroid carcinoma with irregular margins and microcalcification

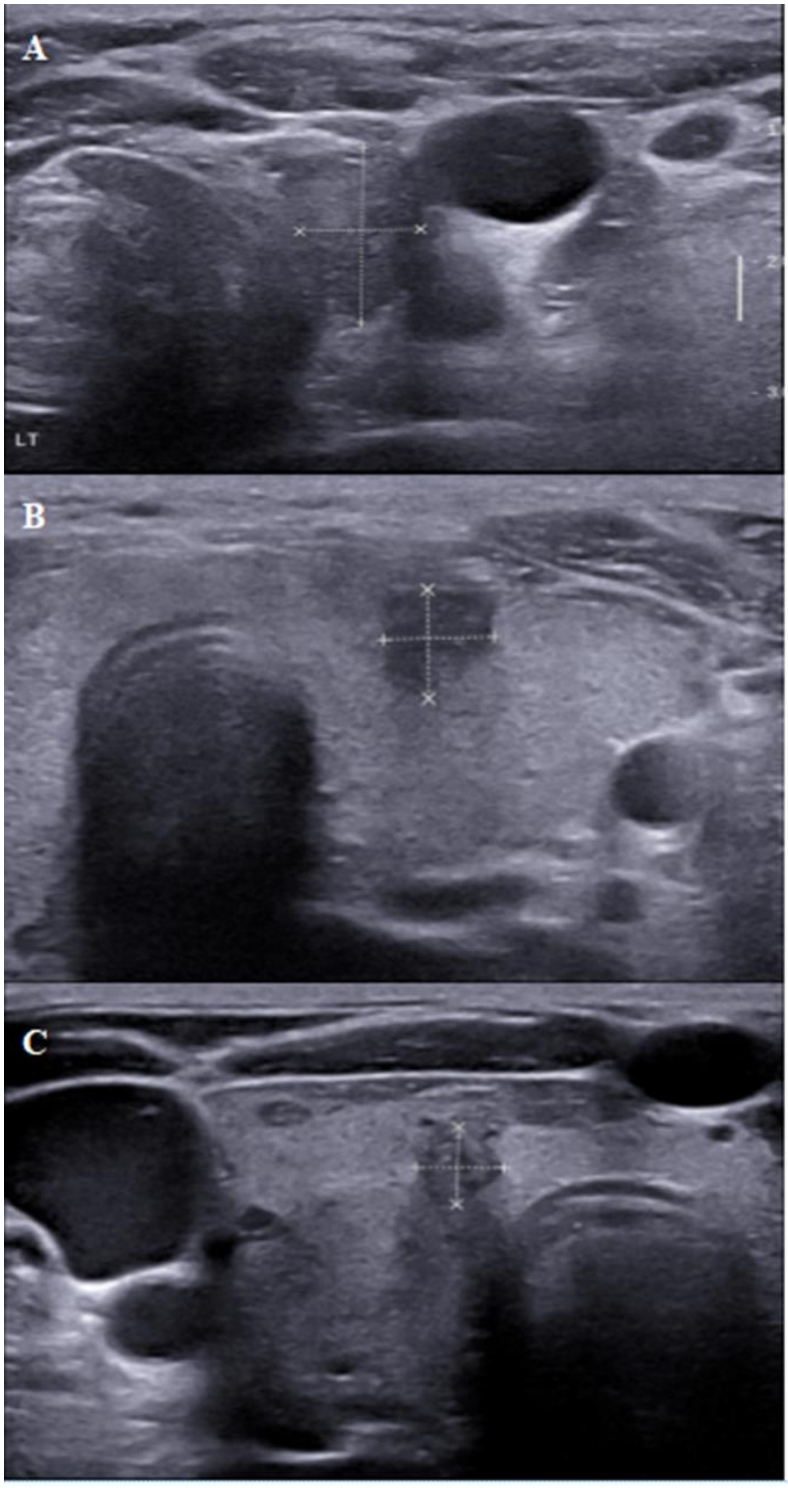

Figure 2.7.9 Transverse grey scale Illustration of classical feature “aspect ratio (tall/wide >1) in A (1.34; 0.80 cm), B (0.77; 0.72 cm) and C (0.64; 0.58 cm) respectively obtained from three patients.

2.2.1.5.5.2 Grey-scale ultrasound features of benign thyroid nodules

Benign thyroid nodules have distinct grey-scale features and can be identified easily. Several features are associated with benign thyroid nodules.

Cystic composition

Nodules with greater proportions of cystic components are usually benign. Spongiform (multiple cystic components) nodules also lie in the realm of benignity. However, predominantly solid nodules (> 10% and ≤ 50% of the cystic component) should be investigated in more detail. It should be noted that not every cystic nodule is benign. PTC tends to appear cystic when it is necrotic and very large in size (Dudea and Botar-Jid, 2015).

Comet tail sign

This sign is highly specific to benign thyroid nodules and represents colloid lesion. The overall sensitivity, specificity, and accuracy of this sign are 74%, 83%, and 81%, respectively (Ahuja et al., 1996). There is a high resemblance between the ultrasonography appearance of colloid and small punctate calcifications (a highly specific feature of PTC) and one can easily be confused when differentiating these two features, since both are hyperechoic. However, the distinction can be made by noticing the presence of the comet tail artefact behind the colloid, whereas punctate calcifications do not exhibit comet tail artefacts (Malhi et al., 2014).

Margins (regular border)

In comparison with malignant thyroid nodules that usually have irregular margins due to infiltration and stromal changes, benign thyroid nodules tend to have well-defined borders, possibly because they are localized and do not proliferate in an uneven manner (Algin et al., 2010).

Peripheral halo sign

In benign thyroid nodules, the halo appears thin and complete, possibly because there is rapid albeit controlled growth of thyroid neoplastic cells that causes compression in the adjacent thyroid parenchyma and results in the formation of the halo. A halo may also appear in malignant lesions; however, these halos are usually incomplete, possibly due to uneven and uncontrolled cell growth of thyroid cancer cells. In most cases, a halo sign is absent in malignant thyroid lesions (Asteria et al., 2008, Ünlütürk et al., 2012).

Multinodularity

Multinodularity is commonly observed in benign thyroid lesions. Malignant thyroid nodules are usually solitary (Ahuja and Evans, 2000). However, the risk of thyroid cancer with multinodularity should not be underestimated (Mengal et al.). Benign and malignant thyroid nodules may be found in the same gland. It has previously been reported that 10% - 20% of PTC are multicentric (Wisner and Nyland, 1998).

Figure 2.8.1 Benign thyroid nodule characterizing isoechogenecity and complete Halo sign

2.3 Review of literature for Study 1

2.3.1 Soft tissue elasticity

Mechanical properties (e.g. elasticity or stiffness) of biological soft tissues depend on molecular constitution, such as fat deposits, water content, collagen, elastin fibres, and micro/macro structural organization of the tissue. Desmoplastic reaction in response to tissue insult or neoplasia might be responsible for excessive collagen production and infiltration inside malignant cells that alter tissue elasticity and stiffness. Koperek et al. (2007) observed desmoplastic reaction and microcalcification in PTC and suggested that desmoplastic reaction might be associated with tissue stiffness (Koperek et al., 2007). To date, there is no study available in the literature that measures the increased stiffness of PTC nodules due to desmoplastic reaction. Unfortunately, modern imaging techniques such as scintigraphy, MRI (except for MR elastography), CT, and GSU do not measure elastic properties of healthy/pathological tissues. Considering the strengths and limitations of available imaging techniques as well as the increased incidence of thyroid nodules, there is a need for a reliable, non-invasive, quantitative imaging technique that can measure changes in stiffness of soft tissues during the pathological course and aids in minimizing the number of unnecessary biopsies.

2.3.2 Elastography principle and technique

Sonoelastography is a novel technique that quantifies elastic properties of healthy/pathological soft tissues. This technique provides

information on tissue stiffness and evaluates the degree of distortion of tissue under stress. The basic principle of sonoelastography is that the force applied to the soft tissue is proportional to the tissue strain (deformation). It can be expressed as Young's modulus: $E = \sigma/\varepsilon$, (σ = applied force, ε = resultant tissue deformation) (Papini et al., 2002). The elasticity (E) is dependent on the applied stress, and therefore the tissue strain is only comparable to elasticity maps under a homogenous stress field. Ultrasound elastography allows tissue to undergo reversible deformation and provides data on acoustic and mechanical properties of the area under study (AUS). Softer parts in a tissue are thus less resistant to strain compared to stiffer regions (Dudea and Botar-Jid, 2015). There are two main variants of elastography techniques, strain elastography (SE) and shear wave elastography (SWE), which provide qualitative and quantitative assessments of tissue stiffness, respectively. The former technique requires manual compression of tissue that generates a colour-coded map called 'elastogram' representing tissue elasticity superimposed on a grey-scale sonogram. SE can provide both qualitative and semi-quantitative information about tissue stiffness (Dudea and Botar-Jid, 2015, Bhatia et al., 2013). SWE uses high-intensity acoustic radiation force impulses (ARFI). ARFI pulses of short duration are focused at varying magnitudes of depth in tissue of interest to induce perturbation resulting in generation of shear waves. These shear waves with their transverse component propagate away from the source (ultrasound waves), at higher speed in stiffer tissues and at slower speed in softer counterparts. (Bhatia et al., 2012b, Lin et al., 2014, Zhang et al.,

2013). SWE measures tissue stiffness by tracking the speed of shear waves through the tissue of incidence and yields an elastogram with absolute quantification of tissue stiffness in the form of an elasticity index. Since SWE provides absolute quantitative data, it is regarded as more objective, accurate, and reproducible than SE. Contrary to SE, SWE is less operator-dependent and does not involve elasticity quantification of adjacent healthy tissue. Therefore, stiffness values obtained from SWE do not represent a 'ratio'; rather, SWE provides absolute tissue stiffness.

2.3.2.1 Strain Elastography (SE)

Strain elastography (SE) also known as free-hand quasi-static elastography or real-time elastography (RTE), is an add-on module incorporated with standard ultrasound units. It is widely available in commercial units and can be used with a conventional ultrasound transducer (Sebag et al., 2010a). The technology employs mechanical force (either external force applied by a transducer, or an internal source of compression such as carotid pulsation) to induce tissue strain (deformation) that results in axial displacement. Ultrasound waves are sent before and after tissue displacement. A high degree of tissue displacement is associated with the softer regions of tissue while stiffer regions exhibit minimal or no displacement. The time difference between ROIs of two consecutive images is recorded while dedicated software evaluates tissue strain. This results in the generation of a colour-coded elastography image, called elastogram (Veyrieres et al., 2012a, Sebag et al., 2010a).

There is no standardized method available for the qualitative interpretation of an elastogram (Kim et al., 2013). However, two assessment methods are commonly used in clinical practice: the ‘elastography scoring system’ and the ‘strain ratio’. The former method, which is based upon four to six scales, assesses relative tissue stiffness within the lesion. According to this assessment method, softer lesions are assigned lower elastography scores and stiffer lesions are assigned higher elastography scores. For strain ratio (SR) measurements, the sonographer/sonologist selects ROIs on the target lesion and the reference tissue. The SR is computed as the ratio of the strain of the target lesion and the strain of the reference tissue within the same image. In general, an SR > 1 suggests that the target lesion has higher stiffness than the reference tissue. The risk of malignancy of a lesion can be interpreted as ‘higher’ with increasing strain ratio and vice versa. SE uses an elastography scoring system and SR as diagnostic parameters, and is thus more subjective and prone to inter-observer variability (Andrioli and Persani, 2014, Asteria et al., 2008, Chong et al., 2013).

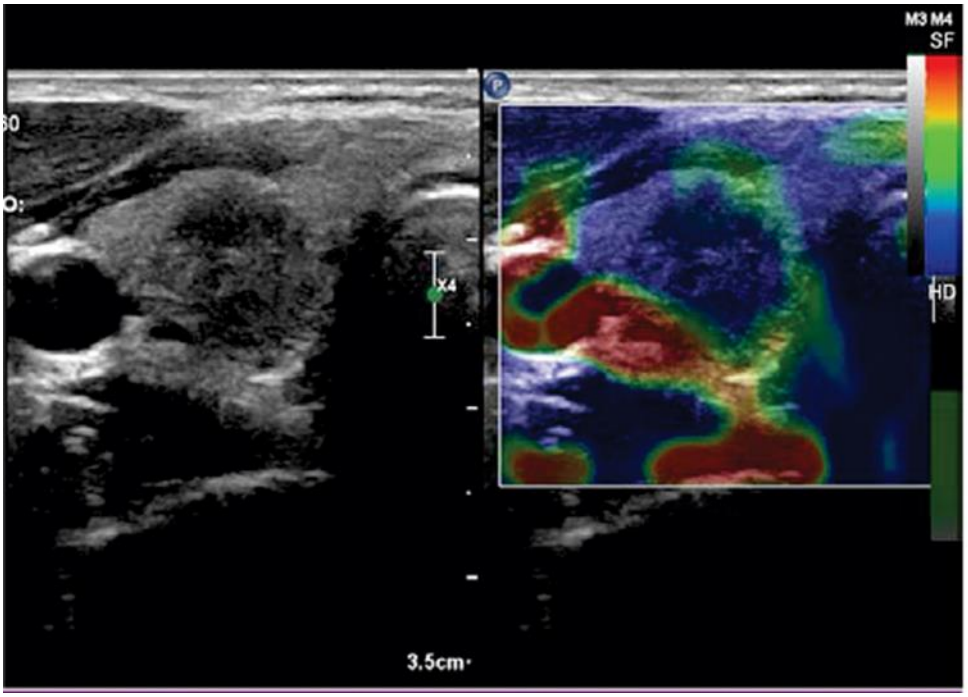

Figure 2.8.2 Strain elastogram of solid thyroid nodule; red – green – blue color map convention, hard nodule: blue nodule. (Stoian et al., 2016)

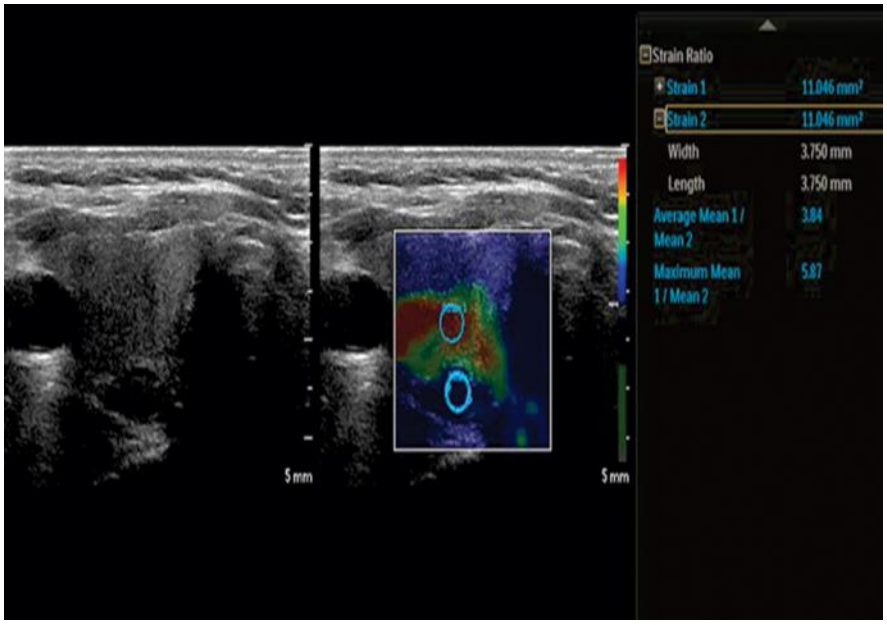

Figure 2.8.3 Transverse image of solid thyroid nodule showing strain ratio: red color (blue-green-red convention map), increased strain ratio: average = 3.84, maximum = 5.87(Stoian et al., 2016).

2.3.2.2 Shear wave elastography (SWE)

SWE is a novel ultrasound technique which provides an estimation of local tissue stiffness without being affected by any hard region in the vicinity of the ROI (Bhatia et al., 2013). SWE does not require manual compression but uses highly focused ultrasound impulses at various depths of the tissue to induce tissue displacement. Tissue displacement of a few microns results in the generation of shear waves which propagate transversely and perpendicular to the direction of ultrasound waves. Shear waves travel at a much faster rate in stiffer medium than in softer regions. Shear wave velocity is directly proportional to the square root of Young's modulus assuming the homogenous density of the medium of propagation. To measure the soft tissue stiffness, the propagation speed of shear waves is tracked by an ultrafast sonographic tracking technique, and the tissue stiffness is quantified and expressed in units of m/s or kPa (Anvari et al., 2016, Azizi et al., 2015).

Since SWE can quantify the soft tissue stiffness and provide the absolute stiffness value of soft tissue, it is considered less operator-dependent, more objective, and better reproducible than SE.

In our first study (Chapter 3), we have investigated the potential of SWE in differentiating benign and malignant thyroid nodules, and its added value to grey-scale ultrasound in the differential diagnosis of thyroid nodules.

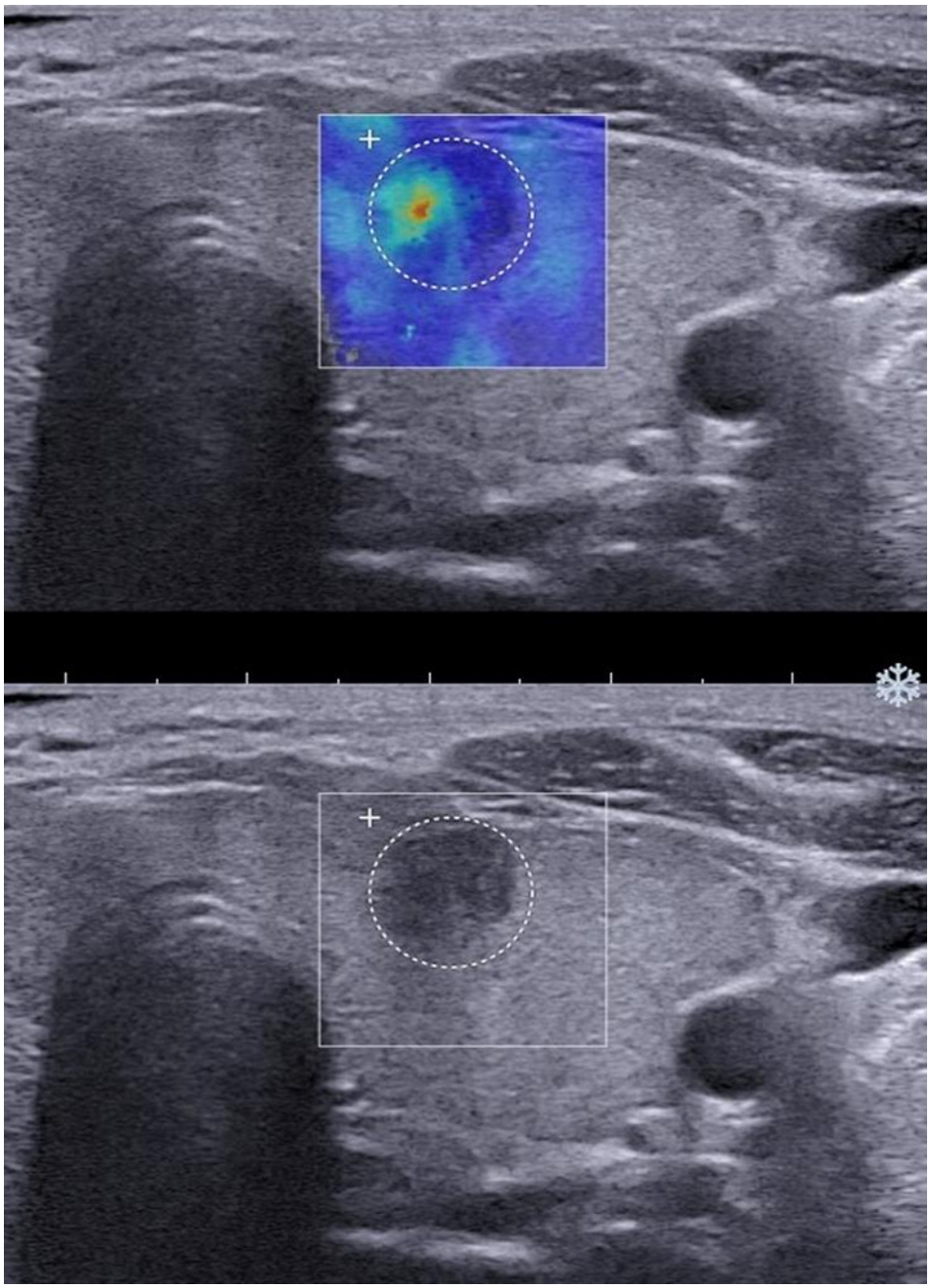

Figure 2.8.4 Transverse shear wave elastogram (upper) and transverse grey-scale elastogram (lower) illustrating papillary thyroid carcinoma in a circle (Region of Interest).

2.4 Review of literature for Study 2

2.4.1 Doppler ultrasound

The ultrasound Doppler imaging technique detects blood flow and provides hemodynamic information based on the 'Doppler effect'. The Doppler effect or Doppler shift refers to the change in the frequency of sound waves due to the reflector (e.g. blood cells in a blood vessel) moving relative (away or towards) to the source of the sound wave (transducer) (Kremkau, 2001). The frequency of reflected ultrasound waves increases when blood cells move towards the transducer and reduces when they are moving away from the transducer. The Doppler effect can be explained by the following equation (Hatle et al., 1980):

$$F = 2fV\cos\emptyset/C \text{ (equation 1)}$$

where *F* = Doppler frequency shift, *f* = frequency transmitted from transducer, *V* = velocity of moving blood cells, C = velocity of ultrasound waves in blood (media), and ∅ = the angle between the direction of ultrasound beam and the direction of blood flow.

Blood velocity can be directly measured by re-arranging equation 1:

$$V = FC / 2f\cos\emptyset \text{ (equation 2)}$$

The Doppler shift can easily be influenced by blood flow velocity, angle of insonation, and transmitted ultrasound frequency. There is a direct relationship between the Doppler shift and the transmitted frequency or blood flow velocity. However, the Doppler shift has an inverse relationship with the insonation angle (*∅)* of blood vessels. This

means that a decrease in the insonation angle will cause an increase in the Doppler shift, and vice versa (Evans, 1989).

Doppler ultrasound can be useful in detecting blood flow velocity, direction of blood flow, and type of blood flow (arterial or venous, normal, or abnormal). The sensitivity of Doppler ultrasound relies on many factors that must be considered while performing Doppler ultrasound examinations. These factors include the choice of wall filter, the pulse repetition frequency (PRF), noise adjustment, patient body movements, and lack of cooperation by the patient in holding swallowing and breathing movements during a Doppler ultrasound examination (De Nicola et al., 2005). In case of assessing vascularity in thyroid nodules, the depth of the nodule and variation in tissue attenuation are also important factors to consider. Over-compression of thyroid nodules by a transducer may also affect the detection of blood vessels (Chammas et al., 2005).

2.4.1.1 Colour Doppler ultrasound

In colour Doppler ultrasound, Doppler frequency shifts are encoded as different colours that correspond to the direction and magnitude of the blood flow (Mitchell, 1990). A colour Doppler ultrasound image consists of both grey-scale and colour components. The grey-scale component corresponds to the conventional grey-scale ultrasound which demonstrates the morphology of the soft tissues. The colour component corresponds to the colour encoding of the blood flow. Colour Doppler

ultrasound images are affected by aliasing when the blood flow velocity exceeds the measurable limits. Aliasing can be explained as the phenomenon where the velocity of the blood flow and the ultrasound beam angle combine to give a Doppler shift value higher than half of the PRF value that causes ambiguity in the Doppler signal. This ambiguity is called aliasing effect (Ranke et al., 1992). Aliasing provides misleading information about the blood flow direction because the colour signals illustrate a blood flow direction opposite to the true flow direction. Aliasing can be avoided by increasing the PRF or lowering the baseline, which increases the range of positive Doppler frequency shifts but decreases the negative Doppler frequency shift range (Hill et al., 2000).

2.4.1.2 Power Doppler ultrasound

Power Doppler ultrasound displays the integrated amplitude of Doppler signals from the vasculature. The amplitude of Doppler signals is dependent on the number of scatterers in the imaging area. In medical ultrasound, scatterers usually correspond to red blood cells. Since power Doppler ultrasound is based on the number of scatterers which produce Doppler shifts and does not depend on the mean Doppler frequency shift caused by scatterers, it is sensitive to low blood flow, when compared to colour Doppler ultrasound (Martinoli et al., 1998, Bude and Rubin, 1996).

Power Doppler ultrasound has an advantage over colour Doppler ultrasound in that power Doppler ultrasound is independent of the angle of insonation (MacSweeney et al., 1996). Furthermore, power Doppler

ultrasound does not provide directional information and does therefore not display aliasing (Martinoli et al., 1998). The main difference between power Doppler and colour Doppler ultrasound lies in the component of signals that are processed. Colour Doppler ultrasound processes mean frequency shifts representing velocity and the phase shift to depict the direction of blood flow. Power Doppler ultrasound, in contrast, relies on the amount of red blood cells causing Doppler frequency shifts independent of their direction and velocity, and generates colour-coded vascular maps reflecting the strength of the Doppler signals (Bude et al., 1994).

2.4.2 Thyroid nodule vascularity

Angiogenesis is an essential feature for the survival of neoplastic cells, and is associated with malignancy (Weis and Cheresh, 2011, Carmeliet and Jain, 2011). The use of colour Doppler ultrasound and power Doppler ultrasound to assess thyroid nodule vascularity has been reported (Wu et al., 2013, Fukunari et al., 2004, Frates et al., 2003). Vascular distribution patterns (peripheral and central vascularity) in thyroid nodules and their association with malignancy have led to controversial statements about their value in the diagnosis of thyroid cancer. In assessing thyroid nodules, some studies reported that Doppler ultrasound is a useful imaging modality in identifying malignant nodules (Fukunari et al., 2004, Frates et al., 2003, Papini et al., 2002), whilst others found that there was no significant difference in the vascular pattern between benign and malignant thyroid nodules (Rago et al., 1998,

Moon et al., 2010, Lam et al., 2014). A possible reason for these conflicting results might be the subjective assessment of vascular patterns of thyroid nodules that has been used in previous studies. The subjective assessment may lead to inaccurate results and high inter- and intra-observer variation.

In our second study (Chapter 4), we have successfully modified our previously established algorithm that can estimate vascularity and perform automated subdivision of thyroid nodules into peripheral and central regions by using a standardized approach called ‘offsetting’. To the best of our knowledge, this is the first study that used a computer-aided method to perform segmentation of different regions of thyroid nodules and to quantify regional vascularity.

2.5 Review of literature for Study 3

Imaging of microvasculature in the thyroid parenchyma is essential for the accurate assessment of vascular density in healthy and pathological thyroid glands. Colour and power Doppler ultrasound are common imaging tools for the assessment of vasculature in soft tissues including the thyroid gland (Bercoff, 2011). Clinically, the assessment of thyroid vascularity is important because it helps the differential diagnosis of thyroid diseases such as Graves' disease, Hashimoto's disease, acute thyroiditis, and thyroid neoplasms (Demaj et al., 2016, Venkateswarulu and Gowni, 2017, Shah, 2016, Aggarwal et al., 2017). Other useful applications of Doppler ultrasound are in the pre-operative planning of thyroid cancer surgery (Shimamoto et al., 1998) and in monitoring the patients' treatment response (Cooper et al., 2006), as well as in the detection of angiogenesis in developing tumour sites (Lassau et al., 2001).

However, both colour and power Doppler ultrasound have limitations in the assessment of microvasculature of thyroid parenchyma. CDU lacks in providing quantitative information (only mean vascularity at a central frequency can be obtained) (Bercoff, 2011) and is less sensitive in the detection of blood flowing at a low rate (Fleischer et al., 1999, Lyshchik et al., 2007). PDU takes advantage of not being affected by aliasing and angle independence and shows comparatively increased sensitivity to blood flow with low velocity, particularly useful in imaging

tortuous vessels. However, PDU does not provide information about the direction of blood flow (Bercoff, 2011, Moon et al., 2010).

Most recently, SuperSonic Imagine (Aix-en-Provence, France) has launched a new vascularity imaging technology, AngioPLUS (Planewave UltraSensitive™ imaging), which allows assessment of the microvasculature of soft tissues. This technique has the advantage that all pixels of the entire tissue can be reconstructed in real time in a single image. This is achieved by using a wave that is sent into the body at the maximum allowed pulse repetition. AngioPLUS provides 3D wall filtering permitting efficient discrimination between blood flow and soft tissues by analysing space, time, and amplitude information (Bercoff, 2016).

In our third study (Chapter 5), we investigated the value of AngioPLUS when combined with colour and power Doppler ultrasound in the assessment of thyroid vascularity. To the best of our knowledge, this is the first study that explored the effectiveness of this new ultrasound technique in assessing the microvasculature of the thyroid gland.

2.6 Review of literature for Study 4

2.6.1 Introduction

There has been a three-fold increase in the incidence of thyroid cancer over the past 30 years (Zhang et al., 2016, Niedziela, 2014), with an estimated 4% increase per annum (Nix et al., 2005). Currently, surgical resection of thyroid cancer is the ultimate therapeutic option. Radio iodine therapy is usually indicated after surgical treatment for well-differentiated thyroid carcinoma to destroy residual thyroid cancer cell or to treat metastasis (Luster et al., 2008, Sawka et al., 2004). External radiation beam therapy is usually indicated for the treatment of Anaplastic thyroid cancer and is not preferred in treatment of well-differentiated thyroid cancer (Ron et al., 1995, Tsang et al., 1998). The scope of chemotherapeutic drugs in treating thyroid cancer is limited and is often adjunct to radiotherapy or surgery (Carneiro et al., 2015). Current chemotherapeutic agents approved for the treatment of thyroid cancer include doxorubicin hydrochloride, lenvatinib mesylate, sorafenib tosylate, and cabozantinib-S-malate. However, most of these therapeutic regimens are associated with high toxicity (Liebner et al., 2016, Lessin and Min, 2000). Recent studies found that there is a 25% - 37% likelihood of remission of thyroid cancer after surgical treatment (Busaidy and Cabanillas, 2012). Complete remission after surgery followed by radiotherapy has been achieved only in 33% of patients with thyroid cancer (Zhang et al., 2016). Therefore, there is a need to explore new therapeutic strategies to meet the challenges in treating thyroid cancer.

Over the past few years, therapies targeting BRAF, PI3K/ AKT, and RET have shown limited therapeutic effects due to their high sensitivity to the target only. Multi-target therapy provides broad-spectrum sensitivity and might be a more useful therapeutic regimen than compounds with individual high sensitivity and high affinity (Carneiro et al., 2015).

Identification of novel drug targets and new drug discovery is a lengthy and time-consuming process. Moreover, there has been an 146% increase in the cost of developing a new drug, with a recent estimate of US $ 2.56 billion (DiMasi et al., 2014). Even after such an investment, there is no guarantee of further approval by the Food and Drug Administration (FDA). One of the possible strategies to accelerate drug development and to reduce costs is to evaluate the potential of already developed drugs for treating other diseases. This approach is beneficial because biosafety, pharmacokinetic data, and toxicity evaluations are already established. As suggested in previous studies (Gupta et al., 2013, O'Connor and Roth, 2005, Ekins and Williams, 2011, Ashburn and Thor, 2004), repurposing of drugs for other medical conditions than their primary medical indications might help to reduce the economic burden on the drug industry and consumers (i.e. patients).

Among various examples of repurposing of drugs, a few selected examples are listed here. Raloxifene (a selective oestrogen receptor modulator, abbreviated as ‘SERM’) was initially approved for the treatment of breast and prostate cancer. It was later approved for the

management of osteoporosis. Bupropion (a noradrenaline enhancer) was initially launched to treat depression and was later recommended for smoking cessation. Zidovudine (a reverse transcriptase inhibitor) was originally developed to treat various cancers; later, its application was found to be useful in managing HIV/AIDS (Ashburn and Thor, 2004).

Table 2.6.1: Examples of drug repurposing in the treatment of various disease conditions (Ashburn and Thor, 2004)

Drug	Initial use / disease	Repurposing
Raloxifene	Breast cancer and Prostate cancer	Osteoporosis
Bupropion	Depression	Smoking cessation
Zidovudine	Cancer	HIV
Statin	Cholesterol lowering agent	Anti-cancer
Cardiac glycosides	Cardiac arrhythmias and Congestive heart failure	Anti-cancer
Lithium	Mood stabilizer agent	Differentiated thyroid cancer
Cyclooxygenase-2	Anti-inflammatory drug	Adenomatous Polyposis
Enalidomide	Morning sickness	Myelodysplastic syndrome
Gemcitabine	Anti-viral drug	Pancreatic cancer
Sildenafil	Anti-angina	Erectile dysfunction

In a previous study, the authors suggested a potential therapeutic role of anti-lipid, anti-viral, and cardiac medicines in curing thyroid cancer (Zhang et al., 2011). Statin (e.g. simvastatin, rosuvastatin, lovastatin) is a cholesterol-lowering agent that limits the risk of stroke and myocardial infarction by reducing the mevalonate concentration in serum (Baigent et al., 2005). It has been found that malignant cells rely on the sustained availability of mevalonate pathway end-products such as geranylgeranylated RhoB that play a critical role in proliferation, migration, and apoptosis (Zeybek et al., 2011, Swanson and Hohl, 2006). Cardiac glycosides (e.g. digoxin) are known to increase cardiac output force and simultaneously decrease the force of contraction of cardiac muscles by inhibiting the sodium-potassium ATPase pump. Current medical usage of cardiac glycosides is to treat cardiac arrhythmias and congestive heart failure. Recent studies have found that cardiac glycosides have the potential to be used as anti-cancer agents. This notion is based on the rationale that cancerous cells are rapidly dividing and that their DNA is highly susceptible to damage. It is now evident that cardiac glycosides induce topoisomerase II-inhibiting activity. Therefore, limiting the property of repairing DNA in cancer cells might become a useful strategy in the selective killing of cancer cells (Prassas and Diamandis, 2008, Menger et al., 2012).

Lithium (Li) is a psychoactive compound classified under mood stabilizer agent. Its current indication is to treat bipolar disorder (Su et al.,

2004). Under normal physiological conditions, Li accumulation in the thyroid gland is 3 - 4 times higher than in blood serum. Koong et al. (1999) suggested a potential role of Li as adjunct therapy with ^{131}I in treating differentiated thyroid cancer, which has the advantages of increased accumulation and localization of ^{131}I and minimal side effects (e.g. nausea, vomiting, etc.) (Koong et al., 1999). Lithium has also been shown to exhibit anti-cancer properties in MTC. Kunnimalaiyaan et al. (2007) found that MTC xenografts showed a significant reduction in volume when treated with Li in *in vitro* and *in vivo* experimental settings (Kunnimalaiyaan et al., 2007).

2.6.2 Cannabinoids as anti-cancer agents

In our literature search, we were particularly interested in evaluating the therapeutic potential of cannabinoids in treating papillary thyroid cancer. Cannabinoids refer to a group of chemical compounds (~ 60) derived from the hemp plant *Cannabis sativa* as well as synthetic endogenous derivatives of these compounds (Cridge and Rosengren, 2013). Two cannabinoid receptors, CB1 and CB2, are distributed in various systems of the human body. CB1 receptors are mainly found in the central nervous system, the uterus, the testes, the eyes, and the spleen, whilst CB2 receptors are associated with organs of the immune system and tumour cells (Pertwee, 2006, Guzman, 2003). Cannabinoid receptors (CBR) and their endogenous ligands are collectively termed ‘endocannabinoid system’, and have been used as molecular targets for the treatment of various diseases. Cannabis has been used for medicinal

and recreational purposes for a long time. Among various cannabinoids, nabiximols (trade name: Sativex) is already approved for medical use in Canada (Bahji and Mazhar, 2016). Dronabinol (trade name: Marinol) has recently been approved by the FDA for the treatment of patients with HIV in palliative care (Benjamin and Fossler, 2016). Nabilone is still undergoing clinical trials for approval from the FDA (Haney et al., 2013).

Several studies have reported the expression of cannabinoid receptors (CB1 and CB2) and their therapeutic potential associated with various cancers including prostate cancer (Morell et al., 2016), colon cancer (Martínez-Martínez et al., 2015), hepatocellular carcinoma (Mallat and Lotersztajn, 2016), pancreatic carcinoma (Dando et al., 2013), glioma, astrocytoma (Vara et al., 2011), breast cancer (Pérez-Gómez et al., 2015), lung cancer (Ravi et al., 2016), and ovarian cancer (Gaul et al., 2015, Javid et al., 2016). Cannabinoids are reported to induce anti-cancer action by inhibiting proliferation, angiogenesis, metastasis, and apoptosis in a variety of cancers including lymphoma, colon cancer, lung cancer, and breast cancer (De Petrocellis et al., 2013, Carracedo et al., 2006b, Pacher et al., 2006, Blázquez et al., 2003).

2.6.3 Cannabinoid anti-cancer mechanism

The anti-cancer action mechanism of cannabinoids relies on autophagy-mediated apoptotic cell death (Salazar et al., 2009b, Verfaillie et al., 2010). Upon binding to its receptors, the cannabinoid agonist causes the activation of ceramides which are sphingosine-based lipids

that are involved in the regulation of proliferation, differentiation, and apoptosis. Ceramide activation stimulates an endoplasmic reticulum (ER) stress-related signalling pathway that causes misfolding of the proteins. The upregulation of p8 and pseudo kinase tribbles homolog 3 (TRIB3) leads to inhibition of AKT/MTORC1-mediated autophagy (Carracedo et al., 2006b, Carracedo et al., 2006a). Autophagy is a cryoprotective mechanism and may also induce cell death. However, a series of experiments have shown that autophagy induces cell death as a mechanism of anti-cancer action of the cannabinoid agonist (Armstrong et al., 2015, Velasco et al., 2016, del PULGAR et al., 2002).

Another hypothesis is that there is increased accumulation of misfolded proteins in the ER after cannabinoids bind to their receptors. This leads to the upregulation of ceramides and further upregulates protein p8 and its ER stress-related downstream target, namely transcription factor 6 (ATF-6). ATF-6 is a transmembrane glycoprotein located on the endoplasmic reticulum that, upon activation, promotes the transcription of ER chaperones (e.g. CHOP and GRP78). CHOP is a C/EBP protein and is an indicator of autophagy in the ER stress pathway. CHOP expression is upregulated in response to ER stress (Velasco et al., 2016, Sano and Reed, 2013).

2.6.4 Cannabinoids as potential therapeutic agents in papillary thyroid cancer

PTC is the most frequently occurring cancer among all thyroid malignancies. About 40% - 65% of all PTC cases harbour BRAF V600E mutations. A recent study showed that treatment of both BRAF wild-type and mutated melanoma cell lines with cannabinoid agonist THC resulted in autophagy-dependent apoptosis in melanoma (Armstrong et al., 2015). These results indicate that endocannabinoids are effective against cancer cells with activated BRAF/ERK and/or Trk. A previous study had suggested the use of cannabinoids for the treatment of BRAF-positive PTC (Kushchayeva et al., 2014). In another recent study, immunohistochemistry analysis of thyroid surgical specimens (n = 87) revealed that the expression of both cannabinoid receptors, CB1 and CB2, was more frequently observed in PTC (P = 0.001) when compared to benign lesions (Lakiotaki et al., 2015). The study further found that CB2 receptor expression was much higher than CB1 receptor expression. These results provide the foundation for further studies to validate the therapeutic potential of cannabinoid agonists in PTC (both wild-type and BRAF-mutated). While the anti-cancerous effect of the CB1 agonist on PTC has been reported (Armstrong et al., 2015), the anti-cancerous effect of the CB2 agonist on PTC is still unclear.

In our fourth study (Chapter 6), we conducted an *in vitro* study to evaluate the anti-cancer effect of the CB2 receptor agonist (JWH-133) on a normal thyroid follicular cell line and a papillary thyroid cancer cell line.

Chapter Three

Study One

Shear wave elastography combined with conventional grey-scale ultrasound improves diagnostic accuracy in differentiating benign and malignant thyroid nodules

3.1 Introduction

Grey-scale ultrasound (GSU) is recommended by the American Thyroid Association (ATA) as first-line investigation to evaluate every clinically susceptible thyroid nodule (Kim et al., 2015, Kwak and Kim, 2014). GSU can accurately differentiate between cystic and solid thyroid nodules (Cosgrove et al., 2017). Cystic nodules are more commonly associated with benignity and do usually not require aggressive treatment, unless they progress in size over a certain period of time or induce clinical manifestations such as dysphagia, shortness of breath, and laryngeal nerve compression (Edith et al., 1990). Most malignant thyroid nodules (e.g. PTC) have firm stroma due to the collection of excessive collagen and myofibroblasts (Dighe, 2014, Koperek et al., 2007, Sun et al., 2014b). However, not every thyroid cancer has a solid internal structure. Similarly, not every benign nodule is cystic. A previous study found an occurrence of 14% of cystic thyroid cancer in their cohort of patients (Edith et al., 1990). Other than a solid internal structure, GSU

features such as microcalcification, a height-to-width ratio > 1, irregular margins, and hypoechogenicity are also common in malignant thyroid nodules (Gharib et al., 2016, Chan et al., 2003, Moon et al., 2010). Up to date, no single GSU feature is found to be specific enough to correctly identify all thyroid malignant cases (Cappelli et al., 2007, Sun et al., 2014b, Razavi et al., 2013). More recently, the ATA guidelines of thyroid nodules and management of thyroid cancer (versions 2016 & 2017) emphasize that the risk of thyroid malignancy should be highly suspected if microcalcification and a height-to-width ratio > 1 are observed in solid nodules (Hossein Gharib et al., 2010, Haugen et al., 2017, Haugen, 2016). However, the ATA further suggested that GSU should not be used as a single screening tool in the evaluation of thyroid nodules because the sensitivity and specificity of GSU features vary significantly (Gharib et al., 2016).

Fine needle aspiration cytology (FNAC) is a current standard procedure to differentiate between benign and malignant thyroid nodules. Thyroid nodules are heterogeneous entities and may contain solid and cystic components within the same nodule. Therefore, precise and accurate sampling from the suspicious region of the nodule is of utmost importance and demands high skills and competency of the sampler (Mamoon et al., 2013, Agcaoglu et al., 2013). Moreover, the collected aspirate should contain a sufficient number of cells, so that a reliable diagnosis can be established. Neoplastic cellular changes with ongoing pathology in complex, differentiated thyroid nodules are difficult to

classify, because various pathological features of thyroid nodules overlap in different disease conditions (Wienke et al., 2003). FNAC has a 1% - 5% false-positive and a 0% - 7.7% false-negative rate, whilst 20% of cases remain non-diagnostic (Sharma, 2016, M Regina Castro and Gharib, 2003). Similar to GSU, FNAC has a wide range of reported sensitivity (GSU: 52% - 97%; FNAC: 54% - 90%) and specificity (GSU: 26% - 83%; FNAC: 60% - 98%) (Cantisani et al., 2015).

Ultrasound elastography is a non-invasive imaging method that assesses tissue stiffness by applying Young's modulus in biological tissues (Gennisson et al., 2013). There are two main types of ultrasound elastography, namely strain elastography and shear wave elastography. Ultrasound elastography has been used for the assessment of thyroid nodules (Monpeyssen et al., 2013). For strain elastography, one meta-analysis evaluated 5,942 thyroid nodules and suggested that different compression delivery methods (e.g. carotid pulsation, transducer compression) had a significant impact on the evaluation of stiffness of thyroid nodules. The authors concluded that carotid pulsation was a better source of compression than other compression delivery methods (Veer and Puttagunta, 2015).

Another meta-analysis of 3,531 thyroid nodules showed that both the elasticity score and the strain ratio have higher sensitivity than combined or individual grey-scale ultrasonography features in the detection of malignant thyroid nodules (Razavi et al., 2013). The authors

further concluded that the strain ratio performs better than the elasticity score. However, not all studies agree that ultrasound strain elastography has superior diagnostic value over GSU in differentiating benign and malignant thyroid nodules, as some found that strain elastography has limited sensitivity (16% versus 78% - 91%) and a positive predictive value (41% versus 33% - 60%) compared to GSU in differentiating benign and malignant thyroid nodules (Ünlütürk et al., 2012, Lippolis et al., 2011). Despite the extensive work undertaken with strain elastography in differentiating benign and malignant thyroid nodules, the usefulness of strain elastography is hindered by various limitations. Strain elastography is operator-dependent and requires external pressure. In free-hand compression, it is difficult to standardize the compression force for different operators. Individual pressure applied by the operator could vary even when the same operator applies it. Thyroid nodules located on the isthmus should not be evaluated using strain elastography. Anatomically, the thyroid isthmus is located in front of the trachea. Tracheal cartilages are hard tissues. Upon applying external pressure from a transducer, the nodule located on the isthmus is compressed against a hard surface, which may produce false elastography measurements. Moreover, the interpretation of strain elastograms is subjective and vulnerable to inter- and intra-observer variations (Dudea and Botar-Jid, 2015).

Shear wave elastography (SWE) is a novel ultrasound technique that estimates tissue stiffness by tracking shear wave propagation through regions of interest in soft tissue. SWE uses high-intensity

acoustic radiation force pulses of short durations, transmitted at varying depths in the tissue to cause perturbations and generate shear waves. Shear waves with their transverse component propagate faster in harder medium than in softer counterparts. The SWE technique combines the advantages of a higher spatial resolution, operator independency, high reproducibility, and quantitative elastic measurements, and thus surpasses the limitations of strain elastography (operator dependency, poor reproducibility, subjective interpretation of results, lack of quantitative measurements) (Veyrieres et al., 2012b, Dudea and Botar-Jid, 2015, Liu et al., 2015b, Zhang et al., 2013, Lin et al., 2014).

SWE has been widely used in the assessment of thyroid nodules. Sebag et al. (2010) applied SWE in the differentiation of benign and malignant thyroid nodules, and noted that a cut-off level > 65 kPa was useful in predicting thyroid malignancy. They further reported that malignant nodules (150 ± 95 kPa) had higher mean elasticity indices than benign thyroid nodules (36 ± 30 kPa). In the same study, the reported sensitivity and specificity of SWE were 85.2% and 93.9%, respectively (Sebag et al., 2010a). Another study investigated 476 thyroid nodules and showed that elasticity indices were significantly higher ($P < 0.05$) for malignant nodules than benign nodules. The optimal cut-off values for elasticity indices were 94.0 kPa for $E_{maximum}$, 85.2 kPa for E_{mean}, and 54.0 kPa for $E_{minimum}$ (Park et al., 2015a). Another study found that E_{mean} ≥ 34.5 kPa is the most significant predictor of thyroid malignancy, with a sensitivity of 52.9% and a specificity of 77.8% (Bhatia et al., 2012b).

These studies showed a wide range of cut-off values (34.5 - 90 kPa), sensitivity (76.9% - 90.3%), and specificity (71.1% - 93.9%). Potential reasons for the variations in the results may be related to different characteristics of the population under study, different sample sizes, and different experimental protocols.

Previous literature studies have compared the individual diagnostic accuracies of GSU and SWE in differentiating benign and malignant thyroid nodules. There are only few studies that evaluated the diagnostic accuracy of a combination of GSU and SWE in the differential diagnosis of thyroid nodules. In addition, previous studies used different methods to draw ROIs. In some studies, the ROI was drawn in such a way that it only encompassed the hardest region of the nodule (Sebag et al., 2010a). Other researchers set the ROI at 5 mm the apparent limit of the nodule (Calvete et al., 2013, Shweel and Mansour, 2013). Such methods are a potential source of inter- and intra-observer variations in the placement of the ROI and are not highly reproducible. Therefore, stiffness measurements calculated in earlier studies are generally not accurate.

In this study, we aimed at evaluating the feasibility of using a shear wave elastography index ($E_{maximum}$, E_{mean}, $E_{minimum}$) in differentiating between benign and malignant thyroid nodules. In addition, we further evaluated the diagnostic accuracy of SWE in differentiating benign and malignant thyroid nodules when it was used alone and in combination with GSU.

3.2 Materials and Methods

3.2.1 Subject recruitment

This retrospective study received approval from the Human Subject Ethics Subcommittee (HSESC) of the Hong Kong Polytechnic University and the Institutional Review Board of the Prince of Wales Hospital. Ultrasound images of 111 patients were reviewed. Altogether, 122 consecutive patients (100 females and 22 males; age range: 21- 95 years; mean age: 53 ± 13.7 years) were recruited from the Department of Surgery at the Prince of Wales Hospital. Informed written consent was obtained from all patients prior to ultrasound examination in accordance with the WORLD Medical Association Declaration of Helsinki: Ethical principles for medical research involving human subjects, 2008 (Association, 2008). The privacy rights of the human subjects in the study were strictly observed.

The inclusion criterion was clinical or radiological detection of at least one thyroid nodule on either side of the neck. Exclusion criteria included completely cystic nodules or any forms of inflammatory thyroid diseases, such as acute thyroiditis, chronic thyroiditis, Grave's disease, and sub-acute thyroiditis, which are associated with increased thyroid parenchymal stiffness.

3.2.2 Ultrasound examination of the thyroid gland

All patients received GSU and SWE examinations of the thyroid gland on both sides of the neck. The reference diagnosis was based on

cytopathology or histopathology results of the nodules. Thyroid ultrasound examinations were performed by the same operator, who at the time had more than 23 years of experience in ultrasonography. All ultrasound examinations were performed using the same ultrasound unit in conjunction with a 4 - 15-MHz linear transducer (Super Linear™ SL15-4, Aixplorer, Supersonic Imagine, Aix-en-Provence, France). Patients were positioned in supine posture on the examination couch with their shoulders supported by a pillow. The patient's neck was slightly hyperextended and the head was turned away from the side under examination. Ultrasound examination was performed with generous amounts of coupling gel. Transverse and longitudinal scans of the thyroid were performed. The transducer was scanned from the jaw to the clavicle, and over the entire thyroid lobe to detect thyroid nodule. When the thyroid nodule was identified, multiple transverse and longitudinal sonograms of the nodule were acquired. For each thyroid nodule, emphasize was given to identify suspicious GSU features, namely microcalcification, a height-to-width ratio > 1, hypoechogenicity, an absent halo sign, internal solid echotexture, and irregular margins (Figures 3.1 and 3.2).

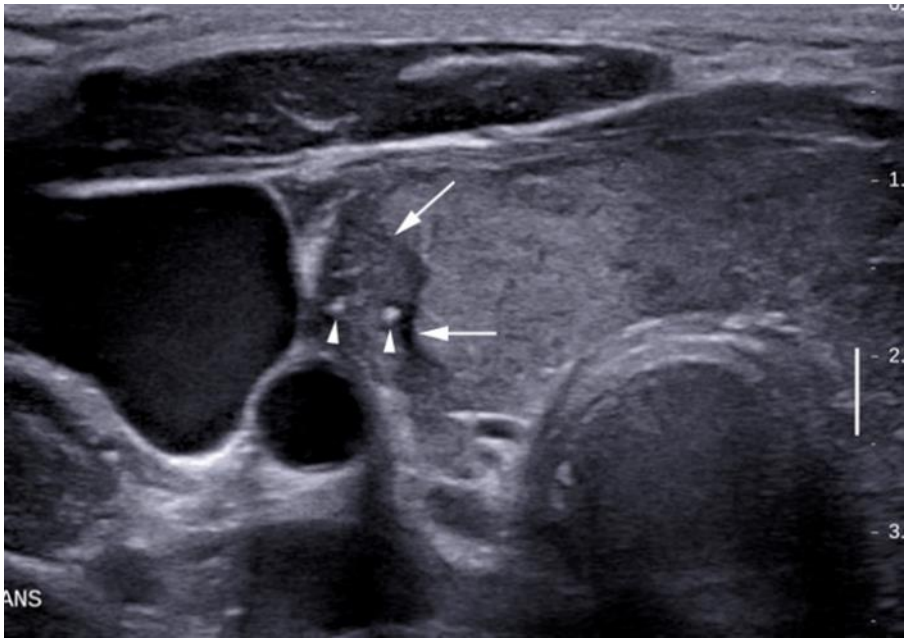

Figure 3.1 Transverse grey-scale sonogram showing a papillary carcinoma in the right thyroid lobe of a 43-year-old patient (arrows). The tumor is hypoechoic when compare to the adjacent thyroid parenchyma, and has multiple microcalcifications (arrowheads).

Figure 3.2 Longitudinal grey-scale sonogram showing a papillary carcinoma in the left thyroid lobe of a 51-year-old patient (arrows). The nodule appears hypoechoic, ill-defined and had multiple microcalcifications (arrowheads).

3.2.3 Shear wave elastography evaluation of thyroid nodules

GSU was followed by SWE evaluation of thyroid nodules. In the case of multiple thyroid nodules, the nodule with at least one suspicious GSU feature (as described above) and/or the largest nodule were selected. While performing the SWE examination, the size of the SWE acquisition area was adjusted so that it was large enough to cover the entire nodule. For image acquisition, the transducer was held stationary for at least two seconds to allow SWE signals to settle and to minimize variability. Caution was exercised to avoid applying pressure onto the patient's neck with the transducer, which might affect the measured stiffness of thyroid nodules. For each nodule, several longitudinal and transverse shear wave elastograms were acquired (Figures 3.3 and 3.4). While acquiring shear wave elastograms, scan planes showing calcification or cystic regions within the nodule were avoided. Following the ultrasound examination, FNAC was performed on the targeted nodule. Thyroid nodules with proven malignancy (papillary carcinoma, follicular carcinoma, or medullary carcinoma) or indeterminate cytology (follicular neoplasm, follicular lesion of undetermined significance, atypia of undetermined significance, or repeated non-diagnostic cytology) were subsequently evaluated by surgical resection and histopathological examination.

3.2.4 Image analysis

Acquired grey-scale sonograms and shear wave elastograms were reviewed by a single observer (Faisal N. Baig) who at the time had two

years of experience in thyroid ultrasound and was trained by M.Y. The observer was blinded to the clinical diagnosis and the cytopathology/histopathology results. GSU features of thyroid nodules were qualitatively analysed and the presence or absence of suspicious features (i.e. microcalcification, hypoechogenicity, a height-to-width ratio > 1, irregular margins, and internal solid echotexture) were assessed and recorded.

The elasticity of the thyroid nodules was calculated by using the inbuilt quantification tool (Q-box^{TM}) of the ultrasound on the shear wave elastograms. The quantification region of interest (ROI) was placed such that it covered the entire thyroid nodule. Shear wave elastography indices ($E_{maximum}$, E_{mean}, and $E_{minimum}$) were automatically calculated by dedicated software in units of kilopascals (kPa) (Figures 3.3 and 3.4). Elasticity was measured in the range of 0 kPa to ≥ 100 kPa. For each nodule, the five images with the highest stiffness values were selected in both transverse and longitudinal scans, and the means of $E_{maximum}$, $E_{mean,}$ and $E_{minimum}$ were calculated.

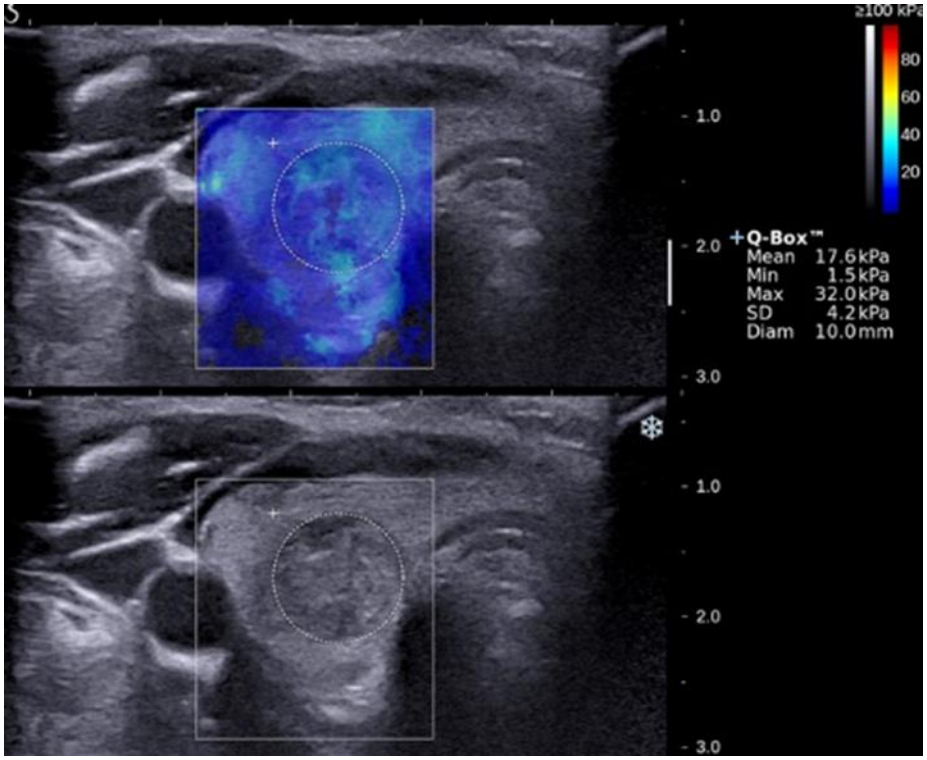

Figure 3.3 Transverse elastogram (upper) and grey-scale sonogram (lower) of a benign nodule in the right thyroid lobe of a 37-year-old patient. The value of elasticity indices ($E_{maximum}$ = 32 kPa and E_{mean} =17.6 kPa) were lower than the respective cut-off values reported in the present study.

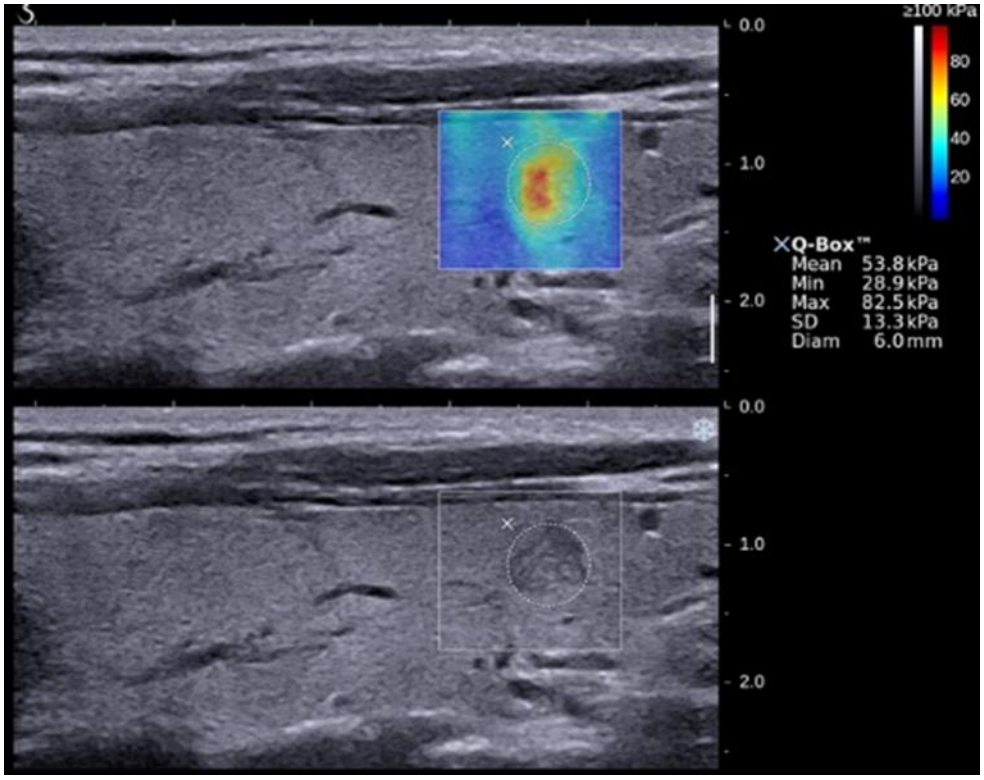

Figure 3.4 Longitudinal elastogram (upper) and grey-scale sonogram (lower) of a papillary carcinoma in the right thyroid lobe of a 57-year-old patient. The value of elasticity indices ($E_{maximum}$ = 82.5 kPa and E_{mean} =53.8 kPa) were higher than the respective cut-off values reported in the present study.

3.2.5 Data analysis

Chi-square tests were performed to determine the significance of differences in GSU features between benign and malignant nodules, whereas the significance of differences in SWE indices between benign and malignant nodules was calculated by Mann-Whitney U tests. The diagnostic performance of GSU was evaluated by deducing the frequency of true-positive (TP), true-negative (TN), false-positive (FP), and false-negative (FN) cases and sensitivity, specificity, negative predictive value (NPV), positive predictive value (PPV) and accuracy were calculated by the following formulas:

Sensitivity (%) = TP/(TP+FN) *100

Specificity (%) = TN/(TN+FP) *100

PPV (%) = TP/(TP+FP) *100

NPV (%) = TN/(TN+FN) *100

Accuracy (%) = (TP+TN)/(TP+TN+FP+FN) *100

Receiver operating characteristic (ROC) curves were used to determine the optimal cut-off points of different SWE indices in distinguishing benign and malignant nodules, and their associated diagnostic performance.

The diagnostic performance of combining GSU and SWE was determined based on the criterion that a thyroid nodule was malignant when it presented with at least one suspicious GSU feature and when the SWE index was equal to or greater than the optimal cut-off. All statistical analyses were performed using the Statistical Package for the Social Sciences (SPSS) software (Version 20, IBM Corporation, Armonk, NY,

USA), and a two-tailed *P* value < 0.05 was defined as significant.

3.3 Results

3.3.1 Histology results

Among all evaluated 122 thyroid nodules, 73 nodules were confirmed as benign by FNAC. Of the remaining 49 nodules, histopathological examination upon surgical resection confirmed 27 nodules as malignant and 11 as benign. The remaining 11 nodules were excluded from the study because surgical resection had not been performed and a final diagnosis could not be obtained. Therefore, altogether, 111 thyroid nodules (27 malignant and 84 benign) were included in this study. Among the 27 malignant nodules, there were 23 papillary thyroid carcinomas, three follicular thyroid carcinomas, and one Hurthle cell carcinoma.

3.3.2 Grey-scale ultrasound

The grey-scale sonographic features of thyroid nodules are summarized in Table 3.1. Among different grey-scale sonographic features, microcalcification (77.8% and 7.1%, respectively), a height-to-width ratio > 1 (59.3% and 13.1%, respectively), hypoechogenicity (92.6% and 33.3%, respectively) and irregular margins (55.6% and 16.7%, respectively), were significantly more common in malignant nodules than in benign nodules (all *P* < 0.05). There was no significant difference in the absent halo sign and internal solid echotexture between malignant and benign nodules (*P* > 0.05). Based on the above results,

further data analysis was performed to determine the diagnostic performance of GSU in distinguishing benign and malignant thyroid nodules. In the data analysis, thyroid nodules with at least one of the above four significant grey-scale sonographic features (i.e. microcalcification, a height-to-width ratio > 1, hypoechogenicity, and irregular margins) were defined as malignant, whereas others were classified as benign. Using these assessment criteria, 26 malignant nodules and 39 benign nodes were correctly identified. The results showed that the sensitivity, specificity, positive predictive value (PPV), negative predictive value (NPV), and overall accuracy of GSU in distinguishing benign and malignant nodules were 96.3%, 46.4%, 36.6%, 97.5%, and 58.5%, respectively (Table 3.1).

Table 3.1 Grey scale sonographic features of benign and malignant thyroid nodules.

Grey scale ultrasound features	Number of nodules (percentage)		*P* value (95% Confidence Interval)
	Benign (n=84)	Malignant (n=27)	
Microcalcification			
Yes	6 (7.1%)	21 (77.8%)	.000
No	78 (92.9%)	6 (22.2%)	(0.12 - 0.49)
Tall/width ratio > 1			
Yes	11 (13.1%)	16 (59.3%)	.000
No	73 (86.9%)	11 (40.7%)	(0.29 - 0.74)
Hypoechogenicity			
Yes	28 (33.3%)	25 (92.6%)	.000
No	56 (66.7%)	2 (7.4%)	(0.42 - 0.71)
Irregular margins			
Yes	14 (16.7%)	15 (55.6%)	.000
No	70 (83.3%)	12 (44.4%)	(0.38 - 0.83)
Absent Halo sign			
Yes	74 (88.1%)	26 (96.3%)	.061
No	10 (11.9%)	1 (3.7%)	(0.65 – 1.01)
Internal solid echotexture			
Yes	61 (72.6%)	27 (100%)	.005
No	23 (27.4%)	0 (0%)	(0.6 - 0.8)

3.3.3 Shear wave elastography

Table 3 shows the SWE indices of benign and malignant thyroid nodules. The results showed that malignant thyroid nodules were associated with higher SWE indices. The median of $E_{maximum}$ of malignant nodules (85.2 ± 8.1 kPa) was significantly higher than that of benign nodules (50.3 ± 3.1 kPa; $P < 0.05$). Similarly, the median of E_{mean} of malignant nodules was 26.6 ± 2.5 kPa and that of benign nodules was 20.2 ± 1 kPa, and the difference was statistically significant ($P < 0.05$). However, no significant difference was found in $E_{minimum}$ between benign and malignant nodules ($P > 0.05$).

Since significant differences were found between benign and malignant nodules in $E_{maximum}$ and E_{mean} only, the evaluation of diagnostic accuracy was performed in these two SWE indices. With the use of ROC curves (Figure 5), the optimal cut-off of $E_{maximum}$ and E_{mean} in distinguishing benign and malignant nodules were defined as 67.3 kPa and 23.1 kPa, respectively. Using the optimal cut-off of $E_{maximum}$, 19 malignant and 59 benign nodules were correctly evaluated. The sensitivity, specificity, and overall accuracy of $E_{maximum}$ were 70.4%, 70.2%, and 70.3%, respectively. Using the optimal cut-off of E_{mean}, 20 malignant and 56 benign nodules were correctly assessed, and the sensitivity, specificity, and overall accuracy of E_{mean} were 74.1%, 66.7%, and 68.5%, respectively (Table 3.2).

Table 3.2 Diagnostic performance of GSU, SWE indices and combination of GSU and SWE in evaluation of thyroid nodules.

Ultrasound modality	Sensitivity (%)	Specificity (%)	PPV (%)	NPV (%)	Accuracy (%)	AUC
GSU	96.3	46.4	36.6	97.5	58.5	0.714
$E_{maximum}$ (67.3 kPa)	70.4	70.2	43.2	88.1	70.3	0.785
E_{mean} (23.1 kPa)	74.1	66.7	41.7	88.9	68.5	0.710
GSU + $E_{maximum}$ (67.3 kPa)	70.4	83.3	57.6	89.7	80.2	0.769
GSU + E_{mean} (23.1 kPa)	74.1	79.8	54.1	90.5	78.4	0.775

GSU, grey scale ultrasound

PPV, positive predictive value

NPV, negative predictive value

AUC, area under the curve

3.3.4 Combination of grey-scale ultrasound and shear wave elastography

Our results showed that GSU had a high sensitivity (96.3%) but a low specificity (46.4%), leading to an overall accuracy of 58.5% in assessing thyroid nodules. When GSU was combined with SWE ($E_{maximum}$ or E_{mean}), the overall accuracy increased to 80.2% for $E_{maximum}$ and to 78.4% for E_{mean}, with a sensitivity of 70.4% and 74.1% and a specificity of 83.3% and 79.8%, respectively (Table 3.2, Figure 3.6). When GSU was combined with $E_{maximum}$ or E_{mean}, 19 or 20 malignant and 70 or 67 benign thyroid nodules were correctly identified, respectively.

Table 3.3 Shear wave elastography measurement of benign and malignant thyroid nodules.

SWEI	**Median ± 1 standard error**		***P* value (95% Confidence Interval)**
	Benign	**Malignant**	
$E_{maximum}$	50.3 ± 3.1	85.2 ± 8.1	0.000 (50.9 – 63.5; 73.0 – 106.1)
E_{mean}	20.2 ± 1.0	26.6 ± 2.5	0.002 (19.5 – 23.5; 23.5 – 33.9)
$E_{minimum}$	3.9 ± 0.6	3.8 ± 1.2	0.045 (4.2 – 6.4; 3.7 – 8.8)

SWEI**:** Shear wave elastography index

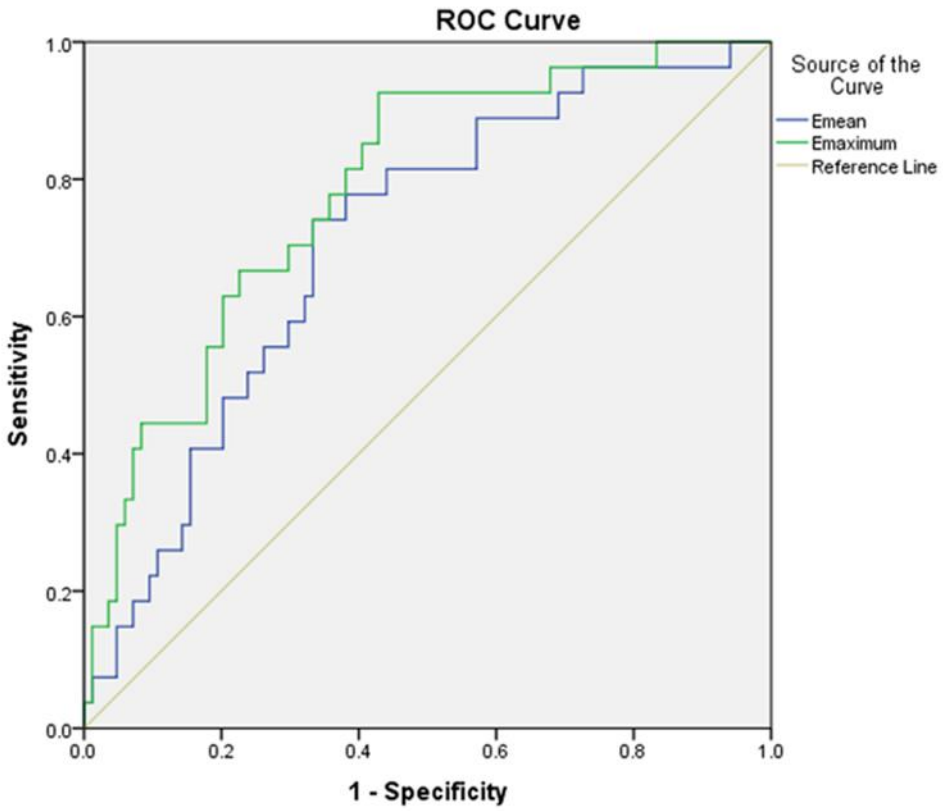

Figure 3.5 Receiver operating characteristic (ROC) curves used to determine the optimal cut-off level of $E_{maximum}$ and E_{mean} in distinguishing benign and malignant thyroid nodules.

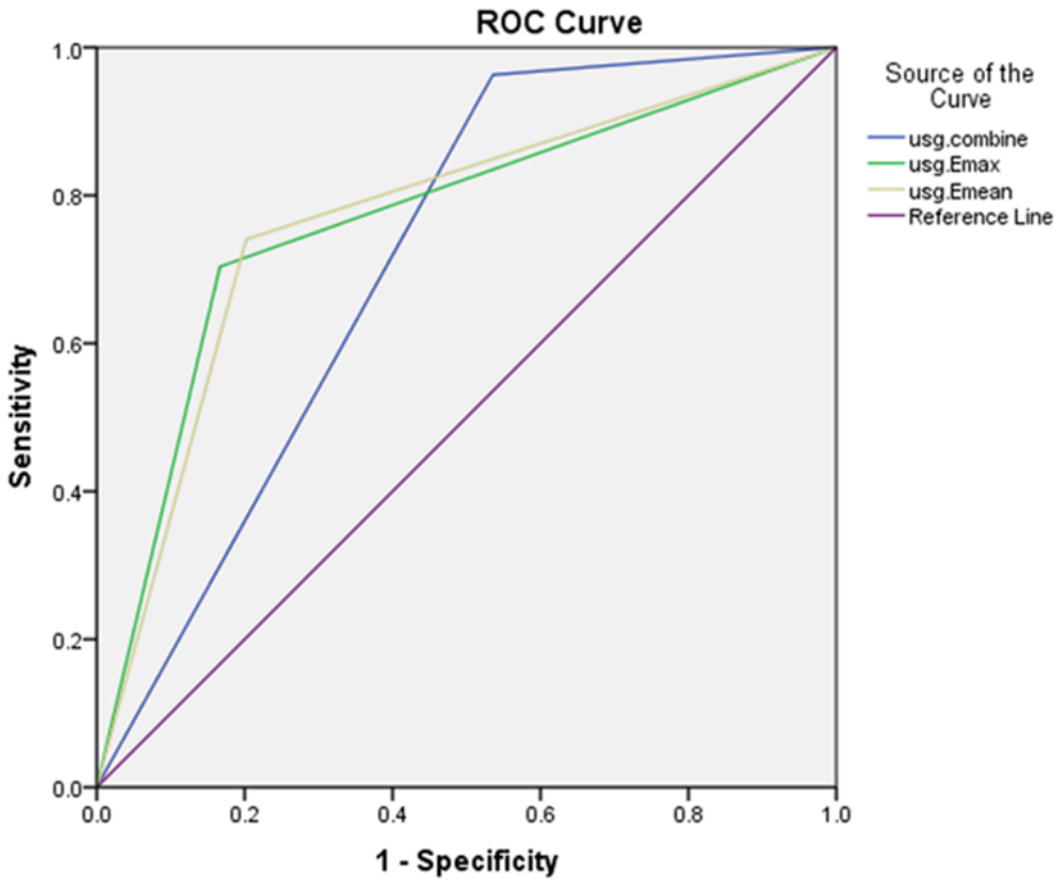

Figure 3.6. Receiver operating characteristic (ROC) curves showing a comparison between grey-scale ultrasound features alone (usg.combine) and in combination with $E_{maximum}$ (usg.$E_{maximum}$) and E_{mean} (usg.E_{mean}) in distinguishing benign and malignant thyroid nodules.

3.4 Discussion

The differential diagnosis of thyroid nodules to predict malignancy poses a diagnostic dilemma in clinical settings. GSU is commonly used to assess thyroid nodules, but no single GSU feature can accurately predict thyroid malignancy (Duan et al., 2016). SWE is a novel ultrasound technique that measures tissue elasticity by tracking shear wave propagation through body tissues and provides quantitative measurements. The technique is less operator-dependent than GSU and highly reproducible (Sun et al., 2014a).

SWE evaluation of thyroid nodules has been documented. However, the reported cut-off levels to differentiate benign and malignant nodules vary, probably due to different methodologies used in earlier studies. Among the available literature, the highest cut-off values of SWE indices for evaluating thyroid malignancy were ≥ 95 kPa for $E_{maximum}$, ≥ 85.2 kPa for E_{mean}, and ≥ 54.2 kPa for $E_{minimum}$ (Park et al., 2015b). However, Bhatia et al. (2012) found that an E_{mean} of 34.5 kPa or higher was a significant predictor of malignancy, with a sensitivity of 52.9% and a specificity of 77.8% (Bhatia et al., 2012c). Other studies suggested that SWE was useful in differentiating benign and malignant thyroid nodules when cut-off levels of 66 kPa and 65 kPa for $E_{maximum}$ were used, respectively (Sebag et al., 2010b, Veyrieres et al., 2012b). However, Szczepanek-Parulska et al. (2013) found that a threshold value of 50 kPa for $E_{maximum}$ was the most useful SWE parameter in the differentiation of benign and malignant nodules (Szczepanek-Parulska et al., 2013).

Using cut-off values of ≥ 53.2 kPa for $E_{maximum}$, ≥ 34.5 kPa for E_{mean}, and ≥ 21.8 kPa for $E_{minimum}$, Duan et al. (2016) found that SWE was superior to conventional GSU in identifying malignant nodules. Among different SWE indices, they found that E_{mean} yielded the highest diagnostic accuracy (79.6%) (Duan et al., 2016). Liu et al. (2014) reported that an E_{mean} ≥ 38.3 kPa was the most useful predictor among all SWE indices in differentiating benign and malignant thyroid nodules (Liu et al., 2014).

In the present study, the optimum cut-off points for $E_{maximum}$ and E_{mean} for distinguishing benign and malignant nodules were 67.3 and 23.1 kPa, respectively, consistent with the results of previous reports of $E_{maximum}$ (Sebag et al., 2010b, Veyrieres et al., 2012b). In the current study, there was no significant difference in the $E_{minimum}$ of benign and malignant nodules, which is inconsistent with previous studies (Duan et al., 2016, Liu et al., 2014, Park et al., 2015b). This discrepancy is presumably due to the different methodologies used in the present and previous studies. Previous studies used ROIs (Q-box^{TM}) of fixed sizes and placed them over the stiffer region of the nodules for the stiffness measurement. This involves a subjective judgement by the operator regarding the placement of the ROI. However, in the present study, the size of the ROI was adjusted so that it covered the entire nodule. This process does not involve an operator's judgement as to where the ROI should be placed, and is thus more objective. In addition, the method

used in the present study allowed a more comprehensive assessment of the nodule, because the ROI covered the entire nodule in the image. Our results suggest that the tissue stiffness within malignant thyroid nodules varies, with some areas significantly stiffer than benign nodules (as demonstrated by significantly higher $E_{maximum}$ and E_{mean} in malignant nodules), whereas some areas showing stiffness similar to benign nodules (as demonstrated by the similar $E_{minimum}$ between benign and malignant nodules). This may be related to the uneven distribution of tumour cells within the nodule. The results of our study demonstrate that $E_{maximum}$ and E_{mean} are potential predictors for thyroid malignancy when using cut-off values of 67.3 kPa and 23.1 kPa, respectively. However, $E_{minimum}$ has limited value in distinguishing benign and malignant nodules.

In the present study, we evaluated the diagnostic performance of GSU alone and a combination of GSU and SWE. The results show that the overall diagnostic accuracy of GSU alone was 58.5%, and that it increased to 80.2% and 78.4% when combined with $E_{maximum}$ (cut-off: 67.3 kPa) and E_{mean} (cut-off: 23.1 kPa), respectively. Our results also demonstrate that when GSU is combined with SWE, specificity increased from 46.4% to 83.3% when using $E_{maximum}$, and to 79.8% when using E_{mean}. However, sensitivity decreased from 96.3% to 70.4% and 74.1%, respectively. This finding is different to what has been reported previously. Dobruch-Sobczak et al. (Dobruch-Sobczak et al., 2016) reported that a combination of GSU and SWE did not significantly improve the diagnostic accuracy of malignant thyroid nodules. In other

studies, there was no significant difference in the diagnostic accuracy of GSU alone and a combination of GSU and SWE indices in distinguishing benign and malignant thyroid nodules, with reported values ranging between 86.3% and 87.2% (Park et al., 2015b), 81% and 77.9% (Liu et al., 2015a), and 60.3% and 60.3% (Veyrieres et al., 2012b). The same authors also found that when GSU and SWE indices were combined, specificity decreased but sensitivity increased (Park et al., 2015b, Veyrieres et al., 2012b, Liu et al., 2015a). The differences in results between previous reports and the present study are presumably due to the different criteria in determining malignant thyroid nodules when combining GSU and SWE. In previous studies, thyroid nodules were considered malignant when they either had one or more malignant grey-scale sonographic features or an SWE index value greater than the cut-off. This criterion increased sensitivity by yielding more true-positive findings, but it also increased the number of false-positive findings, leading to decreased specificity (Dobruch-Sobczak et al., 2016, Park et al., 2015b, Veyrieres et al., 2012b, Liu et al., 2015a). Since the extent of changes in specificity and sensitivity was similar, there was no significant improvement in the overall diagnostic accuracy when GSU was combined with SWE in previous reports. However, in the present study, we considered thyroid nodules to be malignant when they had both malignant grey-scale sonographic features (one or more features) and an SWE index value greater than the cut-off. Using this assessment criterion, there was a substantial improvement in specificity with a moderate decrease in sensitivity leading to a significant improvement in

overall accuracy. In the present study, overall diagnostic accuracy was improved from 58.5% to 80.2% for $E_{maximum}$ and to 78.3% for E_{mean}.

During routine clinical thyroid ultrasound examinations, operators should consider examining the internal cervical chain to identify any metastatic cervical lymph nodes when a malignant thyroid nodule is found. Ultrasound is a useful imaging tool to assess cervical lymph nodes. Metastatic cervical lymph nodes from papillary thyroid carcinoma are usually hyperechoic when compared to adjacent muscles, round in shape, without echogenic hilus, and show punctate calcification (Ahuja et al., 1995). In addition, the combination of ultrasound and computed tomography can help to predict extrathyroidal extension (Lee et al., 2014), and fluorodeoxyglucose positron emission tomography/computed tomography (FDG-PET/CT) scans should be considered for detecting metastases in post-operative patients with an aggressive histology of differentiated thyroid cancer (Nascimento et al., 2015).

In the present study, 84 benign and 27 malignant thyroid nodules were analysed. The calculated power of this sample size in evaluating the performance of GSU and SWE indices in distinguishing benign and malignant thyroid nodules ranged between 0.874 and 0.999 (G*Power version 3.1.9.2, Düsseldorf, Germany).

The present study has several limitations. The majority of the malignant thyroid nodules represented papillary thyroid cancer and we

did thus not evaluate the differences in SWE indices among different types of malignant thyroid nodules. Furthermore, we did not evaluate the intra-operator and inter-operator reliability of SWE measurements of thyroid nodule stiffness. However, a previous study reported that SWE has satisfactory intra-operator (0.65 - 0.78) and inter-operator (0.72 - 0.77) reliability in the evaluation of neck lesions (Bhatia et al., 2012a).

3.5 Conclusions

SWE indices ($E_{maximum}$ and E_{mean}) were independent predictors for thyroid malignancy. Combining GSU with SWE indices (using cut-offs of ≥ 67.3 kPa and ≥ 23.1 kPa for $E_{maximum}$ and E_{mean}, respectively) can improve overall diagnostic accuracy in distinguishing benign and malignant thyroid nodules. SWE is thus a useful adjunct to GSU in the assessment of thyroid nodules.

Chapter Four

Study Two

Computer-aided assessment of regional vascularity of thyroid nodules for prediction of malignancy

4.1 Introduction

Thyroid cancer is the most frequently occurring cancer among all endocrine malignancies. The National Institute of Cancer in the USA registered 64,330 new cases of thyroid cancer in 2016 (Siegel et al., 2016). Despite a wide variation in specificity (54% - 92%) and relatively low sensitivity (66%) of fine needle aspiration cytology (FNAC), it is the current standard method to diagnose thyroid cancer (Wu et al., 2013). Moreover, about 20% - 30% of cytology results remain non-diagnostic with FNAC (Yoon et al., 2011b). Grey-scale ultrasound (GSU) is a common imaging tool for assessing thyroid nodules and different GSU features for identifying malignant thyroid nodules, including micro-calcification, ill-defined borders, hypoechogenicity, an absent halo sign, solid internal structure, and irregular shape, have been reported (Chan et al., 2003, Popli et al., 2012, Wong and Ahuja, 2005, Yunus and Ahmed, 2010). However, GSU assessments of thyroid nodules are subjective and the assessment has thus high inter- and intra-observer variability. In addition, the same features that are used to define malignancy can, even though less frequently, also be found in benign nodules (Anil et al., 2011).

Angiogenesis is a major manifestation of proliferation in neoplastic cells (Weis and Cheresh, 2011, Carmeliet and Jain, 2011). Doppler ultrasound can detect the vasculature of healthy organs and cancerous tissues. Previous studies reported the use of colour Doppler ultrasound and power Doppler ultrasound in the differential diagnosis of prostate cancer, hepatic cancer, ovarian cancer, and breast cancer (Anil et al., 2011, Hossain et al., 2010, Kudo et al., 2004, Shigeno et al., 2000, Tao, 2016). Doppler ultrasound assessments of thyroid cancer vascularity are also reported in the literature. However, the results of these studies are conflicting when describing the usefulness of this technique in detecting malignancy. Several studies indicated that colour Doppler ultrasound has clinical significance in the differential diagnosis of thyroid nodules (Fukunari et al., 2004, Frates et al., 2003, Papini et al., 2002), whilst other studies suggested that colour Doppler ultrasound was not useful in distinguishing benign and malignant thyroid nodules (Rago et al., 1998, Bannier et al., 2010, Moon et al., 2010, Lam et al., 2014, Frates et al., 2005, Bartolotta et al., 2006). These controversial findings might be due to the subjective assessment of thyroid nodules and a lack of standard quantitative methods in previous studies, and these factors cause high inter- and intra-observer variability in the evaluation of the vascularity of thyroid nodules (Moon et al., 2010).

Few reports in the literature found that hypervascularity of a thyroid nodule is an independent predictor of thyroid malignancy (Chan et al.,

2003, Hoang et al., 2007). However, in previous studies, the diagnosis of thyroid cancer was based on visual assessments, which are subjective and highly vulnerable to inter- and intra-observer variability (Wu et al., 2013, Bartolotta et al., 2006). For an accurate and reliable assessment of thyroid nodular vascularity, a quantitative and objective method is needed.

In previous studies, we developed a computer-aided algorithm that can quantify the vascularity of thyroid parenchyma and cervical lymph nodes in colour or power Doppler sonograms (Lam et al., 2014, Ying et al., 2016, Ying et al., 2009). Previous studies suggested that 'peripheral vascularity' is usually associated with benign nodules and 'central vascularity' is common in malignant thyroid nodules (Papini et al., 2002, Frates et al., 2003). However, these previous studies used subjective and qualitative methods to assess the vascular distribution of thyroid nodules, which are not accurate and reliable. In the present study, we modified our previously reported algorithm so that it can perform segmentation of thyroid nodules into peripheral and central regions and quantify the vascularity of these regions. This study also aimed to evaluate the diagnostic accuracy of using regional vascularity of thyroid nodules in differentiating benign and malignant nodules, and to investigate the added value of this new assessment method (i.e. computer-aided assessment of regional vascularity of thyroid nodules) to conventional GSU examinations of thyroid nodules.

4.2 Materials and Methods

This institutional review board-approved retrospective study involved 111 consecutive patients (20 males, 91 females; mean age = 52.5 ± 13.6 years) who were recruited from the Department of Surgery at the Prince of Wales Hospital, Hong Kong. All patients provided informed written consent. The inclusion criteria comprised the presence of thyroid nodule(s) and the availability of cytology/histology results of the nodule(s). Exclusion criteria included associated thyroid diseases (e.g. Grave's disease and Hashimoto disease) and patients with unconfirmed cytological or histological results of the nodules.

4.2.1 Ultrasound evaluation

All patients underwent grey-scale and colour Doppler ultrasound examinations of the thyroid gland on both sides of the neck. An expert sonographer (more than 23 years' experience in ultrasound) carried out all ultrasound examinations using the same scanning protocol. The same ultrasound unit in conjunction with a 4 - 15-MHz linear transducer was used (Aixplorer, Supersonic Imagine, Aix-en-Provence, France).

During ultrasound examination of the thyroid gland, patients lay supine on the examination couch with their shoulders supported by a pillow so that the neck was hyperextended. The patient's head was turned away from the side under examination to facilitate the ultrasound

scanning. The transducer gently scanned over the entire thyroid lobe without exerting pressure onto the patient's neck. After the nodule was localized, multiple transverse and longitudinal images were acquired in grey-scale and colour Doppler ultrasound modes. For each nodule, the grey-scale sonographic features of the thyroid nodule were assessed with GSU, whereas the vascularity of the nodule was evaluated with colour Doppler ultrasound. In GSU, the nodule was assessed for the presence/absence of microcalcification, the regularity of the nodular margins, echogenicity, and the height-to-width ratio of the nodule. The margin of the nodule was classified as either regular or irregular. The echogenicity of nodules was classified into hypoechoic, isoechoic, and hyperechoic, compared to the adjacent thyroid parenchyma. The height-to-width ratio of the nodule was also assessed by measuring the antero-posterior (i.e. height) and medio-lateral (i.e. width) dimensions of the nodule in the transverse scan that showed the maximum cross-sectional area of the nodule. The height-to-width ratio of nodules was classified into ≤ 1 or > 1.

In colour Doppler ultrasound examinations, scanning settings were standardized to ensure high sensitivity, with the use of a medium wall filter and a pulse repetition frequency (PRF) of 1000 Hz. Colour gain was standardized by initially increasing so that the noise was apparent and then gradually decreasing until the noise disappeared (Lam et al., 2014). For each nodule, multiple transverse and longitudinal colour Doppler sonograms were obtained.

Quantitative analysis of colour Doppler sonograms was performed by an independent observer using a customized algorithm incorporated in MATLAB software (version 7.3.0.267 R2006b; The Math Works, Natick, MA, USA). The observer was blind to the clinical diagnosis results. All image analyses were performed in a computer workstation with MATLAB installed. To determine the vascularity of thyroid nodules, the nodule (i.e. the region of interest, ROI) was manually outlined on the Doppler ultrasound image using Microsoft Paint (version 5.1: Microsoft Corporation, Redmond, W.A, USA). After drawing the ROI on the Doppler sonogram, it was saved in tagged image file (TIF) format and further processed with MATLAB. Using the customized software algorithm developed by our team, the ROI was extracted and the number of colour pixels as well as the total number of pixels (grey-scale pixels + colour pixels) were counted. The vascularity index (VI) of the nodule was calculated and expressed as the percentage of the number of colour pixels divided by the total number of pixels within the ROI. This calculation method was the same as described in our previous studies (Ying et al., 2016, Lam et al., 2014, Ying et al., 2009). For each thyroid nodule, the colour Doppler ultrasound image that showed the highest VI was selected for further analysis of the regional vascularity of the nodule.

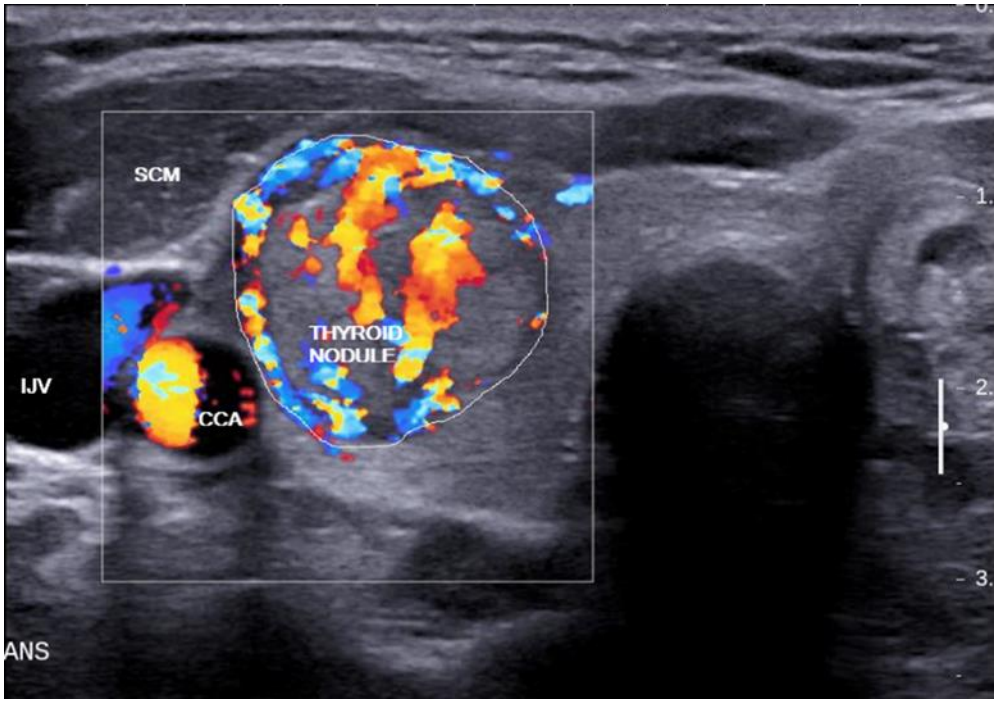

Figure 4.1 Transverse color Doppler sonogram of a nodule in the right thyroid lobe which was proven to be follicular thyroid carcinoma (outlined). The nodule showed both peripheral (arrows) and central (arrowheads) vascularity. SCM, sternocleidomastoid muscle; CCA, common carotid artery; IJV, internal jugular vein.

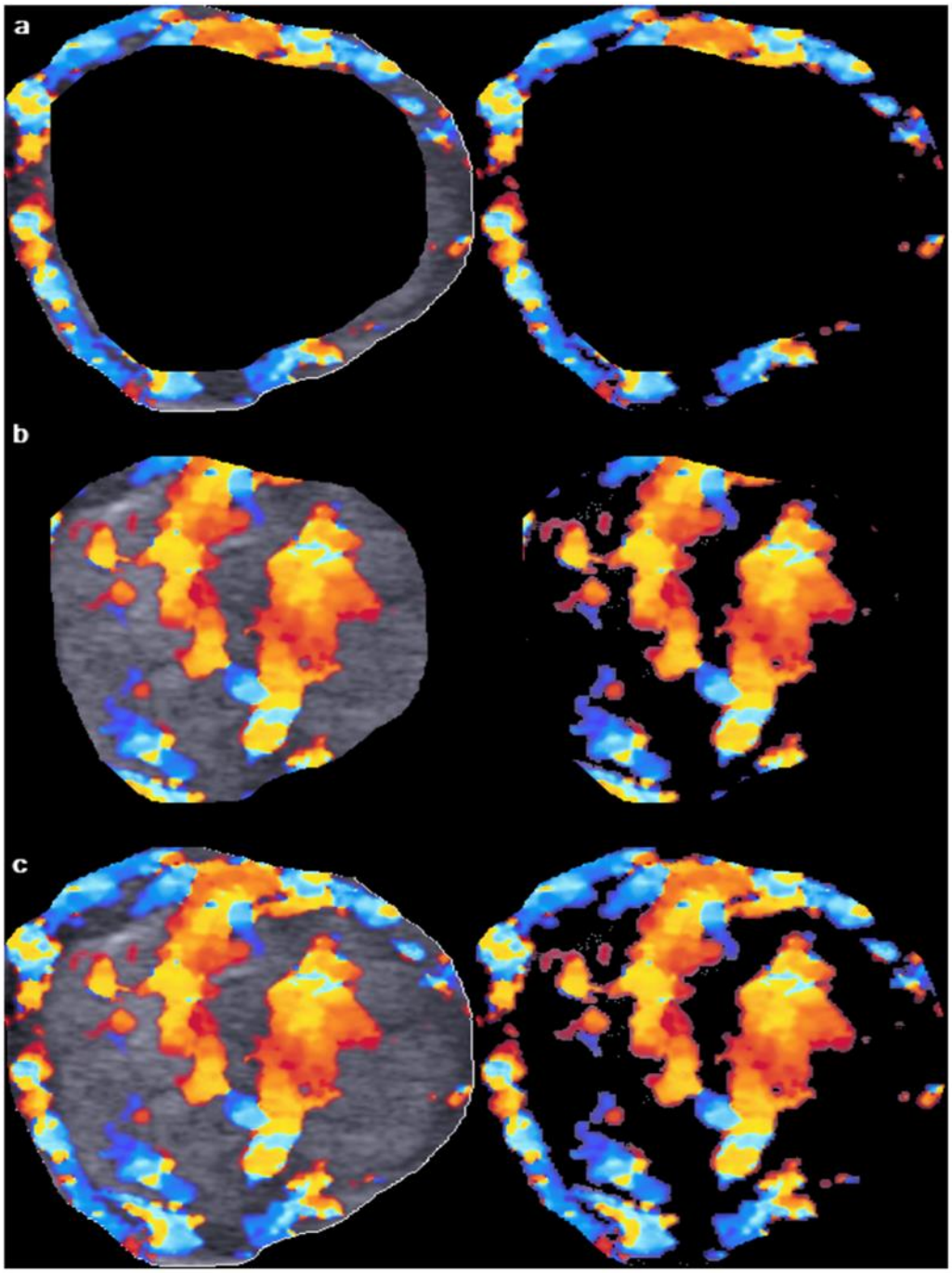

Figure 4.2 Image analysis of peripheral, central, and overall vascular index (VI) of the thyroid nodule as shown in Figure 2. The primary region of interest (ROI), i.e. the thyroid nodule, was extracted from the outlined area. Using an offset level of 10%, the peripheral (a, left) and central (b, left) regions of the nodule

were segmented and the total number of the pixel within the segmented area was counted by the computer algorithm. The color pixels coded by the color Doppler ultrasound were extracted by eliminating the grey-scale pixels, and the color pixels were counted by the algorithm (a right and b, right). The VI of peripheral and central regions of the nodule was the percentage of the number of color pixels to the total number of pixels within the segmented area. The overall VI of the nodule was evaluated by counting the total number of the pixel within the ROI (c, left) and the number of color pixel in the image with the grey-scale pixels eliminated (c, right).

To determine the VI of the peripheral and central regions of the nodule, the primary ROI (i.e. the entire thyroid nodule, Figure 4.1) was sub-divided into peripheral (Figure 4.2a) and central (Figure 4.2b) regions using the so-called ‘offsetting’ method. This sub-division of the nodule was done to investigate whether the vascular distribution is useful for identifying malignant nodules. Figure 4.2c demonstrates the quantification of the overall vascularity of the entire thyroid nodule.

‘Offsetting’ is a method used to increase or decrease the area of arbitrary shapes without distorting the shape and keeping the contour of the ROI. The inner segment (i.e. secondary ROI = central region of the primary ROI) is an inward offset (an operation also known as ‘deflating’ or ‘buffering’ of the primary ROI) (Figure 4.3a and 4.3b). The outer segment is obtained by subtracting the primary ROI by the secondary ROI. (Figure 4.3c). The thickness of the outer segment is determined by the magnitude of the offset (n% offset in Figure 4.3b). The magnitude of offset was varied as a percentage of the maximum diameter of the primary ROI.

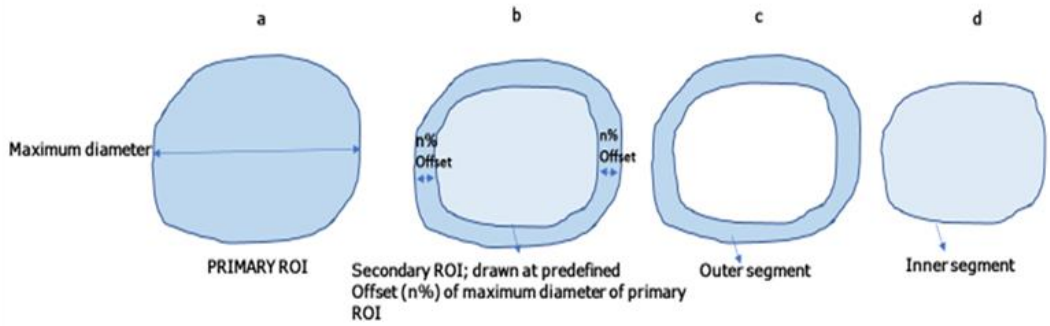

Figure 4.3 Schematic diagrams show the segmentation of peripheral and central regions of a thyroid nodule. After the primary ROI was segmented by the algorithm, the maximum diameter of the ROI was identified (a). With the predefined offset level (n%) given to the algorithm, the secondary ROI was obtained (b). The secondary ROI represents the inner segment (i.e. central region) of the nodule (c). The outer segment (i.e. peripheral region) of the nodule was obtained by subtracting the primary ROI by the secondary ROI (d).

Instead of treating the ROI as a polygon for mathematical offsetting, our algorithm uses a raster image-based approach that iteratively erodes the primary ROI with a small kernel. This approach produces results with the benefit of not having to implement polygon clipping in MATLAB so that the contour of the secondary ROI (i.e. the inner segment of the nodule after offsetting) is smoother and can be maintained as the contour of the primary ROI (i.e. the thyroid nodule).

The optimum offset was determined by exploring the difference in VI between benign and malignant nodules in both inner (i.e. central) and outer (i.e. peripheral) segments. In the present study, we tested a range of offsets with an interval of 5% (i.e. 5%,10%,15%, 20%, and 25%). We did not exceed offset levels of 25%, because previous report suggested that the central region of a thyroid nodule is the inner 90% of the diameter of the nodule (Wu et al., 2013). At each offset level, the VI of the peripheral and central segments of benign and malignant nodules were quantified. The offset level that showed a significant difference ($P < 0.05$) in VI between benign and malignant nodules at both central and peripheral segments was defined as the optimum offset level. The total duration of MATLAB processing of each thyroid nodules to perform setting and to calculate thyroid vascularity in segmented regions is less than a minute. The technique is user-friendly and can be translated to daily clinical use.

The significance of differences in GSU features between benign and malignant thyroid nodules was calculated using Chi-square tests. Unpaired t-tests were used to evaluate the significance of differences in VI between benign and malignant thyroid nodules. Receiver operating characteristic (ROC) curves were used to determine the optimum cut-off of VI in distinguishing benign and malignant thyroid nodules, as well as the associated diagnostic performance at the optimum cut-off level. All statistical analyses were performed using the Statistical Package for the Social Sciences (SPSS) software (Version 24, IBM Corporation, Armonk, NY, USA), and a two-tailed $P < 0.05$ was considered significant.

4.3 Results

4.3.1 Histopathology

The mean age of patients with benign nodules (n = 84) and of patients with malignant nodules (n = 27) was 51.2 ± 12 and 56.6 ± 17.6 years, respectively (P > 0.05). In each patient, a thyroid nodule with confirmed cytological/histological results was included in the study. Among the 111 thyroid nodules in the 111 patients, 62 benign nodules were identified by fine needle aspiration cytology, and the remaining 49 nodules received pathological evaluations after surgical resection. Among these 49 nodules, pathology results revealed 22 benign and 27 malignant nodules (23 papillary thyroid carcinomas, three follicular carcinomas, and one Hurthle cell carcinoma).

4.3.2 Grey-scale ultrasound

GSU evaluations of 111 thyroid nodules showed that malignant nodules tended to show microcalcification (77.8%), were hypoechoic (92.6%), had irregular margins (55.6%), and a height-to-width ratio > 1 (59.3%), whereas these features were less common in benign nodules (microcalcification: 7.1%; hypoechoic: 33.3%; irregular margins: 16.7%; height-to-width ratio > 1: 13.1%). The differences were statistically significant (P < 0.05).

4.3.3 Colour Doppler ultrasound

The results showed that the mean overall vascular index (VI) of malignant nodules (23.8 ± 4.6%) was significantly higher than that of

benign nodules (16.6 ± 1.8%) ($P < 0.05$). Table 4.1 shows the mean VI of the peripheral and central regions of benign and malignant nodules at different offset levels. When the offset level increased from 5% to 20%, the mean VI of the central region of malignant nodules was significantly higher than that of the benign nodules ($P < 0.05$), whereas there was no significant difference in the mean VI of the peripheral region of benign and malignant nodules ($P > 0.05$).

Table 4.1. Vascular index (VI) of peripheral and central regions of benign and malignant thyroid nodules at different offset levels.

Offset levels	Mean Peripheral VI ± SD (*P* value)	Mean Central VI ± SD (*P* value)
5%-Offset Benign Malignant	 21.7 ± 20.3% 23.5 ± 19.3% (0.692)	 15.2 ±15.3% 23.4 ± 17.7% (0.014)
10%-Offset Benign Malignant	 21.4 ± 19.6% 25.3 ± 18.7% (0.324)	 13.5 ± 14.6% 23.3 ± 18.0% (0.021)
15%-Offset Benign Malignant	 20.0 ± 18.4% 24.0 ± 16.6% (0.336)	 12.4 ± 14.5% 22.3 ± 19.3% (0.025)
20%-Offset Benign Malignant	 18.7 ± 17.1% 25.0 ± 17.0% (0.098)	 12.0 ± 14.7% 21.6 ± 20.1% (0.028)
21%-Offset Benign Malignant	 18.4 ± 16.9% 25.0 ± 17.1% (0.083)	 11.9 ± 14.9% 21.3 ± 20.1% (0.031)
22%-Offset Benign Malignant	 18.2 ± 16.7% 26.5 ± 16.2% (0.036)	 11.9 ± 15.1% 21.7 ± 19.6% (0.039)
23%-Offset Benign Malignant	 17.9 ± 16.5% 11.9 ± 15.4% (0.020)	 24.9 ± 17.1% 20.9 ± 20.3% (0.051)
24%-Offset Benign Malignant	 17.8 ± 16.4% 24.9 ± 17.2% (0.013)	 11.9 ± 15.6% 20.6 ± 20.1% (0.065)
25%-Offset Benign Malignant	 17.7 ± 16.3% 26.6 ± 18.7% (0.008)	 11.9 ± 16.0% 20.4 ± 20.1% (0.752)

In contrast, at an offset level of 25%, the mean VI of the peripheral region of malignant nodules was significantly higher than that of the benign nodules ($P < 0.05$), whereas there was no significant difference in the mean VI of the central region of benign and malignant nodules ($P > 0.05$). To determine the optimum offset level, we evaluated the VI of the nodules at the offset levels of 21%, 22%, 23%, and 24%. The results showed that at an offset level of 22%, the mean VI of both central and peripheral regions of malignant nodules was significantly higher than that of benign nodules ($P < 0.05$); we thus determined the optimum offset level to be 22%.

Receiver operating characteristic (ROC) curves demonstrated the optimum cut-off values of VI when the overall VI, peripheral VI, and central VI of the nodule were used to differentiate benign and malignant nodules; the results are summarised in Table 4.2.

Using the overall VI to distinguish benign and malignant nodules, we achieved a diagnostic accuracy of 70.3% with a sensitivity of 74.1%, a specificity of 69%, a negative predictive value (NPV) of 89.2%, and a positive predictive value (PPV) of 43.5% at the optimum cut-off level of 20.2 (Table 4.2).

At the 22% offset, both the peripheral VI and central VI had a diagnostic accuracy of 64% with a sensitivity of 74.1%, a specificity of 60.7%, a NPV of 87.9%, and a PPV of 37.7% at the optimum cut-off levels of 19.7% and 9.1%, respectively (Table 4.2).

Table 4.2. Comparison of the diagnostic performance of peripheral VI, central VI and overall VI at 22% offset in distinguishing benign and malignant nodules.

Color Doppler VI at 22% Offset	Optimum Cut-off (%)	SEN (%)	SPEC (%)	NPV (%)	PPV (%)	Accuracy (%)
Peripheral VI	19.7	74.1	60.7	87.9	37.7	64.0
Central VI	9.1	74.1	60.7	87.9	37.7	64.0
Overall VI	20.2	74.1	69.0	89.2	43.5	70.3

VI, vascular index

SEN, sensitivity

SPEC, specificity

NPV, negative predictive value

PPV, positive predictive value

After determining optimum cut-off levels of the peripheral, central, and overall VI, the criterion was set that a thyroid nodule was considered malignant when all three vascular indices (peripheral VI, central VI, and overall VI) were equal or greater than their respective cut-off values. True positive, true negative, false positive, and false negative cases were evaluated. The diagnostic accuracy of the combined VI assessment in distinguishing benign and malignant nodules was 71.2% (Table 4.3, Figure 4.1).

In the evaluation of the diagnostic performance of GSU, a thyroid nodule was considered malignant when it presented with at least one of the suspicious GSU features (i.e. microcalcification, a height-to-width ratio >1, hypoechoic, and irregular margins). The diagnostic accuracy of GSU in differentiating benign and malignant thyroid nodules was 58.6% (Table 4.3). The diagnostic performance of combining GSU and VI was determined based on the criterion that a thyroid nodule was malignant when it presented with at least one suspicious GSU feature and the combined VI was equal to or greater than the optimum cut-offs (i.e. peripheral VI > 19.7%, central VI > 9.1%, and overall VI > 20.2%). The combination of colour Doppler VI and GSU significantly increased the overall diagnostic accuracy from 58.6% to 79.3% ($P < 0.05$) (Table 4.3, Figure 4.1).

Table 4.3: Comparison between diagnostic performance of grey scale ultrasound, combined color Doppler vascular indices and their combination in the differentiation of benign and malignant thyroid nodules.

	SEN (%)	**SPEC (%)**	**NPV (%)**	**PPV (%)**	**Accuracy (%)**
GSU alone	96.3	46.4	97.5	36.6	58.6
Combined vascular indices	70.4	71.4	88.2	44.2	71.2
Combined vascular indices + GSU	66.7	83.3	88.6	56.3	79.3

GSU, grey scale ultrasound

SEN, sensitivity

SPEC, specificity

NPV, negative predictive value

PPV, positive predictive value

4.4 Discussion

Angiogenesis has been reported as an important manifestation of proliferation in cellular neoplasms and is linked to malignancy (Appetecchia and Solivetti, 2006, Lyshchik et al., 2007, Varverakis et al., 2007). Increased vascularization in the central region of thyroid nodules detected on Doppler ultrasound is an indication for fine needle aspiration cytology (FNAC) of the nodules, as recommended in the guidelines provided by the American Association of Clinical Endocrinologists (AACE), the American College of Endocrinology (ACE), and the Associazione Medici Endocrinologi (AME) (Papini et al., 2002, Mandel, 2004, Nodules, 2006, Frates et al., 2003).

One previous study evaluated 254 thyroid nodules and found that the prevalence of malignancy was higher (41.9%) in hypervascular nodules than in hypovascular nodules, whereas only 14% of malignant cases were reported (Frates et al., 2003). In another study, the vascularity of 55 cases of papillary thyroid carcinoma was evaluated, and the results show that 19% had central vascularity (Chan et al., 2003). Rago et al. (1998) evaluated the vascular pattern of benign and malignant thyroid nodules and found that there was no significant difference between the two (Rago et al., 1998). Moon et al. (2010) reported that assessments of thyroid nodular vascularity alone or in combination with GSU features were not as useful as GSU features alone in predicting thyroid malignancy (Moon et al., 2010). However, Brunese et al. (2008), Fobbe et al. (1998), Chammas et al. (2005), and Varverakis et al. (2007)

found that intranodular vascularity was significantly associated with thyroid malignancy. The controversial findings of previous studies may be due to the fact that thyroid nodular vascularity was subjectively evaluated, and that blood flow in peripheral and central regions of nodules was assessed by visual judgement rather than by a standardised quantitative method. The subjective visual assessment of intranodular vascularity is prone to inter- and intra-observer variations and the results may therefore not be accurate.

In the present study, we have developed an innovative method that can automatically divide thyroid nodules into central and peripheral regions on sonograms and compute the overall VI of the nodule as well as the regional VI of the peripheral and central areas of the nodule. Standardised and automated regional subdivision of thyroid nodules and quantification of regional vascularity of nodules are useful to eliminate human errors and variances in the assessment of intranodular vascularity of thyroid nodules. In this study, we found that a 22% offset level is optimal in the differentiation of benign and malignant nodules. To the best of our knowledge, this is the first study that uses a computer-aided method to subdivide thyroid nodules into different regions in ultrasound images, and quantify the regional vascularity of the nodule.

Lyshchik et al. (Lyshchik et al., 2007) analysed power Doppler images of 86 thyroid nodules and found significant increases in central vascularity of benign nodules with increases in tumour size. The authors

found that the sensitivity and specificity in assessing intranodular vascularity varied with the size of the thyroid nodule, and they suggested that quantitative analysis is useful for assessing nodules smaller than 2 cm. However, only the overall vascularity of the nodules was evaluated in this, study whereas a regional subdivision of the nodule and an analysis of regional vascularity were not performed (Lyshchik et al., 2007).

Sultan et al. (Sultan et al., 2015) analysed 100 thyroid nodules and quantified the vascular fraction area, the mean flow velocity index, and the flow volume index of thyroid nodules in Doppler ultrasound images. Without assessing the diagnostic accuracy to determine the optimal separation of different regions of the nodule, they manually segmented thyroid nodules into three equal sections (peripheral, intranodular, and surrounding parenchyma). The authors concluded that quantitative evaluation of central vascularity of thyroid nodules has higher value in the differential diagnosis of benign and malignant nodules. In Sultan et al. (Sultan et al., 2015), manual segmentation was used to divide the nodule into different regions. This method was subjective and prone to lead to intra- and inter-operator variations. In comparison to Sultan et al. (2015), we adopted a more standardized method by using a dedicated algorithm that uses the optimum offset level to divide the thyroid nodule into peripheral and central regions, accurately and objectively. Using the same optimum offset level, different thyroid nodules can be assessed

consistently, and the same regional division of nodules can be performed. The new approach developed in the present study is more robust, objective, and highly reproducible, with a quantitative evaluation of vascularity that could not be achieved with visual inspection methods.

In this study, 27 malignant and 84 benign thyroid nodules were analysed. The calculated power of this sample size in assessing the diagnostic performance of regional vascularity of thyroid nodules in distinguishing malignant and benign nodules ranged between 0.62 and 0.71. A further study with a larger sample size is suggested. Besides the sample size, there is another limitation of the present study. Of the malignant nodules in the study, the majority represented papillary thyroid carcinoma (n = 23), only three cases were follicular carcinoma, and one case represented Hurtle cell carcinoma. The value of assessing intranodular VI in distinguishing different types of malignant nodule was thus not determined in this study.

4.5 Conclusions

To conclude, the present study developed a novel image processing algorithm which allows accurate and objective division of thyroid nodules into peripheral and central regions in ultrasound images. The algorithm also allows the quantification of VI of the peripheral and central regions of thyroid nodules. Our results show that the optimum offset level of dividing central and peripheral vascularity of thyroid nodules is 22%. Malignant thyroid nodules tend to be more vascular than benign nodules. The optimum cut-off values of VI for overall, peripheral, and central vascularity in differentiating benign and malignant thyroid nodules were 20.2%,19%, and 9.1%, respectively. The combination of VI assessment and GSU can improve the diagnostic accuracy for thyroid malignancy.

Chapter Five

Study Three

AngioPLUS enhances the sensitivity of colour flow Imaging and directional colour power imaging in assessing the vascularity of the thyroid gland

5.1 Introduction

Doppler ultrasound is a non-invasive imaging technique that can assess the vasculature of organs and soft tissues. In the assessment of the thyroid gland, the detection of blood flow is of utmost clinical importance, as it helps the differential diagnosis of thyroid diseases such as Graves' disease, Hashimoto's disease, acute thyroiditis, and thyroid neoplasms (Demaj et al., 2016, Venkateswarulu and Gowni, 2017, Shah, 2016, Aggarwal et al., 2017). Certain thyroid diseases are associated with hypervascularity of the gland, such as papillary thyroid carcinoma, Grave's disease, thyrotoxicosis, and acute thyroiditis (Gong et al., 2016, Xue et al., 2016), whilst diminished blood flow to the thyroid parenchyma is common in most benign or cystic thyroid nodules and hypo-functioning thyroid glands (Rago et al., 1998). Another useful application of Doppler ultrasound is to monitor treatment responses of patients with thyroid diseases by serial assessment of thyroid vascularity (Lagalla et al.,

1998). Colour Doppler ultrasound (CDU) is commonly used to assess the vascularity of soft tissues including the thyroid gland (Fleischer et al., 1999, Lee et al., 2016). Power Doppler ultrasound (PDU) is less dependent on the ultrasound beam insonation angle and has significant clinical value in detecting blood flow with high sensitivity (Cao and Yuan, 2011, Chammas et al., 2005).

Most recently, a new ultrasound technology, namely AngioPLUS (Planewave UltraSensitive™ imaging), provides superb sensitivity in the detection of soft tissue vascularity. The advantage of this technique is that all colour pixels of the soft tissue can be reconstructed in a single image (Bercoff, 2016). This is achieved by using a plane of non-focused ultrasound waves that are sent into the body at the maximum allowed pulse repetition. AngioPLUS provides high resolution and 3D wall filtering that allow efficient discrimination between blood flow and other soft tissues by analysing space, time, and amplitude information (Bercoff, 2016).

Anatomical asymmetries exist between the right and left thyroid lobes. A previous study that included thyroid glands of 62 healthy volunteers reported differences in size and volume between the right and left thyroid lobes. The results of this study suggested that the right thyroid lobe is larger in volume and size than the left thyroid lobe ($P<0.05$) (Ying and Yung, 2009). Another study that involved the assessment of anatomical variations of thyroid glands in 72 cadavers reported that the

mean size of the right thyroid lobe was larger than the mean size of the left thyroid lobe (Prakash et al., 2012). Moreover, the right thyroid lobe is slightly higher in position than the left thyroid lobe (Ahuja and Evans, 2000). Considering these differences in anatomical relations of the thyroid gland, it would be of great clinical interest to evaluate whether there exist any asymmetries in the vasculature of the two thyroid lobes. Since certain thyroid diseases alter the vascularity of the thyroid parenchyma, knowing the differences in vascularity of the right and left thyroid lobes may help to establish the differential diagnosis of thyroid diseases. Ying et al. (2009) evaluated the asymmetry in vascularity of the right and left thyroid lobes by using conventional colour Doppler and power Doppler ultrasound and found no significant difference between the two lobes of the thyroid (Ying et al., 2009). In this prospective study, we hypothesized that AngioPLUS can increase the sensitivity of Doppler ultrasound in the detection of thyroid vascularity. To the best of our knowledge, this is the first study that investigated the value of AngioPLUS in ultrasound assessments of thyroid vascularity. The aims of the present study were to evaluate the differences in the detection of thyroid vascularity when using CDU, PDU, CDU+AngioPLUS, and PDU+AngioPLUS, and to explore differences in vascularity between the right and left thyroid lobes.

5.2 Materials and Methods

It was a prospective study. The Human Subject Ethics Subcommittee of the Hong Kong Polytechnic University approved this study. Informed written consent was obtained from all subjects recruited in the study, and their data was protected according to the research data protection policies of our institution. The same operator (Faisal N. Baig) performed all study procedures including the ultrasound examination, and a standardized scanning protocol was used. All ultrasound examinations were performed using the same ultrasound unit in conjunction with a 2 - 10-MHz linear transducer (SuperLinear™ SL10-2, Aixplorer, Supersonic Imagine, Aix-en-Provence, France).

A total of 49 healthy volunteers without personal or familial medical history of thyroid disease or relevant signs and symptoms were recruited for this study. Exclusion criteria included the detection of thyroid nodule(s) on grey-scale ultrasound or failure to receive consent from the participant. Physical examinations of the thyroid and serum blood tests for assessing physiological thyroid function were not performed in the subjects, due to ethical issues regarding the collection of blood samples from healthy volunteers.

Grey-scale ultrasound examinations of the thyroid gland were conducted to detect any thyroid nodules in the thyroid lobes. Subjects were asked to lie supine on the examination couch with their neck hyperextended, and a pillow was placed underneath their shoulders for

support. Both sides of the neck were examined, and the subject's head was turned away from the side under examination. Coupling gel was applied to the subject's neck for scanning. Transverse and longitudinal scans were performed from the base of the jaw to the clavicle, and the entire thyroid lobe was examined to detect thyroid nodules. Subjects with thyroid nodules detected in the ultrasound examination were excluded from the study. For subjects without detected thyroid nodules, transverse and longitudinal scans of both thyroid lobes were performed. At the transverse and longitudinal scan planes showing the maximum cross-sectional area of the thyroid lobe, Doppler ultrasound examinations were performed using the following Doppler techniques:

1. CDU
2. CDU+AngioPLUS
3. PDU
4. PDU+AngioPLUS

For PDU, directional power Doppler imaging was used in this study. For each Doppler technique, multiple images showing the thyroid vascularity were acquired (Figure 5.1). Settings of all Doppler techniques were standardized to achieve high sensitivity, and a medium wall filter was used to detect low flow blood vessels within the thyroid parenchyma. To achieve the optimal colour gain setting, the colour gain was first increased to the maximum level and then gradually reduced to the level

where the noise just disappeared. Frequency of AngioPLUS was adjusted to 27Hz.

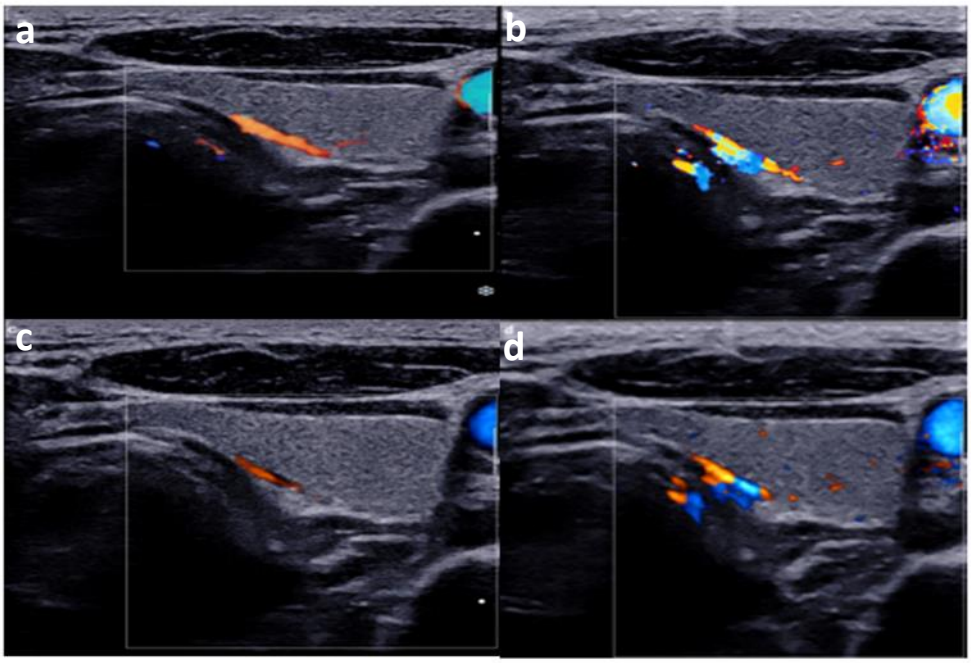

Figure 5.1: Illustration of differences in vascularity detected in left transverse thyroid lobe assessed by (a) Color Flow Imaging (b) Color Flow Imaging + AngioPLUS (c) Directional Color Power Imaging (d) Directional Color Power Imaging + AngioPLUS

Persistence was standardized at ‘medium’ level. For both transverse and longitudinal scans of each thyroid lobe, the three CDU, CDU+AngioPLUS, PDU, and PDU+AngioPLUS images with the most abundant vascularity were chosen for vascularity quantification. Therefore, for each subject, a total of 24 images from the right lobe (12 transverse and 12 longitudinal scan images) and 24 images from the left lobe (12 transverse and 12 longitudinal scan images) were analysed. The Doppler ultrasound images were then exported to an external computer workstation in JPEG format. In each Doppler ultrasound image, the thyroid lobe (i.e. the region of interest, ROI) was outlined manually (Figure 5.2a) in Adobe Photoshop software (version 8.0, Adobe Systems Incorporated, San Jose, CA, USA). The Doppler ultrasound images with manually outlined ROIs were analysed with MATLAB software (version 7.3.0.267 R2006b) in conjunction with our previously established quantification algorithm (Ying et al., 2009, Lam et al., 2014). Briefly, the algorithm extracts the ROI from the Doppler ultrasound image and counts the total number of pixels as well as the number of colour pixels within the ROI. The vascularity index (VI) was calculated in percentage expressed as the number of colour pixels within the ROI divided by the total number of pixels (colour + grey-scale pixels) within the ROI.

For the transverse scan of each thyroid lobe, three images were analysed for each Doppler technique. Among these three images, the one with the highest VI was selected for the data analysis. A similar image selection was applied for the four Doppler techniques as well as for the

longitudinal scan of each thyroid lobe. Therefore, for each thyroid lobe, a total of four transverse Doppler ultrasound images (one each for CDU, CDU+AngioPLUS, PDU, PDU+AngioPLUS) and four longitudinal Doppler ultrasound images (one each for CDU, CDU+AngioPLUS, PDU, and PDU+AngioPLUS) were included in the data analysis. For each Doppler technique, the total VI of the thyroid lobe was calculated as the summation of the VI in the transverse and longitudinal Doppler ultrasound images.

In the current study, the thyroid vascularity between CDU and CDU+AngioPLUS as well as between PDU and PDU+ AngioPLUS was compared. The Shapiro-Wilk test was used to determine the normality of the vascular indices of the right and left thyroid lobes (when sample size was < 50, n = 45) whilst the Kolmogorov-Smirnov test was used to evaluate the normality of the vascularity index assessed by different ultrasound modalities (sample size > 50, n = 90). Parametric tests were used when the data was normally distributed, whereas non-parametric tests were used when the data was not normally distributed. Paired t-tests were used to determine the level of significance of differences in thyroid vascularity between different Doppler ultrasound techniques. The Wilcoxon signed-rank test was used to determine the significance of differences in vascularity between the left and right thyroid lobes. All statistical analyses were performed using the Statistical Package for the Social Sciences (SPSS) software (version 20, IBM Corporation, Armonk, NY, USA) and a two-tailed *P* value < 0.05 was considered significant.

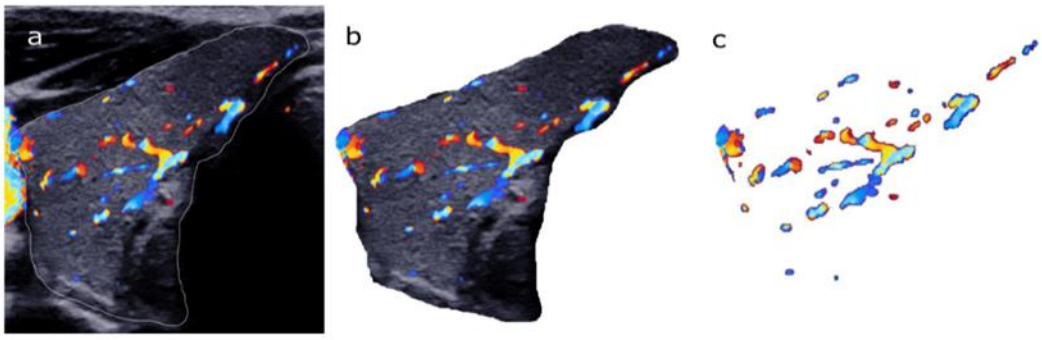

Figure 5.2: The sequence of image analysis of combination of color flow imaging + AngioPLUS (a) illustrates region of interest, ROI i.e. transverse view of right thyroid lobe in 28-year-old male healthy volunteer (b) represents extraction of ROI with use of dedicated algorithm that quantifies number of colors and grey pixels to deduce vascularity within the ROI (c) shows vascularity within the ROI (vascular index 12.47%).

5.3 Results

Among the 49 subjects that were recruited, one subject refused to provide consent and three subjects were found to have thyroid nodules and were therefore excluded from the study. There were 12 females and 33 males, and the age range of the subjects was 22 - 51 years (mean age: 29.6 years). Of the 45 subjects included in the study, a total of 90 thyroid lobes (45 right + 45 left) were assessed with the four Doppler ultrasound techniques, and the VI of the thyroid lobes was evaluated.

The results suggested that the mean VI of thyroid lobes in CDU+AngioPLUS (14.7 ± 9.4%) was significantly higher than that in CDU (8.8 ± 7.3%) ($P < 0.05$). Similarly, the mean VI of thyroid lobes in PDU+AngioPLUS (13.4 ± 9%) was significantly higher than that in PDU (4.7 ± 5.4%) ($P < 0.05$).

In the comparison between colour Doppler and power Doppler ultrasound, the mean VI of thyroid lobes in CDU and CDU+AngioPLUS was significantly higher than that in PDU and PDU+AngioPLUS, respectively ($P < 0.05$).

Comparing the VI between the right and left thyroid lobes as evaluated by the same Doppler ultrasound technique, there was no significant difference ($P > 0.05$) (Table 5.1).

Table 5.1: Comparison of vascularity index between right and left thyroid lobes as evaluated using color Doppler ultrasound (CDU), power Doppler ultrasound (PDU) and their combination with AngioPLUS.

Doppler Ultrasound Techniques	Median (Interquartile range)		
	Left thyroid lobes (n=45)	Right thyroid lobes (n=45)	*P-value*
CDU	6.5 (8.3)	6.1 (9.6)	0.349
CDU+AngioPLUS	12.5 (13.6)	12.7 (17.1)	0.302
PDU	2.6 (5.5)	3.0 (6.6)	0.219
PDU+AngioPLUS	10.8 (11.4)	9.5 (14.4)	0.401

Table 5.2. Comparison of vascularity index of 90 thyroid lobes measured with color Doppler ultrasound (CDU), power Doppler ultrasound (PDU) and their combination with AngioPLUS.

VI of thyroid lobes	Number of thyroid lobes (%)			
	CDU	CDU+AngioPLUS	PDU	PDU+AngioPLUS
0	0	0	4 (4.4%)	0
< 0.1	55 (61.1%)	37 (41.1%)	73 (81.1%)	44 (48.9%)
≥0.1 and <0.2	28 (31.1%)	24 (26.7%)	9 (10%)	26 (28.9%)
≥0.2 and <0.3	5 (5.6%)	25 (27.8%)	4 (4.4%)	16 (17.8%)
≥0.3 and <0.4	2 (2.2%)	3 (3.3%)	0	3 (3.3%)
≥0.4 and < 0.5	0	1 (1.1%)	0	1 (1.1%)
≥ 0.5	0	0	0	0

5.4 Discussion

Doppler ultrasound has clinical value in the differential diagnosis of thyroid diseases (Donkol et al., 2013, Eaton et al., 2002, Corona et al., 2008). CDU and PDU have provided promising results in assessing the vascularity of target soft tissues and organs (Corona et al., 2008, Ceylan et al., 2014). However, imaging of smaller blood vessels and vessels with low blood flow is critical, because changes in vascularity may be subtle in some patients, particularly in patients who are at the early stage of the disease or at the early stage of treatment. Power Doppler ultrasound has limited temporal and spatial resolution when assessing slow blood flow velocities in tortuous and smaller vessels (Rubin et al., 1996). Therefore, quantification of VI in soft tissues or organs with small blood vessels is needed to be re-evaluated when using CDU or PDU.

Most recently, a new microvascular imaging technology, AngioPLUS, has been made available, which can improve colour sensitivity and spatial resolution of Doppler ultrasound imaging while maintaining the image quality of grey-scale ultrasound. The present study prospectively evaluated the VI of thyroid glands of 45 healthy subjects with CDU, PDU, and their respective combination with AngioPLUS. The results of the study showed that there was a significant increase in the VI of the thyroid lobes when CDU (8.8 ± 7.3%) or PDU (4.7 ± 5.4%) were combined with AngioPLUS (14.7 ± 9.4% and 13.4 ± 9%, respectively). The higher VI of the thyroid glands when using AngioPLUS was probably

due to the technique's higher sensitivity in detecting weak Doppler signals from slow blood flow in minute blood vessels. The higher sensitivity of AngioPLUS in detecting weak Doppler signals owes to the 3D wall filtering which allows efficient discrimination between blood flow and tissue by analysing space, time, and amplitude information (Bercoff, 2016).

In the present study, vascular signals were detected on all thyroid lobes as evaluated by the four Doppler ultrasound techniques, except for four thyroid lobes that did not demonstrate vascular signals on PDU. Most of the thyroid lobes that demonstrated vascularity on Doppler ultrasound had a VI < 0.3 (95.5% - 97.8%). Less than 5% of thyroid lobes had a VI between 0.3 and 0.5, and none of the thyroid lobes had a vascular index > 0.5 (Table 2). These findings are consistent with previous studies showing that normal thyroid glands have minimal to moderate vascularity whereas hypervascularity is usually associated with thyroid pathologies (Godding and Clark, 1992, Folkman, 1986, Lohan et al., 2008). Despite higher sensitivity of AngioPLUS in detecting minute blood vessels, none of the thyroid lobes in the present study demonstrated abnormal hypervascularity in CDU+AngioPLUS and PDU+AngioPLUS.

Some previous reports suggested that the right thyroid lobe is generally more vascular than the left thyroid lobe (Lanzer and Topol, 2013, Kohn et al., 1993, Salvatore et al., 2011). However, in our study, no significant differences in the VI of the right and left thyroid lobes were found. This finding is in agreement with our previous study that suggested

that there is no asymmetry in vascularity between the right and left thyroid lobes (Ying et al., 2009).

The main purpose of study 3 was to determine the value of AngioPLUS in combination with colour Doppler ultrasound and power Doppler ultrasound to detect thyroid vasculature in normal thyroid parenchyma. This study only involved healthy volunteers and thyroid cancer patients were not included because of limited time of the study and unavailability of significant number of thyroid cancer patients. However, the results of study 3 can be translated to the vascularity of thyroid nodules as both the normal thyroid parenchyma and thyroid nodules have tiny, subtle vasculature with minute blood flow or blood flow at slower rate. The results of the present study suggest that AngioPLUS has significantly increased the sensitivity of CDU and PDU in detecting blood flow through thyroid parenchyma. These results have clinical value when translating to thyroid nodules that AngioPLUS in combination with CDU or PDU, based on increased sensitivity in detection of tissue vascularity, allows more accurate assessment of thyroid nodule vascularity of which the sensitivity in detecting tiny and subtle vascularity is increased.

AngioPLUS has the potential to be used in the differential diagnosis of thyroid diseases, as most thyroid diseases alter the vascularity of the thyroid gland. Some thyroid diseases such as Graves' disease and thyrotoxicosis increase thyroid vascularity (Arslan et al., 2000), whilst

other pathological conditions such as hypothyroidism and Riedel's thyroiditis cause reduced blood supply to the thyroid gland (Shrestha and Hennessey, 2015). AngioPLUS can thus provide useful and accurate information to help the disease diagnosis. Angiogenesis in cancer involves the formation of minute blood vessels. With the advent of AngioPLUS, it may be useful to detect angiogenesis of thyroid nodules facilitating early diagnosis of neoplasms. Further studies investigating the value of AngioPLUS in identifying malignant thyroid nodules are needed.

A limitation of this study is that thyroid function tests were not performed in the subjects, due to ethical issues regarding the collection of blood samples from healthy volunteers. Moreover, only healthy subjects were recruited for this study and a comparison of the VI between normal and abnormal thyroid glands was thus not conducted.

5.5 Conclusions

In conclusion, AngioPLUS is a useful ultrasound imaging technique that increases the sensitivity of CDU and PDU in mapping the vasculature of the thyroid gland. Using a dedicated algorithm to quantify thyroid vascularity was feasible in images obtained from different Doppler ultrasound techniques. This computer-aided quantification method allows objective and accurate evaluation of thyroid vascularity.

Chapter Six

Study Four

JWH-133 (cannabinoid receptor agonist 2) induces death in papillary thyroid cancer cell lines

6.1 Introduction

Despite their recreational and palliative use, several studies have documented the potential anti-cancer role of cannabinoids in *in vitro* and *in vivo* experiments (Maida and Daeninck, 2016, Sarfaraz et al., 2006, De Petrocellis et al., 2013, Velasco et al., 2016). Certain studies have claimed that cannabinoids induce autophagy in several cancer cell lines (Salazar et al., 2009a, Salazar et al., 2009b, Koay et al., 2014, Dando et al., 2013, Donadelli et al., 2011).

Autophagy is an essential, catabolic degradation process that removes damaged or long-lived proteins from the cell to sustain cellular metabolism and homeostasis. The ultimate outcome of autophagy relies upon the internal cellular context and the strength and duration of signalling inducing autophagy. In the case of cancer, autophagy plays a dual role. It can act via a cytoprotective mechanism by removing the damaged proteins or organelles and thus limit the tumour cell growth

(Mathew et al., 2009), or it may act through the mechanism of programmed cell death induced by sustained autophagy or prolonged stress stimuli (Yang et al., 2011).

Previous literature has shown cross-talk between ER stress and autophagy (Verfaillie et al., 2010). Different conditions, which induce ER stress, also contribute to the initiation of autophagy (Yorimitsu and Klionsky, 2007). It is well established that under normal physiological conditions, the ER is responsible for protein translocation, protein folding, protein transportation to the Golgi apparatus, and the protein's further determination, either secretion from vesicles or display on the plasma surface (Schwarz and Blower, 2016).

Cannabinoid agonists, when binding to their endogenous receptors, perturb the physiological function of the ER, leading to the accumulation of unfolded proteins in the lumen of the ER. A sustained increase in the accumulation of unfolded protein triggers ER stress, resulting in a condition called 'unfolded protein response' (UPR) (Sano and Reed, 2013). UPR can be marked by three signalling proteins: (1) activating transcription factor 6 (ATF-6), (2) inositol-requiring protein 1-α (IRP1-α), and (3) protein kinase RNA-like ER kinase (PERK). Under physiological conditions, the luminal domains of ATF-6 and PERK remain activated and bound to binding immune globulin protein (BiP). However, a bond cleavage occurs between BiP and ATF-6 or PERK, due to the increased load of unfolded proteins in the lumen of the ER. The released BiP

facilitates the folding of accumulated proteins. However, free ATF-6, PERK, and IRP1-α are activated upon binding with accumulated proteins. This leads to the initiation of signal transduction events that promote the accumulation of misfolded proteins in the ER and inhibit the transportation of misfolded proteins from the lumen of the ER to the cytosol, resulting in 'ER-assisted degradation' (Sano and Reed, 2013).

The activation of autophagy due to prolonged ER stress and a progressive increase in the accumulation of unfolded proteins relies on the accumulation of *de novo* ceramide that causes dilation of the lumen of the ER and phosphorylation of eukaryotic translation initiation factor 2A (EIF2A). This causes upregulation of CHOP-, ATF-4-, and TRB3-dependent inhibition of the Akt/mTORc1 axis, and stimulation of autophagy. In several studies, ER stress-mediated autophagy-induced cancer cell death has been regarded as an upstream pathway of autophagy (Salazar et al., 2009b, Armstrong et al., 2015). One recent study reported the distinguished distribution of both cannabinoid receptors (cannabinoid receptor 1, CB1, and cannabinoid receptor 2, CB2) on surgical sections of papillary thyroid carcinoma (PTC) (n = 44) and benign thyroid nodules (n = 43), as assessed by immunohistochemistry analysis. The authors found that CB2 expression had a significantly higher association with PTC samples than with benign nodules (Armstrong et al., 2015). PTC is the most common (80% - 85%) malignancy among all types of thyroid cancer (Gild et al., 2011).

However, the literature is devoid of any reports on the effect of cannabinoid receptor 2 agonists in treating PTC.

In the current study, we particularly aimed to investigate whether JWH-133 (a cannabinoid receptor 2 agonist) induces cell death in normal and papillary thyroid cancer cell lines (BCPAP). We further aimed to investigate whether cannabinoid-induced cell death is a direct apoptosis effect or a consequence of autophagy-mediated apoptosis.

6.2 Materials and Methods

6.2.1 Cell lines and reagents

The human normal thyroid follicular epithelial cell line N-thy-ori-3 and the human papillary thyroid cancer cell line B-CPAP were purchased from the European Collection of Cell Cultures (ECACC, UK) and the Leibniz Institute Deutsche Sammlung von Mikroorganismen und Zellkulturen GmbH (DSMZ, Germany), respectively. Cannabinoid agonist drug (JWH-133 in Tocrisolv 100, Batch #7A/188276), cannabinoid antagonist (SR 144528 Batch #1A/184807), and drug base solution (Tocrisolv 100 Batch #10A/173443) were purchased from Tocris, UK. A cell proliferation kit (MTT) was purchased from Roche Diagnostics, Germany.

6.2.2 Cell cultures

Both cell lines were cultured in RPMI Medium1640 (Gibco® Life Technologies™) supplemented with 10% FBS (Gibco® Life Technologies™), L-glutamine, and 2.0 g/L $NaHCO_3$ at standard cell culture conditions (37 ºC, 100% humidity, 5% CO_2).

6.2.3 Determination of cell metabolism and proliferation

Ten thousand cells from each cell line (N-thy-ori-3 and B-CPAP) were resuspended in 100 µl RPMI1640 medium and treated with different concentrations (0, 5, 10, 15, 20, 25, 30 µM) of JWH-133 followed by incubation for 24, 48, and 72 hours at 37 ºC under 100% humidity and 5% CO_2. Untreated cells were used as a control for each time point. At

the end of the treatment, cells were further incubated with 10 µl MTT solution for 4 hours. Purple formazan crystals were formed, which were solubilized with 100 µl MTT solubilization solution and incubated for another 12 hours in humidified atmosphere (37 ºC, 5% CO2). Optical density was measured by using the Microplate Manager (Bio-Rad, USA, version 5.2) at an absorbance of 550 nm -660 nm. Each condition was performed in triplicate. Means were calculated and expressed as percent viability relative to controls. Data are shown as mean ± standard deviation.

To inhibit the effect of JWH-133, 4 µM of SR 144528 (selective cannabinoid receptor 2 antagonist) were added 20 minutes post treatment with JWH-133 at concentrations of 0, 5, 10, 15, 20, 25, and 30 µM for 24, 48, and 72 hours.

6.2.4 Statistical Analysis

One-way ANOVA was used to determine whether JWH-133 treatment had a significant effect on cell viability at different concentrations, and, specifically, to evaluate the significance of the interaction between predictors (drug concentration, type of cells, and time points) and outcomes (an optical density; O.D value representing cell viability).

All statistical analyses were performed using the Statistical Package for the Social Sciences (SPSS) software (Version 20, IBM Corporation, Armonk, NY, USA) and a two-tailed *P* value < 0.05 was significant.

6.3 Results

6.3.1 JWH-133 inhibits cell viability of BCPAP cells

The viability of N-thy-ori-3 and BCPAP cells treated with different concentrations of JWH-133 was determined using an MTT assay and are summarised in Figure 6.1. In N-thy-ori-3 cells, after 24 hours of incubation, JWH-133 induced a decrease in cell viability at doses of 25 and 30 µM, but the difference did not reach statistical significance (Figure 6.1a). After 48 hours of incubation, JWH-133 was shown to induce cell death in a dose-dependent manner, with a slight decrease in viability at a dose of 20 µM, reaching statistical significance at a dose of 30 µM. After 72 hours, the results were more stable, showing significant decreases at doses of 25 and 30 µM of JWH-133.

In BCPAP cells after 24 hours of incubation, JWH-133 induced a significant decrease of > 50% in viability at doses of 25 and 30 µM ($P < 0.05$) (Figure 6.1b). These results remained consistent after a 48- and a 72-hour incubation, showing a progressive decrease in viability in a dose-dependent manner.

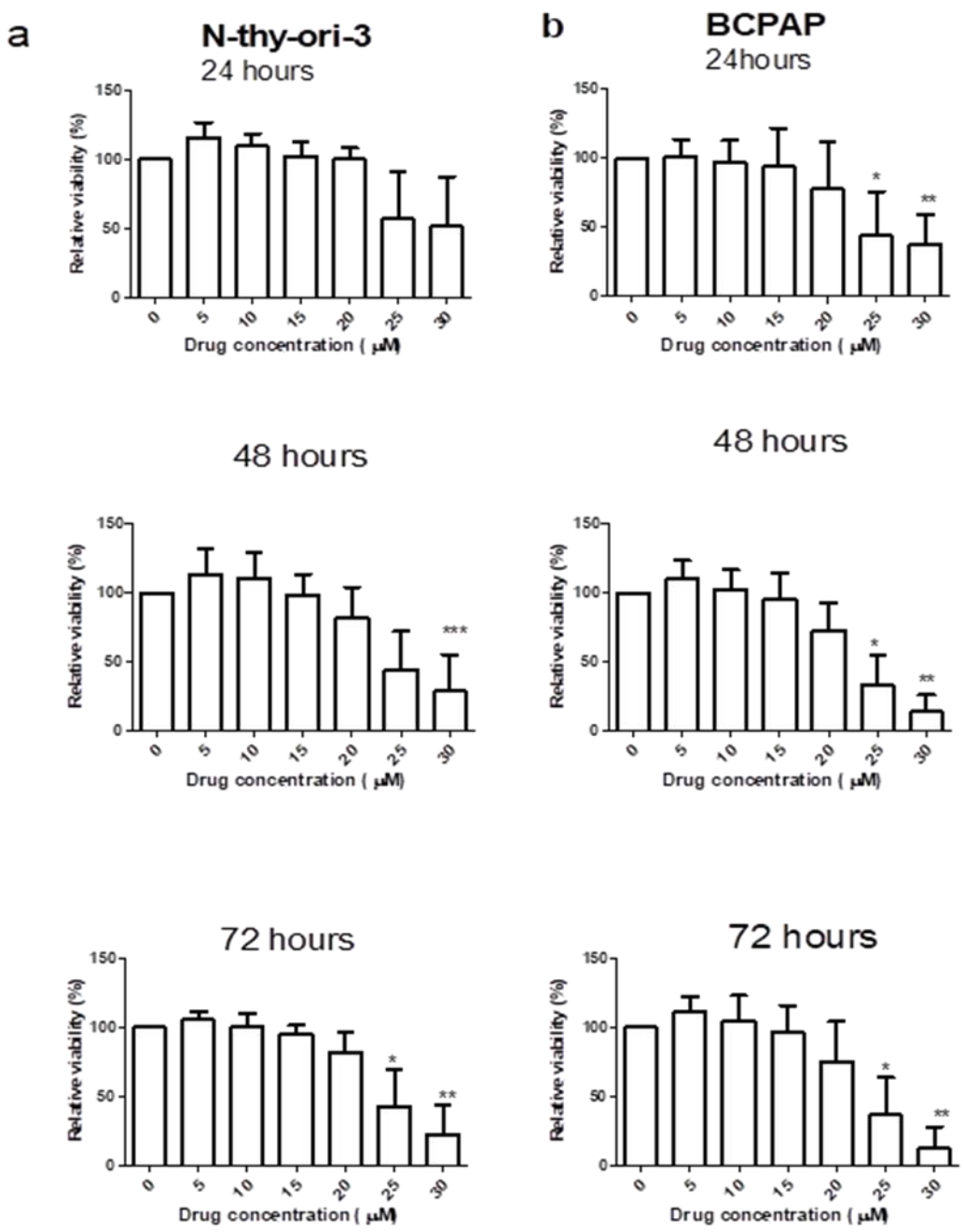

Figure 6.1: Cytotoxic effect of cannabinoid receptor 2 agonist (JWH-133) Viability of (a) N-thy-ori-3 and (b) BCPAP cell lines after 24, 48 and 72 hours incubation. Data shown were mean ± S.D from three independent experiments *P <0.05, **P<0.01 (n=3).

6.3.2 SR144528 inhibition of cytotoxic effect mediated by JWH-133

Twenty minutes post treatment with JWH-133, 4 µM of SR144528 were added to both cell lines and incubated for 24, 48, and 72 hours. Cell viability measured by MTT is summarized in Figure 6.2. A dose-dependent induction of cell death similar to that in cells treated with JWH-133 alone was observed, and the addition of SR144528 did not induce significant changes in cell viability ($P > 0.05$). Interestingly, the addition of SR144528 alone induced significant cell death in both cell lines after 48 or 72 hours of treatment ($P < 0.05$).

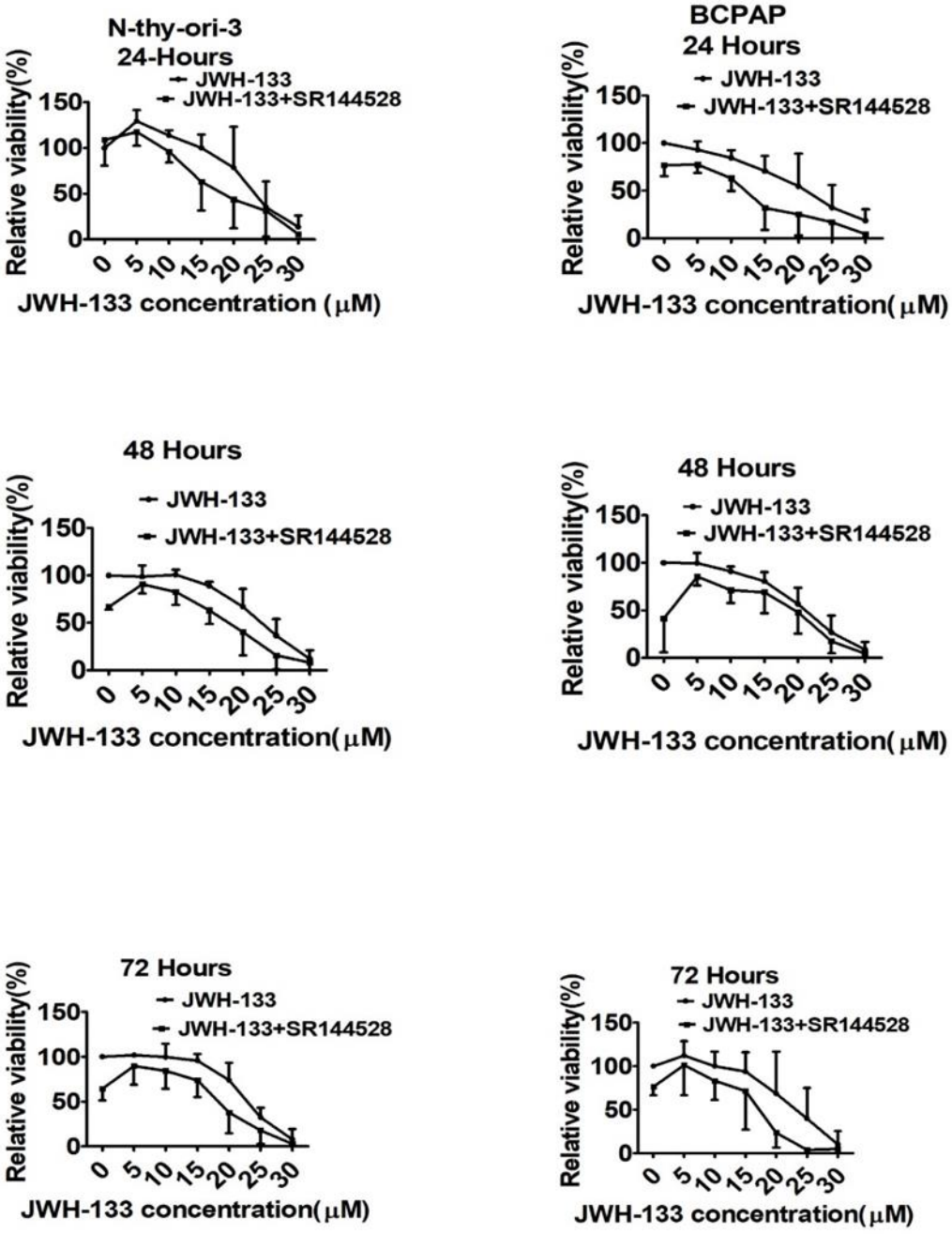

Figure 6.2 Effects of SR144528 (cannabinoid receptor 2 antagonist) on cell viability induced by JWH-133. The viability of (a) N-thy-ori-3 and (b) BCPAP cell lines after 24, 48 and 72 hours incubation. Data shown were mean ±S. D from three independent experiments *P <0.05, **P<0.01 (n=3).

6.4 Discussion

A high rate (> 33%) of cancer recurrence after surgical treatment (Busaidy and Cabanillas, 2012, Zhang et al., 2016) and the high toxicity of currently available pharmaceutical agents (Liebner et al., 2016) emphasize the need for developing new strategies in treating thyroid cancer. ‘Drug repurposing’ can be a useful strategy to bypass some of the challenges posed by the from-scratch development of new drugs (e.g. reduction in financial burden, identification of novel drug targets, and lengthy research period) (O'Connor and Roth, 2005, Ekins and Williams, 2011). Over the past three decades, cannabinoid receptor agonists (CB1 and CB2) have shown marked improvements in treating various cancers. The literature is devoid of any reports on the effects of cannabinoid receptor 2 agonist in treating papillary thyroid cancer. Apart from affecting various other pathways, cannabinoid receptor agonists have shown to induce ER stress- and autophagy-mediated apoptosis (Salazar et al., 2009b). This study was focused on the evaluating therapeutic potential of JWH-133 when used in N-thy-ori-3 and BCPAP cell lines, with a particular interest in identifying the mode of induction of death in both cell lines.

The results of the current study suggested that JWH-133 has both time- and dose-dependent effects on cell viability in both cell lines (N-thy-ori-3 and BCPAP). In comparison to the N-thy-ori-3 line where no significant effect on cell viability was observed post 24 hours JWH-133 treatment, the viability of BCPAP cells was reduced by > 50%. Further

incubation for 48 hours showed a significant reduction in cell survival in both cell lines. However, significant reduction in viability of N-thy-ori-3 cells was only observed at a dose of 25 µM of JWH-133 after 72 hours of incubation. These results demonstrated that 25 µM of JWH-133 can induce a rate of > 50% cell death in papillary thyroid cancer cell lines (BCPAP), even after 24 hours of incubation. Our results suggested that BCPAP cells are more sensitive to JWH-133 than N-thy-ori-3 cells. One possible explanation for the higher sensitivity of BCPAP cells might be their higher expression of CB2 receptors, compared with normal follicular thyroid cells. This explanation is supported by a finding in a recent study that showed significantly higher distribution of CB2 receptors over papillary thyroid cancer nodules than over benign thyroid nodules (Lakiotaki et al., 2015).

The effects of cannabinoid receptor 2 antagonists (SR144528) were also evaluated in this study. SR144528 has high affinity and exhibits an > 700-fold selectivity for CB2 over CB1 receptors (Rinaldi-Carmona et al., 1998). Previous studies showed that SR144528 has strong inverse-agonist activities and blocked mitogen-activated protein kinase activity coupled to the CB2 receptor in Chinese hamster ovary cell lines transfected with the CB2 receptor (Bouaboula et al., 1999). In another study, the apoptotic effects induced in Jurkat cells by a CB2 receptor agonist (THC 1.5 µM) was inhibited by 2 µM of SR144528. (Herrera et al., 2006). In the most recent study, it was shown that the effects of JWH-133 in reducing pulmonary oedema were significantly reversed by

SR144528 (Fujii et al., 2016). In contrast to these previous studies, SR144528 showed no effect to reverse the cytotoxic effect mediated by JWH-133 in the current study, even though a dose of 4 µM was used. The cell death caused by SR144528 alone that we observed is unexpected, and further experiments are needed to determine the underlying mechanisms.

There might be several reasons that explain why SR144528 did not show an effect in the current study. In contrast to previous studies which used *in vivo* experimental models, we used an *in vitro* experimental setting. Several chemical compounds have different outcomes in *in vitro* and *in vivo* models, potentially because of metabolite degradation in *in vivo* settings (Wightman et al., 2001). In comparison, in a study conducted by Herrera et al. (2016), in which *in vitro* experimental settings were used with a different CB2 receptor agonist (TCH), a dose of 2 µM of SR144528 could reverse the apoptotic effect of TCH on Jurkat cells. The results of our study may imply that the action of JWH-133 on thyroid cells is too strong to be inhibited by SR144528. Moreover, in previous studies, SR144528 was used to reverse the non-detrimental action of cannabinoid receptor 2 agonists; however, this study investigated the potential of SR144528 in inhibiting the cytotoxic action of JWH-133 in different thyroid cell lines. In addition, the type of cancer being studied is also an important factor, since that means that the same chemical agents can have different intrinsic effects even under the same conditions. Heterogeneity within tumour cells may alter the effect of drugs in treating

cancer (Cohen et al., 2008). To further test the effect of SR144528, cells may be treated with SR144528 prior to be treated with JWH-133. This action will block the available receptors sites (CB2) and can potentially limit the cytotoxic action of JWH-133.

Since cannabinoid receptor 2 agonists have the potential to induce ER stress that can stimulate autophagy and leads to cell death, we further plan to investigate the ER stress pathway and the Akt/mTORc1 axis, to confirm that the death induced in the papillary thyroid cancer cell line in the current study is a consequence of autophagy-mediated apoptosis. We aim to perform western blot and investigate the expression and regulation of proteins associated with the ER stress pathway (ATF6, CHOP) and autophagy (Bcl2, LC3B-I and -II, and p62).

A limitation of this study is that we have only investigated the CB2 agonist, and have not evaluated the efficacy of the CB1 agonist. Another limitation is that we have only employed a very specific inhibitor of JWH-133 and have not investigated the efficacy of other available cannabinoid antagonists. Further investigation is warranted to investigate the role of cannabinoids in the treatment of PTC in more detail.

6.5 Conclusion

In conclusion, the cannabinoid receptor 2 agonist (JWH-133) has anti-cancer properties other than its documented palliative effects in patients with cancer. Its cytotoxic effects in a BCPAP cell line suggest its potential usefulness in treating papillary thyroid carcinoma.

Chapter Seven

Summary of the Thesis

This PhD study investigated novel applications of ultrasound and the use of computer-aided assessments of vascularity facilitating the diagnosis of thyroid cancer. It further investigated the therapeutic potential of a non-cancer drug (JWH-133) in treating papillary thyroid cancer.

The accurate diagnosis of thyroid cancer is challenging, due to the overlapping of cytology/histology features in biological samples obtained from thyroid nodules. Moreover, grey-scale ultrasound features of thyroid nodules are qualitatively analysed, which carries the risk of inter- and intra-observer variations. Altogether, this leads to an increase in the number of unnecessary biopsies and in the incidence of skipped diagnoses.

Certain ultrasound features of thyroid nodules can be accurately quantified and yield highly reproducible results as well as minimizing the risks of inter- and intra-observer variations. ‘Tissue elasticity’ and ‘vascularity index quantification’ are two potential predictors of malignancy that can be quantified in numerical figures and evaluate the tissue stiffness and the vasculature of thyroid nodules, respectively.

Shear wave elastography (SWE) is a novel ultrasound technique that quantitatively measures tissue stiffness by making use of high-intensity acoustic radiation force to generate shear waves within the tissue. Shear waves travel faster in stiffer medium than in softer or cystic counterparts. Malignant lesions including thyroid cancer tend to be harder. Thus, shear wave elastography indices ($E_{maximum}$, E_{mean}, and $E_{minimum}$) have the potential to predict thyroid malignancy, because malignant nodules might have higher value of these indices.

Our first study (Chapter 3) involved 111 patients with thyroid nodules, and we assessed the feasibility of using SWE alone and in combination with grey-scale ultrasound to differentiate malignant and benign thyroid nodules. Our study results suggested that $E_{maximum} \geq 67.3$ kPa and $E_{mean} \geq 23.1$ kPa are useful independent predictors of thyroid malignancy. Our results also showed that $E_{maximum}$ was the best adjunct parameter to grey-scale ultrasound and enhances diagnostic accuracy in determining thyroid malignancy from 58.5% when using grey-scale ultrasound alone to 80.2% when used in combination ($P < 0.05$). Our study results have significant clinical value for a more accurate diagnosis of thyroid malignancy, and we recommend the use of SWE evaluation for every thyroid nodule that is found to have at least one suspicious grey-scale feature of malignancy prior to a decision about biopsy.

Vascularity is an important indicator of maintaining homeostasis and promoting proliferation in normal tissues and body organs. The thyroid gland receives rich blood supply from the superior and inferior thyroid arteries. Certain pathological conditions such as hyper/hypothyroidism, Grave's disease, and malignancies lead to hemodynamic changes in the vasculature of the thyroid parenchyma. In the case of thyroid nodules, hypervascularity is believed to be associated with malignancy. Previous studies also suggested that 'peripheral vascularity' is an indication of benignity whilst 'central vascularity' is suggestive of the malignant potential of a thyroid nodule (Papini et al., 2002, Frates et al., 2003). However, these findings are controversial, mainly due to two potential reasons: (1) vascularity, despite being a dynamic feature, was subjectively evaluated by a visual assessment method, which is a qualitative approach and brings inter- and intra-observer variations into the analysis; (2) the terms 'peripheral' and 'central' regions in thyroid nodules are used extensively in the literature; however, no standardized method was defined to delineate the boundary between central and peripheral regions, and the determination of the boundaries of these regions was performed on a visual basis, which is an inaccurate and unreliable method. Considering these issues as well as the importance of the quantification of vascular indices in establishing the diagnosis of thyroid nodules, we modified our previously developed algorithm that can quantify the overall vascularity of a ROI with the aim to perform 'regional segmentation' of thyroid nodules. The modified algorithm uses a novel approach called 'offsetting' to segment the central

and peripheral regions of a thyroid nodule. After the segmentation, the algorithm can quantify the vascularity index of the peripheral and central regions of thyroid nodules.

Our results showed that the optimum offset for dividing peripheral and central regions of a nodule was 22%. At the optimum offset, the mean VI of peripheral, central, and overall regions of malignant nodules were significantly higher than those of benign nodules (26.5 ± 16.2%, 21.7 ± 19.6%, and 23.8 ± 4.6% versus 18.2 ± 16.7%, 11.9 ± 15.1%, and 16.6 ± 1.8%, respectively, $P < 0.05$). The optimum cut-off of the peripheral, central, and overall VI was 19.7%, 9.1%, and 20.2%, respectively. When compared to GSU alone, a combination of VI assessment and GSU evaluation of thyroid nodules increased the overall diagnostic accuracy from 58.6% to 79.3% ($P < 0.05$).

In conclusion, a novel algorithm for regional segmentation and quantitative assessment of the VI in ultrasound images was established, and the optimum offset and cut-off values were derived. Assessment of an intranodular VI in conjunction with GSU can increase the accuracy in ultrasound diagnosis of thyroid cancer.

Colour and power Doppler ultrasound are useful in the evaluation of the vasculature of healthy and diseased tissues or organs. In the assessment of the thyroid gland, Doppler ultrasound has clinical value in the differential diagnosis of various thyroid diseases such as Hashimoto's

thyroiditis, Reidel's thyroiditis, Grave's disease, thyroid nodules, and others. Another useful application of Doppler ultrasound is monitoring the treatment response during therapy. All the above applications require the detection of the vasculature in a ROI with high resolution and high sensitivity. Power Doppler ultrasound and colour Doppler ultrasound have revolutionized the visualization of blood flow maps through organs or tissues. Most recently, a new ultrasound technology named Angio Plane Wave Ultrasensitive^{TM} (AngioPLUS) imaging has been made available and provides high resolution and 3D wall filtering that allow efficient discrimination between blood flow and other soft tissues by analysing space, time, and amplitude information.

In the third study of this thesis, we compared the sensitivity of CDU and PDU alone and in combination with AngioPLUS in detecting the thyroid vascularity of 45 healthy volunteers. We further investigated any differences in vascularity between the right and left thyroid lobes. The results of this study showed that the combination of CDU+AngioPLUS (14.7 ± 9.4%) and the combination of PDU+AngioPLUS (13.4 ± 9%) demonstrated a significant higher thyroid VI than CDU (8.8 ± 7.3%) and PDU (4.7 ± 5.4%) alone, respectively ($P < 0.05$). No asymmetry was found between the VI of the right and left thyroid lobes ($P > 0.05$). This study suggested that AngioPLUS provides enhanced detection of the thyroid vasculature when combined with CDU and PDU. Its application is particularly useful in identifying smaller blood vessels and vessels with low blood flow.

In current clinical practice, surgery is the ultimate therapeutic option to treat thyroid cancer. Chemotherapy has a limited role in managing thyroid cancer due to its higher toxicity. Identification of novel drug targets and the development of a novel drug is a lengthy and costly process. ‘Drug repositioning’ can be a useful strategy for the identification of new markers beyond their primary use.

Cannabinoids are derivatives of the marijuana plant *sativa.* Cannabinoids have been used for recreation and for the relief of pain. Few cannabinoid derivatives have been approved for palliative care in patients with cancer. Two cannabinoid receptors (CB1 and CB2) are known to be distributed in various organs and body systems including the immune system, the central and peripheral nervous system, the testes, the ovaries, the spleen, and the thymus. Different studies have shown the distribution of cannabinoid receptor expression in several types of cancer, including lung cancer, prostate cancer, breast cancer, hepatic cancer, and colorectal cancer. Cannabinoids have been shown to have anti-cancer effects including the inhibition of cancer cell proliferation, a reduction in tumour size and volume, anti-angiogenic effects, anti-migration effects, cell cycle arrest, and apoptosis. Most recently, cannabinoid receptor expression was noted on histological specimens of 87 thyroid nodules (44 papillary thyroid cancer cases, 43 benign). CB1 and CB2 were both found to be frequently distributed on PTC nodules, compared with benign nodules, whereas CB2 expression was much

higher than CB1 receptor expression on PTC nodules than benign nodules ($P < 0.05$). This finding highlights the potential role of the CBR2 agonist in managing PTC.

In our fourth study, we evaluated the therapeutic potential of JWH-133 (CBR2 agonist) on a papillary thyroid cancer cell line (BCPAP), using a normal follicular thyroid cell line (N-thy-ori-3) as the control. Cells were treated with different drug concentrations (0, 5, 10, 15, 20, 25, and 30 µM) and incubated over 24, 48, and 72 hours under standardized conditions. Drug toxicity analysis was performed with MTT.

The results of our study showed that JWH-133 induced death in the BCPAP cell line, whilst it demonstrated little effect on N-thy-ori-3 cellular viability. The results further demonstrated that BCPAP cells were more sensitive to the cytotoxic effects of JWH-133 than N-thy-ori-3 cells ($P < 0.05$). We found that a 25-µM dose produced the most lethal effect on cell viability after a 48-hour incubation period. The results of our study suggest that JWH-133 has the potential to induce anti-cancer effects in managing PTC.

In summary, this thesis compiles novel useful findings for diagnosing and treating thyroid cancer, and concludes with the following recommendations:

1. In thyroid ultrasound examination, when a thyroid nodule demonstrates one or more suspicious grey-scale ultrasound features, the nodule should be evaluated with SWE. Nodules found to have an $E_{maximum} \geq 67.3$ kPa or an $E_{mean} \geq 23.1$ kPa are highly suspicious for malignancy, and fine needle aspiration cytology (FNAC) should be performed on these nodules.
2. In Doppler ultrasound evaluations of thyroid vascularity, computer-aided assessments of regional vascularity of thyroid nodules as well as AngioPLUS are recommended. These methods increase diagnostic accuracy and sensitivity in detecting thyroid vascularity, which may help disease diagnosis and treatment monitoring.
3. The applications of SWE and computer-aided VI quantification can be considered in cases where grey-scale ultrasound features are suspicious for malignancy and FNAC is inconclusive in differentiating between benign and malignant thyroid nodules.
4. For the management of PTC, a new chemotherapeutic agent (JWH-133) has shown anti-cancer effects in *in vitro* experiments. Further *in vitro* and *in vivo* studies are needed to validate the effect of JWH-133 in PTC cell lines as well as in animal models.

References

ABBOUD, B. & TANNOURY, J. 2010. Surgical treatment of papillary thyroid carcinoma. *Le Journal medical libanais. The Lebanese medical journal,* 59**,** 206-212.

AGCAOGLU, O., AKSAKAL, N., OZCINAR, B., SARICI, I. S., ERCAN, G., KUCUKYILMAZ, M., YANAR, F., OZEMIR, I. A., KILIC, B. & CAGLAYAN, K. 2013. Factors that affect the false-negative outcomes of fine-needle aspiration biopsy in thyroid nodules. *International journal of endocrinology,* 2013.

AGGARWAL, A., AGGARWAL, J. & AWASTHI, S. 2017. Non Invasive Assessment of Malignancy in Solitary Non Palpable Thyroid Nodules: A Comparative and Complimentary Evaluation of Grey Scale Ultrasound and Color Doppler Parameters–Way Towards a New Scoring System? *Acta Medica International,* 4.

AGRAWAL, K., ESMAIL, A. A., GNANASEGARAN, G., NAVALKISSOOR, S., MITTAL, B. R. & FOGELMAN, I. Pitfalls and Limitations of Radionuclide Imaging in Endocrinology. Seminars in nuclear medicine, 2015. Elsevier, 440-457.

AHMED, S., JOHNSON, P. T., HORTON, K. M., LAI, H., ZAHEER, A., TSAI, S. & FISHMAN, E. K. 2012. Prevalence of unsuspected thyroid nodules in adults on contrast enhanced 16-and 64-MDCT of the chest. *World journal of radiology,* 4**,** 311.

AHUJA, A., CHICK, W., KING, W. & METREWELI, C. 1996. Clinical significance of the comet-tail artifact in thyroid ultrasound. *Journal of clinical ultrasound,* 24**,** 129-133.

AHUJA, A. T., CHOW, L., CHICK, W., KING, W. & METREWELI, C. 1995. Metastatic cervical nodes in papillary carcinoma of the thyroid: ultrasound and histological correlation. *Clin Radiol,* 50**,** 229-31.

AHUJA, A. T. & EVANS, R. M. 2000. *Practical head and neck ultrasound*, Cambridge University Press.

AIN, K. & ROSENTHAL, M. S. 2010. *The complete thyroid book*, McGraw Hill Professional.

ALGIN, O., ALGIN, E., GOKALP, G., OCAKOĞLU, G., ERDOĞAN, C., SARAYDAROGLU, O. & TUNCEL, E. 2010. Role of duplex power Doppler ultrasound in differentiation between malignant and benign thyroid nodules. *Korean journal of radiology,* 11**,** 594-602.

ALI, S. Z., FISH, S. A., LANMAN, R. B., RANDOLPH, G. W. & SOSA, J. A. 2013. Use of the Afirma® gene expression classifier for preoperative identification of benign thyroid nodules with indeterminate fine needle aspiration cytopathology. *PLOS Currents Evidence on Genomic Tests*.

ANDERSEN, S., PEDERSEN, K. M., BRUUN, N. H. & LAURBERG, P. 2002. Narrow individual variations in serum T4 and T3 in normal subjects: a clue to the understanding of subclinical thyroid disease. *The Journal of Clinical Endocrinology & Metabolism,* 87**,** 1068-1072.

ANDRIOLI, M. & PERSANI, L. 2014. Elastographic techniques of thyroid gland: current status. *Endocrine,* 46**,** 455-461.

ANIL, G., HEGDE, A. & CHONG, F. 2011. Thyroid nodules: risk stratification for malignancy with ultrasound and guided biopsy. *Cancer Imaging,* 11**,** 209-223.

ANVARI, A., DHYANI, M., STEPHEN, A. E. & SAMIR, A. E. 2016. Reliability of Shear-Wave elastography estimates of the young modulus of tissue in follicular thyroid neoplasms. *American Journal of Roentgenology,* 206**,** 609-616.

APPETECCHIA, M. & SOLIVETTI, F. 2006. The association of colour flow Doppler sonography and conventional ultrasonography improves the diagnosis of thyroid carcinoma. *Hormone Research in Paediatrics,* 66**,** 249-256.

ARMSTRONG, J. L., HILL, D. S., MCKEE, C. S., HERNANDEZ-TIEDRA, S., LORENTE, M., LOPEZ-VALERO, I., ANAGNOSTOU, M. E., BABATUNDE, F., CORAZZARI, M. & REDFERN, C. P. 2015. Exploiting cannabinoid-induced cytotoxic autophagy to drive melanoma cell death. *Journal of Investigative Dermatology,* 135**,** 1629-1637.

ARSLAN, H., UNAL, O., ALGÜN, E., HARMAN, M. & SAKARYA, M. E. 2000. Power Doppler sonography in the diagnosis of Graves' disease. *European Journal of Ultrasound,* 11**,** 117-122.

ASHBURN, T. T. & THOR, K. B. 2004. Drug repositioning: identifying and developing new uses for existing drugs. *Nature reviews Drug discovery,* 3**,** 673-683.

ASSOCIATION, W. M. 2008. *Declaration of Helsinki: Ethical principles for medical research involving human subjects, October 2008*, Canary.

ASTERIA, C., GIOVANARDI, A., PIZZOCARO, A., COZZAGLIO, L., MORABITO, A., SOMALVICO, F. & ZOPPO, A. 2008. US-elastography in the differential diagnosis of benign and malignant thyroid nodules. *Thyroid,* 18**,** 523-531.

AZIZI, G., KELLER, J. M., MAYO, M. L., PIPER, K., PUETT, D., EARP, K. M. & MALCHOFF, C. D. 2015. Thyroid nodules and shear wave elastography: a new tool in thyroid cancer detection. *Ultrasound in medicine & biology,* 41**,** 2855-2865.

BAHJI, A. & MAZHAR, M. N. 2016. Treatment of Cannabis Dependence with Synthetic Cannabinoids: A Systematic Review. *Canadian Journal of Addiction,* 7.

BAIGENT, C., KEECH, A., KEARNEY, P. & BLACKWELL, L. 2005. Efficacy and safety of cholesterol-lowering treatment: prospective meta-analysis of data from 90 056 participants in 14 randomised trials of statins. *The Lancet,* 366**,** 1267.

BALASUBRAMANIAN, T. 2015. Anatomy of Larynx A Review. *Online Journal of Otolaryngology,* 5**,** 1.

BANNIER, E., CIESLAR, K., MOSBAH, K., AUBERT, F., DUBOEUF, F., SALHI, Z., GAILLARD, S., BERTHEZÈNE, Y., CRÉMILLIEUX, Y. & REIX, P. 2010. Hyperpolarized 3He MR for Sensitive Imaging of Ventilation Function and Treatment Efficiency in Young Cystic Fibrosis Patients with Normal Lung Function 1. *Radiology,* 255**,** 225-232.

BARBET, J., CAMPION, L. C., KRAEBER-BODÉRÉ, F., CHATAL, J.-F. & GROUP, G. S. 2005. Prognostic impact of serum calcitonin and carcinoembryonic antigen doubling-times in

patients with medullary thyroid carcinoma. *The Journal of Clinical Endocrinology & Metabolism,* 90**,** 6077-6084.

BARTOLOTTA, T. V., MIDIRI, M., GALIA, M., RUNZA, G., ATTARD, M., SAVOIA, G., LAGALLA, R. & CARDINALE, A. E. 2006. Qualitative and quantitative evaluation of solitary thyroid nodules with contrast-enhanced ultrasound: initial results. *European radiology,* 16**,** 2234-2241.

BENJAMIN, D. M. & FOSSLER, M. J. 2016. Edible cannabis products: it is time for FDA oversight. *The Journal of Clinical Pharmacology,* 56**,** 1045-1047.

BERCOFF, J. 2011. *Ultrafast ultrasound imaging*, INTECH Open Access Publisher.

BERCOFF, J. 2016. White Paper, Angio PL.U.S. PLaneWave UltraSensitive™ ultrasound imaging. *In:* FRAPPART, T. (ed.) *Aixplorer Multiwave*

BHATIA, K., TONG, C. S., CHO, C. C., YUEN, E. H., LEE, J. & AHUJA, A. T. 2012a. Reliability of shear wave ultrasound elastography for neck lesions identified in routine clinical practice. *Ultraschall Med,* 33**,** 463-8.

BHATIA, K. S., LEE, Y. Y., YUEN, E. H. & AHUJA, A. T. 2013. Ultrasound elastography in the head and neck. Part I. Basic principles and practical aspects. *Cancer Imaging,* 13**,** 253.

BHATIA, K. S., TONG, C. S., CHO, C. C., YUEN, E. H., LEE, Y. Y. & AHUJA, A. T. 2012b. Shear wave elastography of thyroid nodules in routine clinical practice: preliminary observations and utility for detecting malignancy. *European radiology,* 22**,** 2397-2406.

BHATIA, K. S., TONG, C. S., CHO, C. C., YUEN, E. H., LEE, Y. Y. & AHUJA, A. T. 2012c. Shear wave elastography of thyroid nodules in routine clinical practice: preliminary observations and utility for detecting malignancy. *Eur Radiol,* 22**,** 2397-406.

BLÁZQUEZ, C., CASANOVA, M. L., PLANAS, A., DEL PULGAR, T. G., VILLANUEVA, C., FERNÁNDEZ-ACEÑERO, M. J., ARAGONÉS, J., HUFFMAN, J. W., JORCANO, J. L. & GUZMÁN, M. 2003. Inhibition of tumor angiogenesis by cannabinoids. *The FASEB Journal,* 17**,** 529-531.

BLUM, M. Ch 6c--ULTRASONOGRAPHY of the THYROID.

BOMFORD, C. K., MILLER, J., KUNKLER, H., SHERRIFF, I., BOMFORD, S. & IH KUNKLER, S. 1993. *Walter and Miller's textbook of radiotherapy: radiation physics, therapy, and oncology*.

BOUABOULA, M., DUSSOSSOY, D. & CASELLAS, P. 1999. Regulation of Peripheral Cannabinoid Receptor CB2Phosphorylation by the Inverse Agonist SR 144528 IMPLICATIONS FOR RECEPTOR BIOLOGICAL RESPONSES. *Journal of Biological Chemistry,* 274**,** 20397-20405.

BRAVERMAN, L. E. & COOPER, D. 2012. *Werner & Ingbar's the thyroid: a fundamental and clinical text*, Lippincott Williams & Wilkins.

BRITO, J. P., GIONFRIDDO, M. R., AL NOFAL, A., BOEHMER, K. R., LEPPIN, A. L., READING, C., CALLSTROM, M., ELRAIYAH, T. A., PROKOP, L. J. & STAN, M. N. 2013. The accuracy of thyroid nodule ultrasound to predict thyroid cancer: systematic review and meta-analysis. *The Journal of Clinical Endocrinology & Metabolism,* 99**,** 1253-1263.

BUDE, R. O. & RUBIN, J. M. 1996. Power Doppler sonography. *Radiology,* 200**,** 21-23.

BUDE, R. O., RUBIN, J. M. & ADLER, R. S. 1994. Power versus conventional color Doppler sonography: comparison in the depiction of normal intrarenal vasculature. *Radiology,* 192**,** 777-780.

BUSAIDY, N. L. & CABANILLAS, M. E. 2012. Differentiated thyroid cancer: management of patients with radioiodine nonresponsive disease. *Journal of thyroid research,* 2012.

BUTCH, R., SIMEONE, J. & MUELLER, P. 1985. Thyroid and parathyroid ultrasonography. *Radiologic Clinics of North America,* 23**,** 57-71.

CALVETE, A. C., RODRÍGUEZ, J. M., DE DIOS BERNÁ-MESTRE, J., RÍOS, A., ABELLÁN-RIVERO, D. & REUS, M. 2013. Interobserver Agreement for Thyroid Elastography. *Journal of Ultrasound in Medicine,* 32**,** 495-504.

CANTISANI, V., GRAZHDANI, H., DRAKONAKI, E., D'ANDREA, V., DI SEGNI, M., KALESHI, E., CALLIADA, F., CATALANO, C., REDLER, A. & BRUNESE, L. 2015. Strain US elastography for the

characterization of thyroid nodules: advantages and limitation. *International journal of endocrinology,* 2015.

CAO, T.-S. & YUAN, L.-J. 2011. *Factors Influencing Doppler Blood Flow and Its Measurements*, INTECH Open Access Publisher.

CAPPELLI, C., CASTELLANO, M., PIROLA, I., CUMETTI, D., AGOSTI, B., GANDOSSI, E. & ROSEI, E. A. 2007. The predictive value of ultrasound findings in the management of thyroid nodules. *Qjm,* 100**,** 29-35.

CARMELIET, P. & JAIN, R. K. 2011. Principles and mechanisms of vessel normalization for cancer and other angiogenic diseases. *Nature reviews Drug discovery,* 10**,** 417-427.

CARNEIRO, R. M., CARNEIRO, B. A., AGULNIK, M., KOPP, P. A. & GILES, F. J. 2015. Targeted therapies in advanced differentiated thyroid cancer. *Cancer treatment reviews,* 41**,** 690-698.

CARRACEDO, A., GIRONELLA, M., LORENTE, M., GARCIA, S., GUZMÁN, M., VELASCO, G. & IOVANNA, J. L. 2006a. Cannabinoids induce apoptosis of pancreatic tumor cells via endoplasmic reticulum stress–related genes. *Cancer research,* 66**,** 6748-6755.

CARRACEDO, A., LORENTE, M., EGIA, A., BLÁZQUEZ, C., GARCÍA, S., GIROUX, V., MALICET, C., VILLUENDAS, R., GIRONELLA, M. & GONZÁLEZ-FERIA, L. 2006b. The stress-regulated protein p8 mediates cannabinoid-induced apoptosis of tumor cells. *Cancer cell,* 9**,** 301-312.

CARRASCO, N. 1993. Iodide transport in the thyroid gland. *Biochimica et Biophysica Acta (BBA)-Reviews on Biomembranes,* 1154**,** 65-82.

CERBONE, G., SPIEZIA, S., COLAO, A., DI SARNO, A., ASSANTI, A., LUCCI, R., SICILIANI, M., LOMBARDI, G. & FENZI, G. 2000. Power Doppler improves the diagnostic accuracy of color Doppler ultrasonography in cold thyroid nodules: follow-up results. *Hormone Research in Paediatrics,* 52**,** 19-24.

CEYLAN, I., YENER, S., BAYRAKTAR, F. & SECIL, M. 2014. Roles of ultrasound and power Doppler ultrasound for diagnosis of Hashimoto thyroiditis in anti-thyroid marker-positive euthyroid subjects. *Quantitative imaging in medicine and surgery,* 4**,** 232-238.

CHAMMAS, M. C., GERHARD, R., OLIVEIRA, I. R. S. D., WIDMAN, A., BARROS, N. D., DURAZZO, M., FERRAZ, A. & CERRI, G. G. 2005. Thyroid nodules: evaluation with power Doppler and duplex Doppler ultrasound. *Otolaryngology—Head and Neck Surgery,* 132**,** 874-882.

CHAN, B. K., DESSER, T. S., MCDOUGALL, I. R., WEIGEL, R. J. & JEFFREY, R. B. 2003. Common and uncommon sonographic features of papillary thyroid carcinoma. *Journal of Ultrasound in Medicine,* 22**,** 1083-1090.

CHOI, J. S., KIM, J., KWAK, J. Y., KIM, M. J., CHANG, H. S. & KIM, E.-K. 2009. Preoperative staging of papillary thyroid carcinoma: comparison of ultrasound imaging and CT. *American Journal of Roentgenology,* 193**,** 871-878.

CHOI, J. Y., LEE, K. S., KIM, H.-J., SHIM, Y. M., KWON, O. J., PARK, K., BAEK, C.-H., CHUNG, J. H., LEE, K.-H. & KIM, B.-T. 2006. Focal thyroid lesions incidentally identified by integrated 18F-FDG PET/CT: clinical significance and improved characterization. *Journal of Nuclear Medicine,* 47**,** 609-615.

CHONG, Y., SHIN, J., KO, E. & HAN, B.-K. 2013. Ultrasonographic elastography of thyroid nodules: is adding strain ratio to colour mapping better? *Clinical radiology,* 68**,** 1241-1246.

CHRISTIANSEN, J. J., DJURHUUS, C. B., GRAVHOLT, C. H., IVERSEN, P., CHRISTIANSEN, J. S., SCHMITZ, O., WEEKE, J., JØRGENSEN, J. O. L. & MØLLER, N. 2007. Effects of cortisol on carbohydrate, lipid, and protein metabolism: studies of acute cortisol withdrawal in adrenocortical failure. *The Journal of Clinical Endocrinology & Metabolism,* 92**,** 3553-3559.

CILEDAG, N., KAYGUSUZ, H., SAHIN, B., AKTAS, E., IMAMOGLU, F. G. B. & ARIBAS, B. K. 2016. The Advantages and Limitations of Ultrasound Elastography in Diagnosis of Thyroid Carcinoma. *Thyroid Cancer-Advances in Diagnosis and Therapy.* InTech.

COHEN, A. A., GEVA-ZATORSKY, N., EDEN, E., FRENKEL-MORGENSTERN, M., ISSAEVA, I., SIGAL, A., MILO, R., COHEN-SAIDON, C., LIRON, Y. & KAM, Z. 2008. Dynamic proteomics of individual cancer cells in response to a drug. *science,* 322**,** 1511-1516.

COOPER, D. S., DOHERTY, G. M., HAUGEN, B. R., KLOOS, R. T., LEE, S. L., MANDEL, S. J., MAZZAFERRI, E. L., MCIVER, B., PACINI, F. & SCHLUMBERGER, M. 2009. Revised American Thyroid Association management guidelines for patients with thyroid nodules and differentiated thyroid cancer: the American Thyroid Association (ATA) guidelines taskforce on thyroid nodules and differentiated thyroid cancer. *Thyroid,* 19**,** 1167-1214.

COOPER, D. S., DOHERTY, G. M., HAUGEN, B. R., KLOOS, R. T., LEE, S. L., MANDEL, S. J., MAZZAFERRI, E. L., MCIVER, B., SHERMAN, S. I. & TUTTLE, R. M. 2006. Management guidelines for patients with thyroid nodules and differentiated thyroid cancer: The American Thyroid Association Guidelines Taskforce. *Thyroid,* 16**,** 109-142.

CORONA, G., BIAGINI, C., ROTONDI, M., BONAMANO, A., CREMONINI, N., PETRONE, L., CONFORTI, B., FORTI, G. & SERIO, M. 2008. Correlation between, clinical, biochemical, color Doppler ultrasound thyroid parameters, and CXCL-10 in autoimmune thyroid diseases. *Endocrine journal,* 55**,** 345-350.

COSGROVE, D., BARR, R., BOJUNGA, J., CANTISANI, V., CHAMMAS, M. C., DIGHE, M., VINAYAK, S., XU, J.-M. & DIETRICH, C. F. 2017. WFUMB Guidelines and Recommendations on the Clinical Use of Ultrasound Elastography: Part 4. Thyroid. *Ultrasound in Medicine & Biology,* 43**,** 4-26.

CRIDGE, B. J. & ROSENGREN, R. J. 2013. Critical appraisal of the potential use of cannabinoids in cancer management. *Cancer Manag Res,* 5**,** 301-313.

DANDO, I., DONADELLI, M., COSTANZO, C., DALLA POZZA, E., D'ALESSANDRO, A., ZOLLA, L. & PALMIERI, M. 2013. Cannabinoids inhibit energetic metabolism and induce AMPK-dependent autophagy in pancreatic cancer cells. *Cell death & disease,* 4**,** e664.

DANESE, D., SCIACCHITANO, S., FARSETTI, A., ANDREOLI, M. & PONTECORVI, A. 1998. Diagnostic accuracy of conventional versus sonography-guided fine-needle aspiration biopsy of thyroid nodules. *Thyroid,* 8**,** 15-21.

DAVIES, T. F. 2017. Physiology and testing of thyroid function. *Endocrine Surgery*.

DE NICOLA, H., SZEJNFELD, J., LOGULLO, Â. F., WOLOSKER, Â. M. B., SOUZA, L. R. M. F. & CHIFERI, V. 2005. Flow pattern and vascular resistive index as predictors of malignancy risk in thyroid follicular neoplasms. *Journal of ultrasound in medicine,* 24**,** 897-904.

DE PETROCELLIS, L., LIGRESTI, A., SCHIANO MORIELLO, A., IAPPELLI, M., VERDE, R., STOTT, C. G., CRISTINO, L., ORLANDO, P. & DI MARZO, V. 2013. Non-THC cannabinoids inhibit prostate carcinoma growth in vitro and in vivo: pro-apoptotic effects and underlying mechanisms. *British journal of pharmacology,* 168**,** 79-102.

DEL PULGAR, T. G., VELASCO, G., SÁNCHEZ, C., AMADOR, H. & GUZMÁN, M. 2002. De novo-synthesized ceramide is involved in cannabinoid-induced apoptosis. *Biochemical Journal,* 363**,** 183-188.

DEMAJ, E., KERMAJ, M., FURERAJ, T., KOLLCAKU, L. & AGRON, Y. 2016. The Important Role Of Doppler Ultrasound In The Differential Diagnosis Between Hashitoxicosis And Graves' Disease. *European Thyroid Journal,* 5**,** 106.

DIGHE, M. K. 2014. Elastography of thyroid masses. *Ultrasound clinics,* 9**,** 13-24.

DIMASI, J., GRABOWSKI, H. & HANSEN, R. 2014. Cost to develop and win marketing approval for a new drug is $2.6 billion. *Tufts Center for the Study of Drug Development,* 18.

DOBRUCH-SOBCZAK, K., ZALEWSKA, E. B., GUMINSKA, A., SLAPA, R. Z., MLOSEK, K., WARELUK, P., JAKUBOWSKI, W. & DEDECJUS, M. 2016. Diagnostic Performance of Shear Wave Elastography Parameters Alone and in Combination with Conventional B-Mode Ultrasound Parameters for the Characterization of Thyroid Nodules: A Prospective, Dual-Center Study. *Ultrasound Med Biol,* 42**,** 2803-2811.

DONADELLI, M., DANDO, I., ZANIBONI, T., COSTANZO, C., DALLA POZZA, E., SCUPOLI, M., SCARPA, A., ZAPPAVIGNA, S., MARRA, M. & ABBRUZZESE, A. 2011. Gemcitabine/cannabinoid combination triggers autophagy in pancreatic cancer cells through a ROS-mediated mechanism. *Cell death & disease,* 2**,** e152.

DONG, M.-J., LIU, Z.-F., ZHAO, K., RUAN, L.-X., WANG, G.-L., YANG, S.-Y., SUN, F. & LUO, X.-G. 2009. Value of 18F-FDG-PET/PET-CT in differentiated thyroid carcinoma with radioiodine-negative whole-body scan: a meta-analysis. *Nuclear medicine communications,* 30**,** 639-650.

DONKOL, R. H., NADA, A. M. & BOUGHATTAS, S. 2013. Role of color Doppler in differentiation of Graves' disease and thyroiditis in thyrotoxicosis. *World J Radiol,* 5**,** 178-183.

DUAN, S. B., YU, J., LI, X., HAN, Z. Y., ZHAI, H. Y. & LIANG, P. 2016. Diagnostic value of two-dimensional shear wave elastography in papillary thyroid microcarcinoma. *Onco Targets Ther,* 9**,** 1311-7.

DUDEA, S. M. & BOTAR-JID, C. 2015. Ultrasound elastography in thyroid disease. *Medical ultrasonography,* 17**,** 74.

EATON, S., EUINTON, H., NEWMAN, C., WEETMAN, A. & BENNET, W. 2002. Clinical experience of amiodarone-induced thyrotoxicosis over a 3-year period: role of colour-flow Doppler sonography. *Clinical endocrinology,* 56**,** 33-38.

EDITH, T., KEYHANI-ROFAGHA, S., CUNNINGHAM, J. J. & MAZZAFERRI, E. L. 1990. Cystic thyroid nodules: the dilemma of malignant lesions. *Archives of internal medicine,* 150**,** 1422-1427.

EKINS, S. & WILLIAMS, A. J. 2011. Finding promiscuous old drugs for new uses. *Pharmaceutical research,* 28**,** 1785-1791.

EL HENNAWY, H., ZAID, H. A., MUJEEB, I. B., EL KAHLOUT, E. A. & BEDAIR, E. S. 2013. Accuracy of Fine Needle Aspiration Cytology of Solitary Thyroid Nodules in Tertiary versus Community Hospital. *Surgical Science,* 4**,** 494.

EVANS, D. H. 1989. *Doppler ultrasound: Physics, instrumentation, and clinical applications*, John Wiley & Sons.

FENG, B., LIANG, P., CHENG, Z., YU, X., YU, J., HAN, Z. & LIU, F. 2012. Ultrasound-guided percutaneous microwave ablation of benign thyroid nodules: experimental and clinical studies. *European journal of endocrinology,* 166**,** 1031-1037.

FIORE, E., RAGO, T., PROVENZALE, M., SCUTARI, M., UGOLINI, C., BASOLO, F., DI COSCIO, G., BERTI, P., GRASSO, L. & ELISEI, R. 2009. Lower levels of TSH are associated with a lower risk of papillary thyroid cancer in patients with thyroid nodular disease: thyroid autonomy may play a protective role. *Endocrine-Related Cancer,* 16**,** 1251-1260.

FLEISCHER, A. C., WOJCICKI, W. E., DONNELLY, E. F., PICKENS, D. R., THIRSK, G., THURMAN, G. B. & HELLERQVIST, C. G. 1999. Quantified color Doppler sonography of tumor vascularity in an animal model. *Journal of ultrasound in medicine,* 18**,** 547-551.

FOLKMAN, J. 1986. How is blood vessel growth regulated in normal and neoplastic tissue?—GHA Clowes Memorial Award Lecture. *Cancer research,* 46**,** 467-473.

FRATES, M. C., BENSON, C. B., CHARBONEAU, J. W., CIBAS, E. S., CLARK, O. H., COLEMAN, B. G., CRONAN, J. J., DOUBILET, P. M., EVANS, D. B. & GOELLNER, J. R. 2005. Management of thyroid nodules detected at US: Society of Radiologists in Ultrasound Consensus Conference Statement 1. *Radiology,* 237**,** 794-800.

FRATES, M. C., BENSON, C. B., DOUBILET, P. M., CIBAS, E. S. & MARQUSEE, E. 2003. Can color Doppler sonography aid in the prediction of malignancy of thyroid nodules? *Journal of ultrasound in medicine,* 22**,** 127-131.

FUJII, M., SHERCHAN, P., SOEJIMA, Y., DOYCHEVA, D., ZHAO, D. & ZHANG, J. H. 2016. Cannabinoid receptor type 2 agonist attenuates acute neurogenic pulmonary edema by preventing neutrophil migration after subarachnoid hemorrhage in rats. *Brain Edema XVI.* Springer.

FUJIMORI, M., HARA, H. & TSUTSUI, H. 2013. CQ51. Are Measurements of Calcitonin and CEA Useful as Markers of Recurrence After Surgery for Medullary Carcinoma? *Treatment of Thyroid Tumor.* Springer.

FUKUNARI, N., NAGAHAMA, M., SUGINO, K., MIMURA, T., ITO, K. & ITO, K. 2004. Clinical evaluation of color Doppler imaging for the differential diagnosis of thyroid follicular lesions. *World journal of surgery,* 28**,** 1261-1265.

GACCHE, R. 2015. Compensatory angiogenesis and tumor refractoriness. *Oncogenesis,* 4**,** e153.

GAUL, D. A., MEZENCEV, R., LONG, T. Q., JONES, C. M., BENIGNO, B. B., GRAY, A., FERNÁNDEZ, F. M. & MCDONALD, J. F. 2015. Highly-accurate metabolomic detection of early-stage ovarian cancer. *Scientific reports,* 5.

GENNISSON, J.-L., DEFFIEUX, T., FINK, M. & TANTER, M. 2013. Ultrasound elastography: principles and techniques. *Diagnostic and interventional imaging,* 94**,** 487-495.

GHARIB, H., PAPINI, E., GARBER, J. R., DUICK, D. S., HARRELL, R. M., HEGEDÜS, L., PASCHKE, R., VALCAVI, R. & VITTI, P. 2016. AMERICAN ASSOCIATION OF CLINICAL ENDOCRINOLOGISTS, AMERICAN COLLEGE OF ENDOCRINOLOGY, AND ASSOCIAZIONE MEDICI ENDOCRINOLOGI MEDICAL GUIDELINES FOR CLINICAL PRACTICE FOR THE DIAGNOSIS AND MANAGEMENT OF THYROID NODULES–2016 UPDATE: APPENDIX. *Endocrine Practice,* 22**,** 1-60.

GHARIB, H., PAPINI, E., PASCHKE, R., DUICK, D., VALCAVI, R., HEGEDÜS, L. & VITTI, P. 2010. American Association of Clinical Endocrinologists, Associazione Medici Endocrinologi, and European Thyroid Association medical guidelines for clinical practice for the diagnosis and management of thyroid nodules. *Endocrine Practice*.

GILD, M. L., BULLOCK, M., ROBINSON, B. G. & CLIFTON-BLIGH, R. 2011. Multikinase inhibitors: a new option for the treatment of thyroid cancer. *Nature Reviews Endocrinology,* 7**,** 617-624.

GODDING, G. A. & CLARK, O. H. 1992. Use of color Doppler imaging in the distinction between thyroid and parathyroid lesions. *The American journal of surgery,* 164**,** 51-56.

GONG, B., LIU, J.-D., YING, H., WANG, T. & JIA, M. The Diagnostic Analysis of High Frequency Color Doppler Ultrasound in Thyroid Cancer. Medicine and Biopharmaceutical: Proceedings of the 2015 International Conference, 2016. World Scientific, 245-250.

GREENSPAN, F. S. & GARDNER, D. G. 1997. *Basic & clinical endocrinology*, Appleton & Lange Stamford, CT.

GUPTA, S. C., SUNG, B., PRASAD, S., WEBB, L. J. & AGGARWAL, B. B. 2013. Cancer drug discovery by repurposing: teaching new tricks to old dogs. *Trends in pharmacological sciences,* 34**,** 508-517.

GUTH, S., THEUNE, U., ABERLE, J., GALACH, A. & BAMBERGER, C. 2009. Very high prevalence of thyroid nodules detected by high frequency (13 MHz) ultrasound examination. *European journal of clinical investigation,* 39**,** 699-706.

GUZMAN, M. 2003. Cannabinoids: potential anticancer agents. *Nature Reviews Cancer,* 3**,** 745-755.

HANEY, M., COOPER, Z. D., BEDI, G., VOSBURG, S. K., COMER, S. D. & FOLTIN, R. W. 2013. Nabilone decreases marijuana withdrawal and a laboratory measure of marijuana relapse. *Neuropsychopharmacology,* 38**,** 1557.

HARACH, H. & ZUSMAN, S. 1991. Cytopathology of the tall cell variant of thyroid papillary carcinoma. *Acta cytologica,* 36**,** 895-899.

HARBERT, J. C., ECKELMAN, W. C. & NEUMANN, R. D. 1996. *Nuclear medicine: diagnosis and therapy*, Thieme Medical Publishers.

HASLERUD, T., BRAUCKHOFF, K., REISÆTER, L., KÜFNER LEIN, R., HEINECKE, A., VARHAUG, J. E. & BIERMANN, M. 2016. F18-FDG-PET for recurrent differentiated thyroid cancer: a systematic meta-analysis. *Acta Radiologica,* 57**,** 1193-1200.

HATLE, L., ANGELSEN, B. & TROMSDAL, A. 1980. Non-invasive assessment of aortic stenosis by Doppler ultrasound. *Heart,* 43**,** 284-292.

HAUGEN, B. R. 2016. 2015 American Thyroid Association Management Guidelines for Adult Patients with Thyroid Nodules and Differentiated Thyroid Cancer: What is new and what has changed? *Cancer*.

HAUGEN, B. R., SAWKA, A. M., ALEXANDER, E. K., PACINI, M., SCHLUMBERGER, M., SCHUFF, K., SHERMAN, S. I., WARTOFSKY, M. & WILLIAMS, M. D. 2017. The ATA Guidelines on Management of Thyroid Nodules and Differentiated Thyroid Cancer Task Force Review and Recommendation on the Proposed Renaming of eFVPTC without Invasion to NIFTP. *Thyroid: official journal of the American Thyroid Association*.

HAYMART, M. R., REPPLINGER, D. J., LEVERSON, G. E., ELSON, D. F., SIPPEL, R. S., JAUME, J. C. & CHEN, H. 2008. Higher serum thyroid stimulating hormone level in thyroid nodule patients is associated with greater risks of differentiated thyroid cancer and advanced tumor stage. *The Journal of Clinical Endocrinology & Metabolism,* 93**,** 809-814.

HEGEDÜS, L. & BENNEDBÆK, F. N. 2005. Nonisotopic techniques of thyroid imaging. *Thyroid-a Fundamental and Clinical Text.* Lippincott Williams/.

HERRERA, B., CARRACEDO, A., DIEZ-ZAERA, M., DEL PULGAR, T. G., GUZMÁN, M. & VELASCO, G. 2006. The CB 2 cannabinoid receptor signals apoptosis via ceramide-dependent activation of the mitochondrial intrinsic pathway. *Experimental cell research,* 312**,** 2121-2131.

HILL, C., BAMBER, J., TER HAAR, G., BAXTER, G., ALLAN, P., MORLEY, P. & FISH, P. 2000. Doppler ultrasound: physics, instrumentation and signal processing.

HOANG, J. K., LEE, W. K., LEE, M., JOHNSON, D. & FARRELL, S. 2007. US features of thyroid malignancy: pearls and pitfalls 1. *Radiographics,* 27**,** 847-860.

HOSSAIN, F., KARIM, M. N., RAHMAN, S. M. M., KHAN, N., SIDDIQUI, M. & HUSSAIN, R. 2010. Preoperative detection of ovarian cancer by color Doppler ultrasonography and CA 125. *Bangladesh Medical Research Council Bulletin,* 36**,** 68-73.

HOSSEIN GHARIB, M., ENRICO PAPINI MD, F., PASCHKE, R., DUICK, D. S., ROBERTO VALCAVI MD, F., HEGEDÜS, L. & VITTI, P. 2010. AMERICAN ASSOCIATION OF CLINICAL ENDOCRINOLOGISTS, ASSOCIAZIONE MEDICI ENDOCRINOLOGI, AND EUROPEAN THYROID ASSOCIATION MEDICAL GUIDELINES FOR CLINICAL PRACTICE FOR THE DIAGNOSIS AND MANAGEMENT OF THYROID NODULES. *Endocrine Practice,* 16**,** 1.

HUSSEIN, R. R., ELSAYED, R. F. & ELSAFY, H. M. E. 2013. Elastography: Novel Development in Ultrasound for the Differential Diagnosis of Thyroid Nodules. *Al-Azhar Medical Journal,* 42**,** 265-272.

HWANG, S. H., KIM, E.-K., MOON, H. J., YOON, J. H. & KWAK, J. Y. 2016. Risk of thyroid cancer in euthyroid asymptomatic patients with thyroid nodules with an emphasis on family history of thyroid cancer. *Korean journal of radiology,* 17**,** 255-263.

IMAM, S. K. 2016. Thyroid: A General Overview. *Thyroid Disorders.* Springer.

JAVID, F. A., PHILLIPS, R. M., AFSHINJAVID, S., VERDE, R. & LIGRESTI, A. 2016. Cannabinoid pharmacology in cancer research: A new hope for cancer patients? *European journal of pharmacology,* 775**,** 1-14.

JOHNSON, T. L., LLOYD, R. V., THOMPSON, N. W., BEIERWALTES, W. H. & SISSON, J. C. 1988. Prognostic implications of the tall cell variant of papillary thyroid carcinoma. *The American journal of surgical pathology,* 12**,** 22-27.

KABALA, J. E. 2006. CT and MRI in Thyroid Cancer. *Practical Management of Thyroid Cancer.* Springer.

KANANI, S., PATEL, J., SHAH, R., NIRVAN, A. & DAVE, R. 2014. A study of venous drainage of thyroid gland in 50 cadavers.

KHADRA, H., BAKEER, M., HAUCH, A., HU, T. & KANDIL, E. 2016. Is vascular flow a predictor of malignant thyroid nodules? A meta-analysis. *Gland Surgery,* 5**,** 576-582.

KHARCHENKO, V. P., KOTLYAROV, P. M., MOGUTOV, M. S., ALEXANDROV, Y. K., SENCHA, A. N., PATRUNOV, Y. N. & BELYAEV, D. V. 2010. *Ultrasound diagnostics of thyroid diseases*, Springer Science & Business Media.

KIM, D. W. 2014. Computed tomography features of papillary thyroid carcinomas. *Journal of computer assisted tomography,* 38**,** 936-940.

KIM, E. K., PARK, C. S., CHUNG, W. Y., OH, K. K., KIM, D. I., LEE, J. T. & YOO, H. S. 2002. New sonographic criteria for recommending fine-needle aspiration biopsy of nonpalpable solid nodules of the thyroid. *AJR Am J Roentgenol,* 178**,** 687-91.

KIM, H., KIM, J.-A., SON, E. J. & YOUK, J. H. 2013. Quantitative assessment of shear-wave ultrasound elastography in thyroid nodules: diagnostic performance for predicting malignancy. *European radiology,* 23**,** 2532-2537.

KIM, S.-Y., KIM, E.-K., MOON, H. J., YOON, J. H. & KWAK, J. Y. 2015. Application of texture analysis in the differential diagnosis of benign and malignant thyroid nodules: comparison with gray-scale ultrasound and elastography. *American Journal of Roentgenology,* 205**,** W343-W351.

KING, A. D. 2008. Imaging for staging and management of thyroid cancer. *Cancer Imaging,* 8**,** 57.

KITAHARA, C. M. & SOSA, J. A. 2016. The changing incidence of thyroid cancer. *Nature Reviews Endocrinology,* 12**,** 646-653.

KOAY, L. C., RIGBY, R. J. & WRIGHT, K. L. 2014. Cannabinoid-induced autophagy regulates suppressor of cytokine signaling-3 in intestinal epithelium. *American Journal of Physiology-Gastrointestinal and Liver Physiology,* 307**,** G140-G148.

KOHN, L., SAJI, M., KOSUGI, M., BAN, T., GIULIANI, C., HIDAKA, A., SHIMURA, H., SHIMURA, Y. & OKAJIMA, F. 1993. Thyroid diseases: Basic Science, Pathology, Clinical and Laboratory

Diagnosis, L. Troncone, B. Shapiro, MA Satta and F. Monaco, eds. Boca Raton, USA: CRC Press.

KOONG, S.-S., REYNOLDS, J. C., MOVIUS, E. G., KEENAN, A. M., AIN, K. B., LAKSHMANAN, M. C. & ROBBINS, J. 1999. Lithium as a Potential Adjuvant to 131I Therapy of Metastatic, Well Differentiated Thyroid Carcinoma 1. *The Journal of Clinical Endocrinology & Metabolism,* 84**,** 912-916.

KOPEREK, O., SCHEUBA, C., PURI, C., BIRNER, P., HASLINGER, C., RETTIG, W., NIEDERLE, B., KASERER, K. & CHESA, P. G. 2007. Molecular characterization of the desmoplastic tumor stroma in medullary thyroid carcinoma. *International journal of oncology,* 31**,** 59-68.

KRAMER, J. L. 2015. Medical marijuana for cancer. *CA: a cancer journal for clinicians,* 65**,** 109-122.

KRÁTKÝ, J., VITKOVA, H., BARTÁKOVÁ, J., TELICKA, Z., ANTOSOVA, M., LIMANOVA, Z. & JISKRA, J. 2014. Thyroid nodules: Pathophysiological insight on oncogenesis and novel diagnostic techniques. *Physiological Research,* 63**,** S263.

KREMKAU, F. W. 2001. *Diagnostic ultrasound: principles and instruments*, WB Saunders Company.

KUDO, M., TOCHIO, H. & ZHOU, P. 2004. Differentiation of hepatic tumors by color Doppler imaging: role of the maximum velocity and the pulsatility index of the intratumoral blood flow signal. *Intervirology,* 47**,** 154-161.

KUNNIMALAIYAAN, M., VACCARO, A. M., NDIAYE, M. A. & CHEN, H. 2007. Inactivation of glycogen synthase kinase-3β, a downstream target of the raf-1 pathway, is associated with growth suppression in medullary thyroid cancer cells. *Molecular Cancer Therapeutics,* 6**,** 1151-1158.

KUSHCHAYEVA, Y., JENSEN, K., BURMAN, K. D. & VASKO, V. 2014. Repositioning therapy for thyroid cancer: new insights on established medications. *Endocrine-related cancer,* 21**,** R183-R194.

KWAK, J. Y. & KIM, E.-K. 2014. Ultrasound elastography for thyroid nodules: recent advances. *Ultrasonography,* 33**,** 75-82.

LAGALLA, R., CARUSO, G. & FINAZZO, M. 1998. Monitoring treatment response with color and power Doppler. *European journal of radiology,* 27**,** S149-S156.

LAKIOTAKI, E., GIAGINIS, C., TOLIA, M., ALEXANDROU, P., DELLADETSIMA, I., GIANNOPOULOU, I., KYRGIAS, G., PATSOURIS, E. & THEOCHARIS, S. 2015. Clinical significance of cannabinoid receptors CB1 and CB2 expression in human malignant and benign thyroid lesions. *BioMed research international,* 2015.

LAM, J., YING, M., CHEUNG, S., YEUNG, K., YU, P., CHENG, H. & AHUJA, A. 2014. A comparison of the diagnostic accuracy and reliability of subjective grading and computer-aided assessment of intranodal vascularity in differentiating metastatic and reactive cervical lymphadenopathy. *Ultraschall in der Medizin-European Journal of Ultrasound*.

LANZER, P. & TOPOL, E. J. 2013. *Pan vascular medicine: integrated clinical management*, Springer.

LASSAU, N., KOSCIELNY, S., OPOLON, P., DE BAERE, T., PERONNEAU, P., LECLERE, J. & ROCHE, A. 2001. Evaluation of contrast-enhanced color Doppler ultrasound for the quantification of angiogenesis in vivo. *Investigative radiology,* 36**,** 50-55.

LEE, D. Y., KWON, T. K., SUNG, M. W., KIM, K. H. & HAH, J. H. 2014. Prediction of extrathyroidal extension using ultrasonography and computed tomography. *Int J Endocrinol,* 2014**,** 351058.

LEE, J. H., SHIN, H. J., YOON, J. H., KIM, E. K., MOON, H. J., LEE, H. S., KWON, H. J. & KWAK, J. Y. 2016. Predicting lymph node metastasis in patients with papillary thyroid carcinoma by vascular index on power Doppler ultrasound. *Head & Neck*.

LESSIN, L. S. & MIN, M. 2000. Chemotherapy for thyroid cancer. *Thyroid Cancer.* Springer.

LIEBNER, D. A., HARALDSDOTTIR, S. & SHAH, M. H. 2016. Chemotherapy of Thyroid Cancer: General Principles. *Thyroid Cancer.* Springer.

LIN, F. I. & IAGARU, A. 2010. Updates on PET-CT and thyroid cancer. *Applied Radiology,* 39**,** 8.

LIN, P., CHEN, M., LIU, B., WANG, S. & LI, X. 2014. Diagnostic performance of shear wave elastography in the identification of malignant thyroid nodules: a meta-analysis. *European radiology,* 24**,** 2729-2738.

LIPPOLIS, P., TOGNINI, S., MATERAZZI, G., POLINI, A., MANCINI, R., AMBROSINI, C., DARDANO, A., BASOLO, F., SECCIA, M. & MICCOLI, P. 2011. Is elastography actually useful in the presurgical selection of thyroid nodules with indeterminate cytology? *The Journal of Clinical Endocrinology & Metabolism,* 96**,** E1826-E1830.

LIU, B., LIANG, J., ZHENG, Y., XIE, X., HUANG, G., ZHOU, L., WANG, W. & LU, M. 2015a. Two-dimensional shear wave elastography as promising diagnostic tool for predicting malignant thyroid nodules: a prospective single-centre experience. *Eur Radiol,* 25**,** 624-34.

LIU, B., LIANG, J., ZHENG, Y., XIE, X., HUANG, G., ZHOU, L., WANG, W. & LU, M. 2015b. Two-dimensional shear wave elastography as promising diagnostic tool for predicting malignant thyroid nodules: a prospective single-centre experience. *European radiology,* 25**,** 624-634.

LIU, B. X., XIE, X. Y., LIANG, J. Y., ZHENG, Y. L., HUANG, G. L., ZHOU, L. Y., WANG, Z., XU, M. & LU, M. D. 2014. Shear wave elastography versus real-time elastography on evaluation thyroid nodules: a preliminary study. *Eur J Radiol,* 83**,** 1135-43.

LOHAN, D. G., TOMASIAN, A., SALEH, R., KRISHNAM, M. & FINN, J. P. 2008. Hypervascular Thyroid Nodules on Time-Resolved MR Angiography at 3 T: Radiologic–Pathologic Correlation. *American Journal of Roentgenology,* 190**,** W255-W260.

LUCK, C., SRIRANGARAMASAMY, J., BALAMURUGAN, M., ARUMUGAM, B. & PADMAVATHY, A. 2017. Evaluation of diagnostic accuracy of FNAC and correlation with histopathology in thyroid lesions. *Tropical Journal of Pathology and Microbiology,* 3.

LUSTER, M., CLARKE, S., DIETLEIN, M., LASSMANN, M., LIND, P., OYEN, W., TENNVALL, J. & BOMBARDIERI, E. 2008. Guidelines for radioiodine therapy of differentiated thyroid cancer. *European journal of nuclear medicine and molecular imaging,* 35**,** 1941.

LYSHCHIK, A., MOSES, R., BARNES, S. L., HIGASHI, T., ASATO, R., MIGA, M. I., GORE, J. C. & FLEISCHER, A. C. 2007. Quantitative analysis of tumor vascularity in benign and malignant solid thyroid nodules. *Journal of ultrasound in medicine,* 26**,** 837-846.

M REGINA CASTRO, M. & GHARIB, H. 2003. Thyroid fine-needle aspiration biopsy: progress, practice, and pitfalls. *Endocrine Practice*.

MACSWEENEY, J., COSGROVE, D. & ARENSON, J. 1996. Colour Doppler energy (power) mode ultrasound. *Clinical radiology,* 51**,** 387-390.

MAIDA, V. & DAENINCK, P. 2016. A user's guide to cannabinoid therapies in oncology. *Current Oncology,* 23**,** 398.

MALHI, H., BELAND, M. D., CEN, S. Y., ALLGOOD, E., DALEY, K., MARTIN, S. E., CRONAN, J. J. & GRANT, E. G. 2014. Echogenic foci in thyroid nodules: significance of posterior acoustic artifacts. *American Journal of Roentgenology,* 203**,** 1310-1316.

MALLAT, A. & LOTERSZTAJN, S. 2016. Targeting cannabinoid receptors in hepatocellular carcinoma? *Gut,* 65**,** 1582-1583.

MAMOON, N., JAMY, R. & KHAN, A. H. 2013. Evaluation of fine needle aspiration cytology as a screening tool in thyroid lesions. *J Pak Med Assoc,* 63**,** 1120-1123.

MANDEL, S. J. 2004. Diagnostic use of ultrasonography in patients with nodular thyroid disease. *Endocrine Practice,* 10**,** 246-252.

MANNING, A. M., YANG, H., FALCIGLIA, M., MARK, J. R. & STEWARD, D. L. 2017. Thyroid Ultrasound-Guided Fine-Needle Aspiration Cytology Results: Observed Increase in Indeterminate Rate over the Past Decade. *Otolaryngology–Head and Neck Surgery***,** 0194599816688190.

MARTÍNEZ-MARTÍNEZ, E., GÓMEZ, I., MARTÍN, P., SÁNCHEZ, A., ROMÁN, L., TEJERINA, E., BONILLA, F., MERINO, A. G., DE HERREROS, A. G. & PROVENCIO, M. 2015. Cannabinoids receptor type 2, CB2, expression correlates with human colon cancer progression and predicts patient survival. *Oncoscience,* 2**,** 131.

MARTINOLI, C., DERCHI, L., RIZZATTO, G. & SOLBIATI, L. 1998. Power Doppler sonography: general principles, clinical applications, and future prospects. *European radiology,* 8**,** 1224-1235.

MATHEW, R., KARP, C. M., BEAUDOIN, B., VUONG, N., CHEN, G., CHEN, H.-Y., BRAY, K., REDDY, A., BHANOT, G. & GELINAS, C. 2009. Autophagy suppresses tumorigenesis through elimination of p62. *Cell,* 137**,** 1062-1075.

MCDOUGALL, I. R. 2013. *Thyroid disease in clinical practice*, Springer.

MCKERNS, K. W. 2013. *Hormonal Control of the Hypothalamo-pituitary-gonadal Axis*, Springer.

MENGAL, M. Z., RAFI, Y. & GONDAL, K. M. Frequency of Thyroid Malignancy in Patients Undergoing Thyroidectomy for Multinodular Goiter.

MENGER, L., VACCHELLI, E., ADJEMIAN, S., MARTINS, I., MA, Y., SHEN, S., YAMAZAKI, T., SUKKURWALA, A. Q., MICHAUD, M. & MIGNOT, G. 2012. Cardiac glycosides exert anticancer effects by inducing immunogenic cell death. *Science translational medicine,* 4**,** 143ra99-143ra99.

MICHELS, J. J., JACQUES, M., HENRY-AMAR, M. & BARDET, S. 2007. Prevalence and prognostic significance of tall cell variant of papillary thyroid carcinoma. *Human pathology,* 38**,** 212-219.

MITCHELL, D. G. 1990. Color Doppler imaging: principles, limitations, and artifacts. *Radiology,* 177**,** 1-10.

MIZRACHI, A., SWARTZWELDER, C. E. & SHAHA, A. R. 2015. Proposal for anatomical classification of the superior pole in thyroid surgery. *Journal of surgical oncology,* 112**,** 15-17.

MONPEYSSEN, H., TRAMALLONI, J., POIRÉE, S., HÉLÉNON, O. & CORREAS, J.-M. 2013. Elastography of the thyroid. *Diagnostic and interventional imaging,* 94**,** 535-544.

MOON, H. J., KWAK, J. Y., KIM, M. J., SON, E. J. & KIM, E.-K. 2010. Can Vascularity at Power Doppler US Help Predict Thyroid Malignancy? 1. *Radiology,* 255**,** 260-269.

MOORE, K. L., PERSAUD, T. & SHIOTA, K. 2000. *Color atlas of clinical embryology*, Elsevier Health Sciences.

MORELL, C., BORT, A., VARA, D., RAMOS-TORRES, A., RODRÍGUEZ-HENCHE, N. & DÍAZ-LAVIADA, I. 2016. The cannabinoid WIN 55,212-2 prevents neuroendocrine differentiation of LNCaP prostate cancer cells. *Prostate cancer and prostatic diseases,* 19**,** 248-257.

MÜLLER, M. & SEITZ, H. 1984. Thyroid hormone action on intermediary metabolism. *Journal of Molecular Medicine,* 62**,** 11-18.

MULLUR, R., LIU, Y.-Y. & BRENT, G. A. 2014. Thyroid hormone regulation of metabolism. *Physiological reviews,* 94**,** 355-382.

NASCIMENTO, C., BORGET, I., AL GHUZLAN, A., DEANDREIS, D., HARTL, D., LUMBROSO, J., BERDELOU, A., LEPOUTRE-LUSSEY, C., MIRGHANI, H., BAUDIN, E., SCHLUMBERGER, M. & LEBOULLEUX, S. 2015. Postoperative fluorine-18-fluorodeoxyglucose positron emission tomography/computed tomography: an important imaging modality in patients with aggressive histology of differentiated thyroid cancer. *Thyroid,* 25**,** 437-44.

NETTER, F. H. 2014. *Atlas of Human Anatomy, Professional Edition E-Book: including NetterReference. com Access with Full Downloadable Image Bank*, Elsevier Health Sciences.

NGUYEN, Q. T., LEE, E. J., HUANG, M. G., PARK, Y. I., KHULLAR, A. & PLODKOWSKI, R. A. 2015. Diagnosis and treatment of patients with thyroid cancer. *American health & drug benefits,* 8**,** 30.

NIEDZIELA, M. 2014. Thyroid nodules. *Best Practice & Research Clinical Endocrinology & Metabolism,* 28**,** 245-277.

NIX, P., NICOLAIDES, A. & COATESWORTH, A. 2005. Thyroid cancer review 1: presentation and investigation of thyroid cancer. *International journal of clinical practice,* 59**,** 1340-1344.

NODA, Y., KANEMATSU, M., GOSHIMA, S., KONDO, H., WATANABE, H., KAWADA, H. & BAE, K. T. 2015. MRI of the thyroid for differential diagnosis of benign thyroid nodules and papillary carcinomas. *American Journal of Roentgenology,* 204**,** W332-W335.

NODULES, A. A. T. F. O. T. 2006. American Association of Clinical Endocrinologists and Associazione Medici Endocrinologi medical guidelines for clinical practice for the diagnosis and management of thyroid nodules. *Endocrine Practice*.

O'CONNOR, K. A. & ROTH, B. L. 2005. Finding new tricks for old drugs: an efficient route for public-sector drug discovery. *Nature reviews Drug discovery,* 4**,** 1005-1014.

PACHER, P., BÁTKAI, S. & KUNOS, G. 2006. The endocannabinoid system as an emerging target of pharmacotherapy. *Pharmacological reviews,* 58**,** 389-462.

PACINI, F. Thyroid nodules.

PAPINI, E., GUGLIELMI, R., BIANCHINI, A., CRESCENZI, A., TACCOGNA, S., NARDI, F., PANUNZI, C., RINALDI, R., TOSCANO, V. & PACELLA, C. M. 2002. Risk of malignancy in nonpalpable thyroid nodules: predictive value of ultrasound and color-Doppler features. *The Journal of Clinical Endocrinology & Metabolism,* 87**,** 1941-1946.

PARK, A. Y., SON, E. J., HAN, K., YOUK, J. H., KIM, J.-A. & PARK, C. S. 2015a. Shear wave elastography of thyroid nodules for the prediction of malignancy in a large scale study. *European journal of radiology,* 84**,** 407-412.

PARK, A. Y., SON, E. J., HAN, K., YOUK, J. H., KIM, J. A. & PARK, C. S. 2015b. Shear wave elastography of thyroid nodules for the prediction of malignancy in a large scale study. *Eur J Radiol,* 84**,** 407-12.

PEETERS, E. Y., SHABANA, W. M., VERBEEK, P. A. & OSTEAUX, M. M. 2003. Use of a curved-array transducer to reduce interobserver variation in sonographic measurement of thyroid volume in healthy adults. *Journal of clinical ultrasound,* 31**,** 189-193.

PÉREZ-GÓMEZ, E., ANDRADAS, C., BLASCO-BENITO, S., CAFFAREL, M. M., GARCÍA-TABOADA, E., VILLA-MORALES, M., MORENO, E., HAMANN, S., MARTÍN-VILLAR, E. & FLORES, J. M. 2015. Role of cannabinoid receptor CB2 in HER2 pro-oncogenic signaling in breast cancer. *JNCI: Journal of the National Cancer Institute,* 107.

PERROS, P., BOELAERT, K., COLLEY, S., EVANS, C., EVANS, R. M., GERRARD, B., GILBERT, J., HARRISON, B., JOHNSON, S. J. & GILES, T. E. 2014. Guidelines for the management of thyroid cancer. *Clinical endocrinology,* 81**,** 1-122.

PERTWEE, R. G. 2006. Cannabinoid pharmacology: the first 66 years. *British journal of pharmacology,* 147.

POPLI, M. B., RASTOGI, A., BHALLA, P. & SOLANKI, Y. 2012. Utility of gray-scale ultrasound to differentiate benign from malignant thyroid nodules. *Indian Journal of Radiology and Imaging,* 22**,** 63.

PRAKASH, RAJINI, T., RAMACHANDRAN, A., SAVALGI, G. B., VENKATA, S. P. & MOKHASI, V. 2012. Variations in the anatomy of the thyroid gland: clinical implications of a cadaver study. *Anatomical Science International,* 87**,** 45-49.

PRASSAS, I. & DIAMANDIS, E. P. 2008. Novel therapeutic applications of cardiac glycosides. *Nature reviews Drug discovery,* 7**,** 926-935.

PUCCI, E., CHIOVATO, L. & PINCHERA, A. 2000. Thyroid and lipid metabolism. *International journal of obesity,* 24**,** S109.

RAGO, T., VITTI, P., CHIOVATO, L., MAZZEO, S., DE LIPERI, A., MICCOLI, P., VIACAVA, P., BOGAZZI, F., MARTINO, E. & PINCHERA, A. 1998. Role of conventional ultrasonography and color flow-doppler sonography in predicting malignancy in'cold'thyroid nodules. *European Journal of Endocrinology,* 138**,** 41-46.

RAMOS, C. D., WITTMANN, D. E. Z., ETCHEBEHERE, E. C. S. D. C., TAMBASCIA, M. A., SILVA, C. A. M. & CAMARGO, E. E. 2002. Thyroid uptake and scintigraphy using 99mTc pertechnetate: standardization in normal individuals. *Sao Paulo Medical Journal,* 120**,** 45-48.

RANKE, C., HENDRICKX, P., ROTH, U., BRASSEL, F., CREUTZIG, A. & ALEXANDER, K. 1992. Color and conventional image-directed Doppler ultrasonography: Accuracy and sources of error in quantitative blood flow measurements. *Journal of clinical ultrasound,* 20**,** 187-193.

RAVI, J., ELBAZ, M., WANI, N. A., NASSER, M. W. & GANJU, R. K. 2016. Cannabinoid receptor-2 agonist inhibits macrophage induced EMT in non-small cell lung cancer by downregulation of EGFR pathway. *Molecular carcinogenesis,* 55**,** 2063-2076.

RAZAVI, S. A., HADDUCK, T. A., SADIGH, G. & DWAMENA, B. A. 2013. Comparative effectiveness of elastographic and B-mode ultrasound criteria for diagnostic discrimination of thyroid nodules: a meta-analysis. *American Journal of Roentgenology,* 200**,** 1317-1326.

RINALDI-CARMONA, M., BARTH, F., MILLAN, J., DEROCQ, J.-M., CASELLAS, P., CONGY, C., OUSTRIC, D., SARRAN, M., BOUABOULA, M. & CALANDRA, B. 1998. SR 144528, the first potent and selective antagonist of the CB2 cannabinoid receptor. *Journal of Pharmacology and Experimental Therapeutics,* 284**,** 644-650.

RON, E., LUBIN, J. H., SHORE, R. E., MABUCHI, K., MODAN, B., POTTERN, L. M., SCHNEIDER, A. B., TUCKER, M. A. & BOICE JR, J. D. 1995. Thyroid cancer after exposure to external radiation: a pooled analysis of seven studies. *Radiation research,* 141**,** 259-277.

ROSARIO, P. W., SILVA, A. L. D., BORGES, M. A. R. & CALSOLARI, M. R. 2015. Is Doppler ultrasound of additional value to gray-scale ultrasound in differentiating malignant and benign thyroid nodules? *Archives of endocrinology and metabolism,* 59**,** 79-83.

ROSENBAUM-KRUMME, S. J., GÖRGES, R., BOCKISCH, A. & BINSE, I. 2012. 18F-FDG PET/CT changes therapy management in high-risk DTC after first radioiodine therapy. *European journal of nuclear medicine and molecular imaging,* 39**,** 1373-1380.

ROSS, D. S. 2008. Diagnostic approach to and treatment of thyroid nodules. I. *UpToDate. Wellesley, MA: UpToDate. Last accessed December*.

RUBIN, J., BUDE, R., CARSON, P., BREE, R. & ADLER, R. 1996. Power Doppler Us: A Potentially Useful Alternative To Mean Frequency-based Color Doppler Us. *Journal of Diagnostic Medical Sonography,* 12**,** 154.

SAEEDAN, M. B., ALJOHANI, I. M., KHUSHAIM, A. O., BUKHARI, S. Q. & ELNAAS, S. T. 2016. Thyroid computed tomography imaging: pictorial review of variable pathologies. *Insights into imaging,* 7**,** 601-617.

SALABE, G. 2001. Pathogenesis of thyroid nodules: histological classification? *Biomedicine & pharmacotherapy,* 55**,** 39-53.

SALAZAR, M., CARRACEDO, A., SALANUEVA, Í. J., HERNÁNDEZ-TIEDRA, S., EGIA, A., LORENTE, M., VÁZQUEZ, P., TORRES, S., IOVANNA, J. L. & GUZMÁN, M. 2009a. TRB3 links ER stress to autophagy in cannabinoid antitumoral action. *Autophagy,* 5**,** 1048-1049.

SALAZAR, M., CARRACEDO, A., SALANUEVA, Í. J., HERNÁNDEZ-TIEDRA, S., LORENTE, M., EGIA, A., VÁZQUEZ, P., BLÁZQUEZ, C., TORRES, S. & GARCÍA, S. 2009b. Cannabinoid action induces autophagy-mediated cell death through stimulation of ER stress in human glioma cells. *The Journal of clinical investigation,* 119**,** 1359-1372.

SALVATORE, D., DAVIES, T. F., SCHLUMBERGER, M., HAY, I. & LARSEN, P. 2011. Thyroid physiology and diagnostic evaluation of patients with thyroid disorders. *Williams Textbook of Endocrinology,* 12**,** 327-50.

SANO, R. & REED, J. C. 2013. ER stress-induced cell death mechanisms. *Biochimica et Biophysica Acta (BBA)-Molecular Cell Research,* 1833**,** 3460-3470.

SARFARAZ, S., AFAQ, F., ADHAMI, V. M., MALIK, A. & MUKHTAR, H. 2006. Cannabinoid receptor agonist-induced apoptosis of human prostate cancer cells LNCaP proceeds through sustained activation of ERK1/2 leading to G1 cell cycle arrest. *Journal of Biological Chemistry,* 281**,** 39480-39491.

SAWKA, A. M., THEPHAMONGKHOL, K., BROUWERS, M., THABANE, L., BROWMAN, G. & GERSTEIN, H. C. 2004. A systematic review and metaanalysis of the effectiveness of radioactive iodine remnant ablation for well-differentiated thyroid cancer. *The Journal of Clinical Endocrinology & Metabolism,* 89**,** 3668-3676.

SCHWARZ, D. S. & BLOWER, M. D. 2016. The endoplasmic reticulum: structure, function and response to cellular signaling. *Cellular and molecular life sciences,* 73**,** 79-94.

SEBAG, F., VAILLANT-LOMBARD, J., BERBIS, J., GRISET, V., HENRY, J., PETIT, P. & OLIVER, C. 2010a. Shear wave elastography: a new ultrasound imaging mode for the differential diagnosis of benign and malignant thyroid nodules. *The Journal of Clinical Endocrinology & Metabolism,* 95**,** 5281-5288.

SEBAG, F., VAILLANT-LOMBARD, J., BERBIS, J., GRISET, V., HENRY, J. F., PETIT, P. & OLIVER, C. 2010b. Shear wave elastography: a new ultrasound imaging mode for the differential diagnosis of benign and malignant thyroid nodules. *J Clin Endocrinol Metab,* 95**,** 5281-8.

SHAH, M. Amiodarone-Induced Thyrotoxicosis and Ventricular Arrhythmias: Case Report and Review of the Literature. The Medicine Forum, 2016. 13.

SHAPIRO, R. S. 2003. Panoramic ultrasound of the thyroid. *Thyroid,* 13**,** 177-181.

SHARMA, C. 2016. An analysis of trends of incidence and cytohistological correlation of papillary carcinoma of the thyroid gland with evaluation of discordant cases. *Journal of Cytology,* 33**,** 192.

SHETTY, S. K., MAHER, M. M., HAHN, P. F., HALPERN, E. F. & AQUINO, S. L. 2006. Significance of incidental thyroid lesions detected on CT: correlation among CT, sonography, and pathology. *American Journal of Roentgenology,* 187**,** 1349-1356.

SHIGENO, K., IGAWA, M., SHIINA, H., WADA, H. & YONEDA, T. 2000. The role of colour Doppler ultrasonography in detecting prostate cancer. *BJU international,* 86**,** 229-233.

SHIMAMOTO, K., SATAKE, H., SAWAKI, A., ISHIGAKI, T., FUNAHASHI, H. & IMAI, T. 1998. Preoperative staging of thyroid papillary carcinoma with ultrasonography. *European journal of radiology,* 29**,** 4-10.

SHRESTHA, R. T. & HENNESSEY, J. 2015. Acute and subacute, and Riedel's thyroiditis.

SHWEEL, M. & MANSOUR, E. 2013. Diagnostic performance of combined elastosonography scoring and high-resolution ultrasonography for the differentiation of benign and malignant thyroid nodules. *European journal of radiology,* 82**,** 995-1001.

SIEGEL, R. L., MILLER, K. D. & JEMAL, A. 2016. Cancer statistics, 2016. *CA: a cancer journal for clinicians,* 66**,** 7-30.

SINHA, R. A., SINGH, B. K. & YEN, P. M. 2014. Thyroid hormone regulation of hepatic lipid and carbohydrate metabolism. *Trends in Endocrinology & Metabolism,* 25**,** 538-545.

SINOS, G. & SAKORAFAS, G. H. 2015. Pyramidal lobe of the thyroid: anatomical considerations of importance in thyroid cancer surgery. *Oncology research and treatment,* 38**,** 309-310.

SOBRINHO-SIMOES, M., ELOY, C., MAGALHAES, J., LOBO, C. & AMARO, T. 2011. Follicular thyroid carcinoma. *Modern Pathology,* 24**,** S10.

SOFFERMAN, R. A. & AHUJA, A. T. 2011. *Ultrasound of the thyroid and parathyroid glands*, Springer Science & Business Media.

SPENCER, C., LOPRESTI, J., FATEMI, S. & NICOLOFF, J. 1999. Detection of residual and recurrent differentiated thyroid carcinoma by serum thyroglobulin measurement. *Thyroid,* 9**,** 435-441.

STEWART, W. B. & RIZZOLO, L. J. 2012. Embryology and surgical anatomy of the thyroid and parathyroid glands. *Surgery of the thyroid and parathyroid glands.* Springer.

STOIAN, D., BOGDAN, T., CRAINA, M., CRACIUNESCU, M., TIMAR, R. & SCHILLER, A. 2016. Elastography: A New Ultrasound Technique in Nodular Thyroid Pathology. *Thyroid Cancer-Advances in Diagnosis and Therapy.* InTech.

SU, Y., RYDER, J., LI, B., WU, X., FOX, N., SOLENBERG, P., BRUNE, K., PAUL, S., ZHOU, Y. & LIU, F. 2004. Lithium, a common drug for bipolar disorder treatment, regulates amyloid-β precursor protein processing. *Biochemistry,* 43**,** 6899-6908.

SULTAN, L. R., XIONG, H., ZAFAR, H. M., SCHULTZ, S. M., LANGER, J. E. & SEHGAL, C. M. 2015. Vascularity assessment of thyroid nodules by quantitative color doppler ultrasound. *Ultrasound in medicine & biology,* 41**,** 1287-1293.

SUN, J., CAI, J. & WANG, X. 2014a. Real-time ultrasound elastography for differentiation of benign and malignant thyroid nodules: a meta-analysis. *J Ultrasound Med,* 33**,** 495-502.

SUN, J., CAI, J. & WANG, X. 2014b. Real-time Ultrasound Elastography for Differentiation of Benign and Malignant Thyroid Nodules. *Journal of Ultrasound in Medicine,* 33**,** 495-502.

SWANSON, K. M. & HOHL, R. J. 2006. Anti-cancer therapy: targeting the mevalonate pathway. *Current cancer drug targets,* 6**,** 15-37.

SZCZEPANEK-PARULSKA, E., WOLINSKI, K., STANGIERSKI, A., GURGUL, E., BICZYSKO, M., MAJEWSKI, P., REWAJ-LOSYK, M. & RUCHALA, M. 2013. Comparison of diagnostic value of conventional ultrasonography and shear wave elastography in the prediction of thyroid lesions malignancy. *PLoS One,* 8**,** e81532.

TAN, G. H. & GHARIB, H. 1997. Thyroid incidentalomas: management approaches to nonpalpable nodules discovered incidentally on thyroid imaging. *Annals of internal medicine,* 126**,** 226-231.

TAN, G. H., GHARIB, H. & READING, C. C. 1995. Solitary thyroid nodule: comparison between palpation and ultrasonography. *Archives of internal Medicine,* 155**,** 2418-2423.

TAO, A. T. 2016. *Advanced Methods in Molecular Breast Imaging.*

TREGLIA, G., CALDARELLA, C., SAGGIORATO, E., CERIANI, L., ORLANDI, F., SALVATORI, M. & GIOVANELLA, L. 2013. Diagnostic performance of 99mTc-MIBI scan in predicting the malignancy of thyroid nodules: a meta-analysis. Springer.

TSANG, R. W., BRIERLEY, J. D., SIMPSON, W. J., PANZARELLA, T., GOSPODAROWICZ, M. K. & SUTCLIFFE, S. B. 1998. The effects of surgery, radioiodine, and external radiation therapy on the clinical outcome of patients with differentiated thyroid carcinoma. *Cancer,* 82**,** 375-388.

TUNBRIDGE, W., EVERED, D., HALL, R., APPLETON, D., BREWIS, M., CLARK, F., EVANS, J. G., YOUNG, E., BIRD, T. & SMITH, P. 1977. The spectrum of thyroid disease in a community: the Whickham survey. *Clinical endocrinology,* 7**,** 481-493.

ÜNLÜTÜRK, U., ERDOĞAN, M. F., DEMIR, Ö., GÜLLÜ, S. & BAŞKAL, N. 2012. Ultrasound elastography is not superior to grayscale ultrasound in predicting malignancy in thyroid nodules. *Thyroid,* 22**,** 1031-1038.

VAN NOSTRAND, D., SCHNEIDER, M. & ACIO, E. R. 2016. Radionuclide Imaging of Thyroid Nodules. *Thyroid Cancer.* Springer.

VARA, D., SALAZAR, M., OLEA-HERRERO, N., GUZMAN, M., VELASCO, G. & DIAZ-LAVIADA, I. 2011. Anti-tumoral action of cannabinoids on hepatocellular carcinoma: role of AMPK-dependent activation of autophagy. *Cell Death & Differentiation,* 18**,** 1099-1111.

VARVERAKIS, E., NEONAKIS, E., TZARDI, M. & CHRYSOS, E. 2007. Role of color Doppler ultrasonography in preoperative management of cold thyroid nodules. *HORMONES-ATHENS-,* 6**,** 44.

VEER, V. & PUTTAGUNTA, S. 2015. The role of elastography in evaluating thyroid nodules: a literature review and meta-analysis. *European Archives of Oto-Rhino-Laryngology,* 272**,** 1845-1855.

VELASCO, G., HERNÁNDEZ-TIEDRA, S., DÁVILA, D. & LORENTE, M. 2016. The use of cannabinoids as anticancer agents. *Progress in Neuro-Psychopharmacology and Biological Psychiatry,* 64**,** 259-266.

VENKATESWARULU, B. & GOWNI, R. 2017. Role of Color Doppler in evaluation of Thyroid Diseases. *Indian Journal of Applied Research,* 6.

VERBURG, F. A., AKTOLUN, C., CHITI, A., FRANGOS, S., GIOVANELLA, L., HOFFMANN, M., IAKOVOU, I., MIHAILOVIC, J., KRAUSE, B. J. & LANGSTEGER, W. 2016. Why the European Association of Nuclear Medicine has declined to endorse the 2015 American Thyroid Association management guidelines for adult patients with thyroid nodules and differentiated thyroid cancer. Springer.

VERFAILLIE, T., SALAZAR, M., VELASCO, G. & AGOSTINIS, P. 2010. Linking ER stress to autophagy: potential implications for cancer therapy. *International journal of cell biology,* 2010.

VEYRIERES, J.-B., ALBAREL, F., LOMBARD, J. V., BERBIS, J., SEBAG, F., OLIVER, C. & PETIT, P. 2012a. A threshold value in Shear Wave elastography to rule out malignant thyroid nodules: a reality? *European journal of radiology,* 81**,** 3965-3972.

VEYRIERES, J. B., ALBAREL, F., LOMBARD, J. V., BERBIS, J., SEBAG, F., OLIVER, C. & PETIT, P. 2012b. A threshold value in Shear Wave elastography to rule out malignant thyroid nodules: a reality? *Eur J Radiol,* 81**,** 3965-72.

WEBER, A. L., RANDOLPH, G. & AKSOY, F. G. 2000. The thyroid and parathyroid glands: CT and MR imaging and correlation with pathology and clinical findings. *Radiologic Clinics of North America,* 38**,** 1105-1129.

WEIS, S. M. & CHERESH, D. A. 2011. Tumor angiogenesis: molecular pathways and therapeutic targets. *Nature medicine,* 17**,** 1359-1370.

WIENKE, J. R., CHONG, W. K., FIELDING, J. R., ZOU, K. H. & MITTELSTAEDT, C. A. 2003. Sonographic features of benign thyroid nodules interobserver reliability and overlap with malignancy. *Journal of Ultrasound in Medicine,* 22**,** 1027-1031.

WIGHTMAN, L., KIRCHEIS, R., RÖSSLER, V., CAROTTA, S., RUZICKA, R., KURSA, M. & WAGNER, E. 2001. Different behavior of branched and linear polyethylenimine for gene delivery in vitro and in vivo. *The journal of gene medicine,* 3**,** 362-372.

WIMMER, I. & PICHLER, R. 2016. FDG PET in Thyroid Cancer. *Thyroid Cancer-Advances in Diagnosis and Therapy.* InTech.

WISNER, E. R. & NYLAND, T. G. 1998. Ultrasonography of the thyroid and parathyroid glands. *Veterinary Clinics of North America: Small Animal Practice,* 28**,** 973-991.

WONG, K. & AHUJA, A. T. 2005. Ultrasound of thyroid cancer. *Cancer Imaging,* 5**,** 157.

WU, M.-H., CHEN, C.-N., CHEN, K.-Y., HO, M.-C., TAI, H.-C., CHUNG, Y.-C., LO, C.-P., CHEN, A. & CHANG, K.-J. 2013. Quantitative analysis of dynamic power Doppler sonograms for patients with thyroid nodules. *Ultrasound in medicine & biology,* 39**,** 1543-1551.

XUE, M., SHI, Q., TAN, K., WU, Y. & ZHOU, R. 2016. The role of color doppler ultrasonography, thyroid function and auto antibody for the screening of Graves' disease in pregnancy. *Zhonghua nei ke za zhi,* 55**,** 470-473.

YANG, Z. J., CHEE, C. E., HUANG, S. & SINICROPE, F. A. 2011. The role of autophagy in cancer: therapeutic implications. *Molecular cancer therapeutics,* 10**,** 1533-1541.

YING, M., CHENG, S. C. & AHUJA, A. T. 2016. Diagnostic Accuracy of Computer-Aided Assessment of Intranodal Vascularity in Distinguishing Different Causes of Cervical Lymphadenopathy. *Ultrasound in medicine & biology,* 42**,** 2010-2016.

YING, M., NG, D. K., YUNG, D. M. & LEE, E. S. 2009. A semi-quantitative approach to compare high-sensitivity power Doppler sonography and conventional power Doppler sonography in the assessment of thyroid vascularity. *Thyroid,* 19**,** 1265-1269.

YING, M. & YUNG, D. 2009. Asymmetry of thyroid lobe volume in normal Chinese subjects: association with handedness and position of esophagus. *The Anatomical Record,* 292**,** 169-174.

YOON, J. H., KWAK, J. Y., MOON, H. J., KIM, M. J. & KIM, E.-K. 2011a. The diagnostic accuracy of ultrasound-guided fine-needle aspiration biopsy and the sonographic differences between benign and malignant thyroid nodules 3 cm or larger. *Thyroid,* 21**,** 993-1000.

YOON, J. H., MOON, H. J., KIM, E.-K. & KWAK, J. Y. 2011b. Inadequate cytology in thyroid nodules: should we repeat aspiration or follow-up? *Annals of surgical oncology,* 18**,** 1282-1289.

YORIMITSU, T. & KLIONSKY, D. J. 2007. Endoplasmic reticulum stress: a new pathway to induce autophagy. *Autophagy,* 3**,** 160-162.

YOUN, Y.-K., LEE, K. E. & CHOI, J. Y. 2014. Surgical Anatomy of the Thyroid Gland. *Color Atlas of Thyroid Surgery.* Springer.

YUNUS, M. & AHMED, Z. 2010. Significance of ultrasound features in predicting malignant solid thyroid nodules: need for fine-needle aspiration. *JPMA-Journal of the Pakistan Medical Association,* 60**,** 848.

ZEYBEK, N. D., GULCELIK, N. E., KAYMAZ, F. F., SARISOZEN, C., VURAL, I., BODUR, E., CANPINAR, H., USMAN, A. & ASAN, E. 2011. Rosuvastatin induces apoptosis in cultured human papillary thyroid cancer cells. *Journal of Endocrinology,* 210**,** 105-115.

ZHANG, B., MA, X., WU, N., LIU, L., LIU, X., ZHANG, J., YANG, J. & NIU, T. 2013. Shear Wave Elastography for Differentiation of Benign and Malignant Thyroid Nodules. *Journal of Ultrasound in Medicine,* 32**,** 2163-2169.

ZHANG, L., HE, M., ZHANG, Y., NILUBOL, N., SHEN, M. & KEBEBEW, E. 2011. Quantitative high-throughput drug screening identifies novel classes of drugs with anticancer activity in thyroid cancer cells: opportunities for repurposing. *The Journal of Clinical Endocrinology & Metabolism,* 97**,** E319-E328.

ZHANG, L., ZHANG, L., CHENG, X., GAO, Y., BAO, J., YU, H., GUAN, H., SUN, Y. & LU, R. 2016. Curcumin induces cell death of human papillary thyroid carcinoma BCPAP cells through endoplasmic reticulum stress. *RSC Advances,* 6**,** 52905-52912.